Late Quaternary environmental history of Rauer Group, East Antarctica

Inaugural-Dissertation

zur

Erlangung des Doktorgrades

der Mathematisch-Naturwissenschaftlichen Fakultät

der Universität zu Köln

vorgelegt von

Sonja Berg

aus Erkelenz

Köln 2010

Berichterstatter: Prof. Dr. Martin Melles

(Gutachter)   PD Dr. Bernd Wagner

                      Prof. Dr. Damian Gore

Tag der mündlichen Prüfung: 30.06.2010

Abstract

In East Antarctica, small ice-free coastal areas are unique environments, located between the East Antarctic Ice Sheet (EAIS) and its outlet glacier systems on the one hand and the Southern Ocean on the other. Rauer Group is an ice-free archipelago in eastern Prydz Bay, which has been visited in March 2007. Geomorphological studies have been conducted there in order to shed light on the glacial history of the area. The recovery of long sediment cores from three marine inlets and one lake provided the possibility to reconstruct the late Pleistocene and Holocene environmental and climate history of the area for the first time. Since knowledge on climate and glacial history around East Antarctica is relatively sparse, this study contributes significantly to a broader understanding of the late Quaternary evolution of the region.

The reconstructions presented in this thesis are based on a multi-proxy approach, comprising sedimentological, biogeochemical and paleontological studies on sedimentary records from lakes and marine inlets. Chronologies of the records have been obtained by radiocarbon dating.

Radiocarbon ages from three different records indicate ice-free conditions on the islands in the late Pleistocene between 40-30 ^{14}C ka BP (44.7-34 cal ka BP). The presence of lacustrine as well as marine environments on/at Filla Island suggest that the EAIS reached only insignificantly beyond its present margin during that period. At the same time, relative sea-level reconstructions point to increased ice load in vicinity of the coast and a steeper than present ice sheet profile.

A subsequent glacial overriding due to EAIS expansion during the Last Glacial Maximum can be inferred from a till layer and a hiatus in sediment cores from two marine basins, respectively. Glacial overriding within the last glacial is also suggested by the geomorphology of the islands.

The inlets became ice-free prior to 11,200 cal yr BP, when biogenic sedimentation started. Deglaciation processes in the catchments, however, influenced the inlets until c. 9200 cal yr BP as evidenced by the input of minerogenic material. Holocene ice retreat was virtually complete prior to the Mid-Holocene, since a sediment record from a marine inlet 1.8 km in front of the present ice sheet, contains a complete marine record of the past 4500 years. Significant ice sheet expansion beyond present ice margins did not occur in Rauer Group since the Mid-Holocene.

Concerning climatic conditions throughout the Holocene, an early Holocene climate optimum in Rauer Group is reflected by elevated marine productivity under relatively open-water conditions until 8200 cal yr BP. In the following cooler period sea ice on the marine inlets increased. In the Mid-Holocene the basins experienced an input of freshwater between c. 5700-3500 cal yr BP. Probably warmer climate conditions caused ice-sheet melting and

increased precipitation on the islands. Neoglacial cooling in the late Holocene is reflected by an increase in sea ice in both inlets.

Zusammenfassung

Eisfreie Küstengebiete in der Ostantarktis sind aufgrund ihrer Lage zwischen dem ostantarktischen Eisschild mit seinen Gletschern und dem Südozean einzigartige Umgebungen. Die Rauer-Gruppe ist eine solche eisfreie Inselgruppe in der östlichen Prydz Bucht und wurde im Rahmen dieser Untersuchung während einer Expedition im März 2007 besucht. Dabei wurden geomorphologische Untersuchungen durchgeführt, um die Glazialgeschichte des Gebietes zu rekonstruieren. Die in diesem Zusammenhang gewonnenen Sedimentkerne ermöglichen zum ersten Mal eine Rekonstruktion der spätpleistozänen und holozänen Umwelt- und Klimageschichte des Gebietes. Da das bisherige Wissen über die ostantarktische Klima- und Glazialgeschichte relativ gering ist, trägt diese Untersuchung maßgeblich zu einem breiteren Verständnis der spätquartären Entwicklung in der Region bei.

Sedimentologische, biogeochemische und paläontologische Parameter dienen in dieser Arbeit als Proxys, um Rekonstruktionen an lakustrinen und marinen Archiven durchzuführen. Die zeitliche Einordnung der Sedimentsequenzen erfolgte auf Grundlage von Radiokarbondatierungen.

Mehrere Alter, die aus verschiedenen Sedimentkernen stammen, indizieren eisfreie Bedingungen auf den Inseln im späten Pleistozän. Dies betrifft einen Zeitraum zwischen etwa 40.000 und 30.000 ^{14}C Jahren vor heute (44.700-34.000 Kalenderjahre vor heute). Das Vorkommen sowohl lakustriner als auch mariner Umgebungen um die Insel Filla weist darauf hin, dass der Eisschild damals nur unwesentlich über seine heutige Begrenzung hinausreichte. Gleichzeitig deuten Rekonstruktionen des relativen Meeresspiegels auf eine erhöhte Eisauflast nahe der Küste und auf ein steileres Eisprofil als gegenwärtig hin. Eine nachfolgende Überfahrung der Rauer-Gruppe durch eine Ausdehnung des ostantarktischen Eisschilds lässt sich zum einen aus dem Vorliegen einer Tilllage in einem der Kerne (Co1011) und zum anderen aus dem Auftreten einer Sedimentationsunterbrechung in einem anderen Kern (Co1010) ableiten. Geomorphologische Befunde deuten ebenfalls auf eine Vereisung der Inselgruppe während des letzten Glazials hin.

Die Buchten wurden vor etwa 11200 Jahren eisfrei, was dem Zeitpunkt des Einsetzens biogener Sedimentation in den Becken entspricht. Mit dem Eisrückzug in Zusammenhang stehende Prozesse beeinflussten die Buchten jedoch noch bis vor ca. 9200 Jahren vor heute durch den vermehrten Eintrag minerogenen Materials. Der holozäne Eisrückzug war scheinbar vor 4500 Jahren bereits abgeschlossen, da ein Sedimentkern aus einem Becken mit einer Entfernung von nur 1,8 km zum heutigen Eisschild eine vollständige marine Abfolge der letzten 4500 Jahre enthält. Eine bedeutende Ausdehnung des Eisschildes über die heutigen Grenzen hinaus hat demnach seit dem mittleren Holozän nicht stattgefunden.

Hinsichtlich der Klimageschichte der Region kann ein Optimum im frühen Holozän bis vor ca. 8200 Jahren nachgewiesen werden, welches mit erhöhter mariner Bioproduktion unter offen-marinen Bedingungen korrespondiert. Während der darauffolgenden kühleren Phase kam es zu verstärkter Meereisbildung in den Buchten. Im mittleren Holozän von ca. 5700 bis 3500 Jahren vor heute erfuhren die Buchten dann einen erhöhten Frischwassereintrag. Vermutlich führten wärmere klimatische Bedingungen zu einem verstärkten Abschmelzen des Eisschildes und zu erhöhtem Niederschlag auf den Inseln. Eine Zunahme der Meereisbedeckung durch eine erneute Abkühlung im Spätholozän schließlich lässt sich in der Rauer-Gruppe anhand paläontologischer Parameter nachweisen.

Acknowledgements

Contents

List of figures

List of tables

1. Introduction

1.1 General introduction

Today approximately 90% of global continental ice masses are stored in Antarctica (SCAR, 2007). These ice masses are glaciologically subdivided in the marine-based West Antarctic Ice Sheet (WAIS), the Antarctic Peninsula (AP) ice masses and the East Antarctic Ice Sheet (EAIS; Figure 1.1). The EAIS is not only the largest ice mass on earth, but also the longest-lived ice sheet. Since the initial glaciation of Antarctica in Tertiary, the EAIS has experienced substantial changes in its mass and dimensions (e.g., Flower and Kennett, 1994; O'Brien et al., 2007; Volpi et al., 2009).
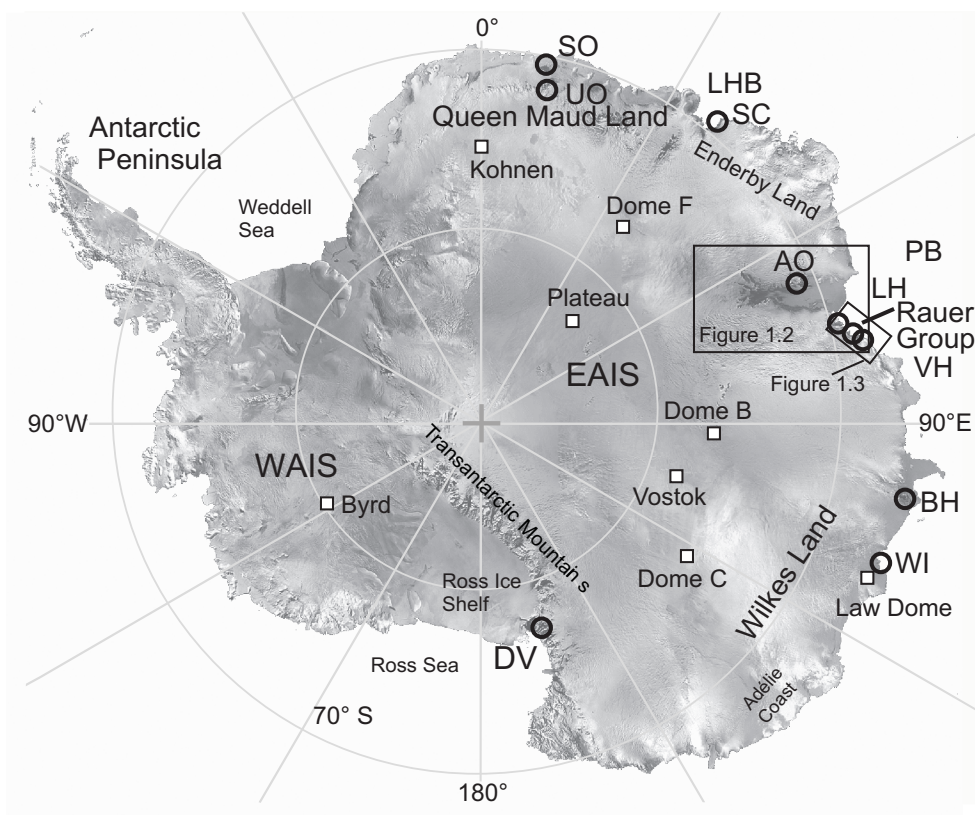
Figure 1.1 Map of Antarctica; WAIS West Antarctic Ice sheet, EAIS East Antarctic Ice Sheet, UO Unterseee Oasis, SO Schirmacher Oasis, LHB Lützow-Holm Bay, SC Sôya Coast, AO Amery Oasis, LH Larsemann Hills, VH Vestfold Hills, PB Prydz Bay, BH Bunger Hills, WI Windmill Islands, DV McMurdo Dry Valleys, rectangles indicate locations of selected ice cores.

In Prydz Bay region, for example, oldest indications for glacial processes on the Antarctic continent have been dated to the Eocene/Oligocene (Strand et al., 2003), with recurring ice expansions far onto the continental shelf (O'Brien et al., 2007). This study, focusing on the late Quaternary and Holocene period, respectively, therefore covers only the most recent chapter of EAIS history.

The ice masses of Antarctica as well as the surrounding sea ice play an important role in earths climate system, since they are influencing global energy balance, ocean currents and

sea level. The potential global impact of changes in the Antarctic region makes it an actuating variable in the discussion about recent and future climate change. At present, the WAIS shows intense ice-dynamic fluctuations (Wingham et al., 2006), and the AP region has been ascribed as one of the fastest warming regions in the world (Vaughan et al., 2003). While the ice sheets of the WAIS and AP region are comparatively small, ice volume of the EAIS equals up to 52 m sea level equivalent (Lythe et al., 2001). Hence, mass balance changes can have a significant impact on sea level. In contrast to the smaller WAIS, mass balance estimations for the EAIS indicate only minor changes in the last decades (Mayewski et al., 2009) however, increased ice loss in coastal region has been observed since 2006 (Chen et al., 2009).
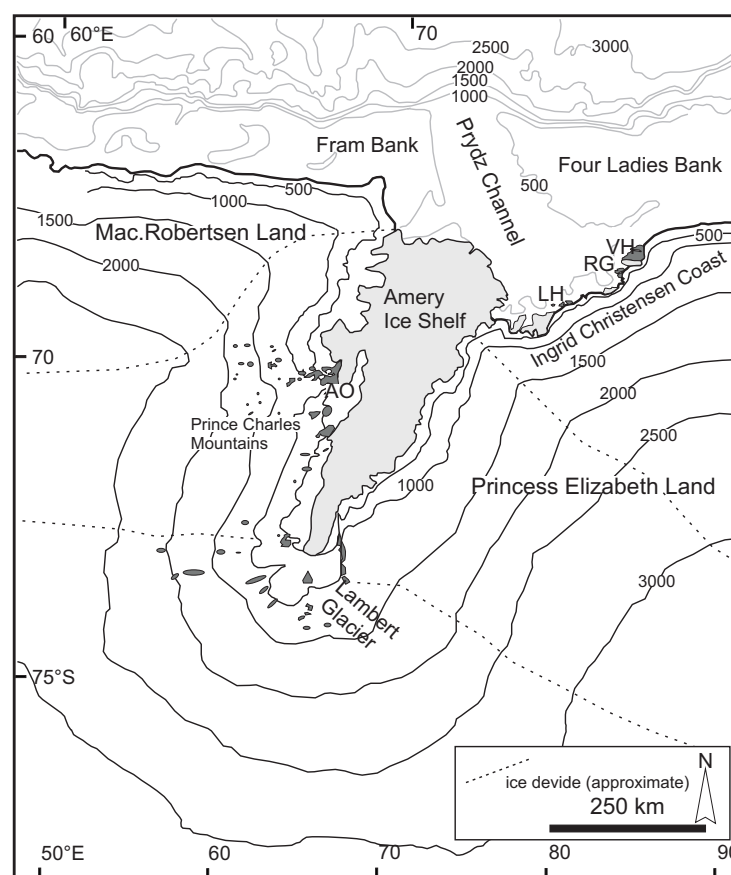
Figure 1.2 Amery Ice Shelf and the Lambert Glacier as well as large topographic features of Prydz Bay, AO Amery Oasis, RG Rauer Group, LH Larsemann Hills, VH Vestfold Hills (Map after O'Brien et al., 2007).

Assessing reactions of the Antarctic system under changing climate conditions is an issue, which can be addressed by paleoenvironmental and paleoclimatic reconstructions. They provide information on the natural variability of ice extent and corresponding climate conditions. Reconstructions of past changes can therefore constitute a framework for predictions of future developments.

Numerous records from very different sites and settings have been employed to reconstruct variability of climate and environments throughout the late Quaternary in East Antarctica.

2

Ice cores retain information about atmospheric composition, temperature, and circulation patterns over periods of up to 800 ka (e.g., Masson et al., 2000; Blunier and Brook, 2001; EPICA, 2004; EPICA, 2006; Petit and Delmonte, 2009). Marine sediment records from the Southern Ocean portray oceanographic conditions like latitudinal extend, and duration of annual sea ice (Hodell et al., 2001; Gersonde et al., 2005; Crosta et al., 2008) or changes in currents, and formation of water masses (Harris, 2000; Harris et al., 2001; Denis et al., 2009).

Besides the ice sheet and the ocean, ice-free terrestrial areas, so-called oases, provide evidence on paleoenvironments and -climates. Today, less than 0,4% of Antarctica is unglaciated (SCAR, 2007) and the relatively small outcrops are far away from each other (Figures 1.1 and 1.2). In East Antarctica, oases lined up along the coast, encompass terrestrial, lacustrine and shallow marine environments hosting unique species assemblages, which are adapted to the extreme conditions (e.g., Karr et al., 2003; Cromer et al., 2006; Convey et al., 2008). Sediment records from these lakes and marine inlets allow detailed reconstructions of past environmental and climate conditions of the areas (e.g., Björk et al., 1996; Roberts and McMinn, 1999; McMinn 2000; Cremer et al., 2003a; Wagner at al., 2004; Verleyen et al., 2005; Hodgson et al., 2006).

The proximity to the ice sheet makes the East Antarctic oases sensitive to dynamics of the ice sheet. Small-scale variation of ice sheet extent can be reconstructed from geomorphological features and glacial deposits like moraine ridges and erratics (e.g., Fitzsimons, 1996; Gore et al., 1996; Fitzsimons 1997; Hall et al., 2002; White et al., 2009). Fossil raised beaches and shorelines, as well as marine/lacustrine transitions recorded in low-lying basins, shed light on the local relative sea level (RSL) evolution, which is closely linked to maximum ice loads and the timing of ice retreat (e.g., Zwartz et al., 1998; Goodwin and Zweck, 2000; Basset et al., 2007). However, fluctuations of the ice sheet can result in erosion of soft sediments and often limit the temporal range of sedimental archives to the period since the previous deglaciation.

1.2 Late Quaternary in coastal East Antarctica

Global ice volume and eustatic sea level are directly linked by the redistribution of water on the earths surface, stored in continental ice masses (e.g., Clark and Mix, 2002). Since eustatic sea level reconstructed from far field observations and isotopic records is an integrated signal, regional ice sheet reconstructions are necessary to allocate spatial and temporal changes in ice sheet extend. Build up of large ice masses during the last glacial resulted in a eustatic sea level of several tenths of metres lower than present (e.g., Bard et al., 1990). The Antarctic contribution to this lowering has mainly been reconstructed from ice sheet modelling (e.g., Huybrechts, 2002; Bassett et al., 2007).

Field evidence for EAIS extend during the last glacial comes from several coastal regions where only moderate ice sheet expansion, compared to the present extent, occurred (e.g., Gore et al., 2001; Cremer et al., 2003a; Hodgson et al., 2003; Hodgson et al., 2009). Radiocarbon ages from sedimentary records indicate biogenic sedimentation in terrestrial and coastal marine environments between c. 45 and 29 cal yr BP, in the second half of Marine Isotope Stage (MIS) 3 (e.g., Cremer et al., 2003a; Hodgson et al., 2003; Hodgson et al., 2009). During the last glacial maximum (LGM, 23-19 cal ka BP; Mix et al., 2001), lower global temperatures (Clark et al., 2009) and a global sea level minimum of c. 120 m below present (Bard et al., 1991) prevailed. In Antarctica, winter sea ice extend was displaced northward for 7-10° in latitude (Gersonde et al., 2005) and the WAIS expanded as far as to the shelf margins (Conway et al., 1999; Anderson et al., 2002), while the EAIS reached maximum extents up to mid-shelf areas (Anderson et al., 2002; Mackintosh et al., 2007). Reconstructions of the EAIS configuration during the LGM show that expansion and retreat did not occur at the same time and to the same extent in individual regions (e.g., Anderson et al., 2002; Denton and Hughes, 2002; Ingólfsson, 2004). Some presently ice-free coastal regions, like Windmill Islands, were completely glaciated (Goodwin, 1993), while others, like Larsemann Hills or Bunger Hills remained widely ice free (Gore et al., 2001; Hodgson et al., 2001a).
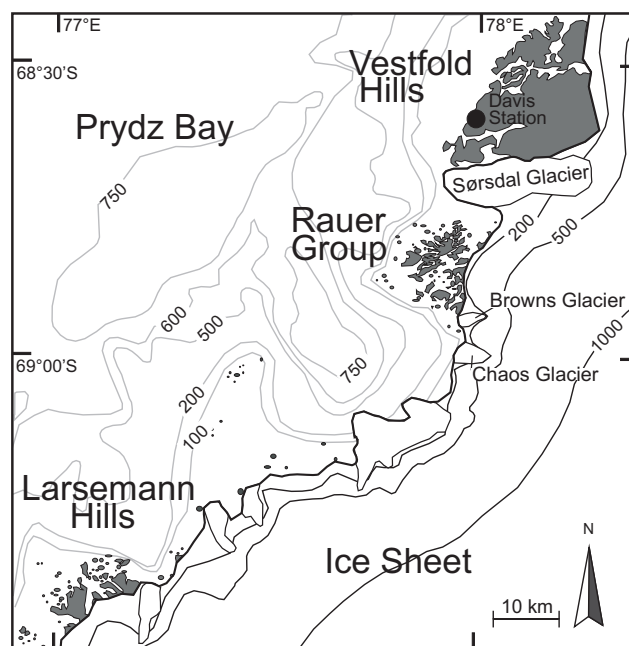
Figure 1.3 Coast of eastern Prydz Bay with ice-free areas (grey), including the study area, Rauer Group and outlet glaciers.

Onset of biogenic production on the shelf as well as in lakes and marine inlets of coastal areas widely occurred at around the Late Pleistocene/Holocene transition (e.g., Roberts and McMinn, 1999; Ingólfsson, 2004; Leventer et al., 2006). Holocene climate in the Antarctic region was characterized by several fluctuations of warmer and colder periods (e.g.,

Bentley et al., 2009). Ice core records from East Antarctica (Figure 1.1) indicate an early Holocene climate optimum with warmer conditions for the period between 11,500 and 9000 yr BP as well as a Mid-Holocene warmer period between 6000 and 3000 yr BP (Masson et al., 2000). Climate fluctuations are also preserved in sedimentary records from around East Antarctica; however, correlations are often difficult between different regions. While sedimentary evidence for an early Holocene optimum is relatively well constrained, for example from lake sediments from Amery Oasis, (Wagner et al., 2004) and Vestfold Hills (Verleyen et al., 2004a and b) and from marine records from Prydz Bay (Taylor and McMinn, 2001) and Bunger Hills (Kulbe et al., 2001), other trends, reconstructed from various sites, are less pronounced (Ingólfsson, 2004). There is a need for well-dated records from East Antarctica to better reveal natural changes in climate conditions throughout the Holocene, and to identify the processes driving climate in coastal East Antarctica.

1.3 Aims and background of the study

The studies presented in this thesis are based on geomorphological investigations as well as on sedimentological, geochemical, and paleontological analysis of sediment cores, which have been recovered in Rauer Group, an ice-free archipelago in eastern Prydz Bay (Figures 1.1, 1.2, and 1.3). Coring locations have been selected at three marine inlets between the islands of Rauer Group and from a lake on one of the islands (Figure 2.1). Rauer Group has not been studied for its paleoenvironmental history, so far, which makes the present studies the first dealing with the late Quaternary environmental history of the islands. The position of the studied area between the two relatively well known ice-free oases Larsemann and Vestfold hills (Figure 1.3) makes Rauer Group an ideal site to refine the regional picture of past glacial and climate developments. On larger scale, Prydz Bay region (c. 65-80°E; Figure 1.2) is a key area for paleoglaciological reconstructions, since the Lambert Glacier/Amery Ice shelf system is the largest drainage system of the EAIS (O'Brien et al., 2007). In addition, Prydz Bay has been identified as a source region for Antarctic bottom-water (AABW; Yabuki et al., 2006), assigning it a role in the global oceanographic system.

The following key questions have been formulated in order to produce a profound picture of the Late Pleistocene/Holocene evolution of Rauer Group

- How did the ice sheet at Rauer Group evolve through time?
- How did environmental conditions change through time and in what way are these changes related to climate?
- Which changes in temperature and precipitation are documented in Rauer Group and how did these changes interact with the glacial history?

- In what way does the climatic and environmental history of Rauer Group differ from reconstructions of other sites, as well within Prydz Bay region as within East Antarctica? And what mechanisms and feedback could explain these differences?

In order to address the questions stated above, a field campaign was carried out in austral summer 2006/07. Rauer Group was visited for about three weeks in March 2007, with logistical support provided by the Alfred-Wegener Institute (AWI) and the crew of RV Polarstern (cruise ANT XXIII/9). Beside the sediment cores, which have been investigated by the author, the field campaign focused on several other aspects to complete the picture of late Quaternary history of Rauer Group. Description and mapping of the geomorphology of the islands was carried out as well as sampling of erratics for exposure dating and levelling of lakes and sills for RSL reconstructions. Wagner et al. (2008) give a detailed compilation of the fieldwork and preliminary results.

In the following chapters the study area is introduced (Chapter 2) and a brief outline of the methods applied in this thesis is given (Chapter 3). Chapter 4.1 gives a list of the author's contribution to subchapters 4.2-4.6, which are stand-alone contributions, each of them dealing with different aspects of the glacial and climatic history of Rauer Group. Chapter 4.2 focuses on the geomorphology and glacial history of Rauer Group, while Chapters 4.3-4.6 discuss the late Quaternary environmental and climatic history of Rauer Group as it was reconstructed from sediment cores. A synthesis in Chapter 5 provides a concluding view on the outcome of this thesis and points out further issues.

2. Study Area

Rauer Group is an ice-free archipelago covering an area of about 300 km^2 in eastern Prydz Bay (77°54'E; 68°48'S; Figure 1.2). Rauer Group consists of several larger islands and numerous small ones and is bounded by the EAIS to the east and by the Sørsdal Glacier to the north (Figure 2.1A). The floating end of the Sørsdal Glacier divides Rauer Group from the Vestfold Hills 30 km to the north (Figure 2.1B). Where the ice sheet margin rests on land, it creates several peninsulas (Figure 2.1D). At the intercept of the ice sheet with the ocean the ice margin has developed as a cliff (Figure 2.1D). Outlet glaciers to the north (Sørsdal Glacier) and to the south (Browns and Chaos glaciers) of Rauer Group drain into Prydz Bay (Figure 1.3).
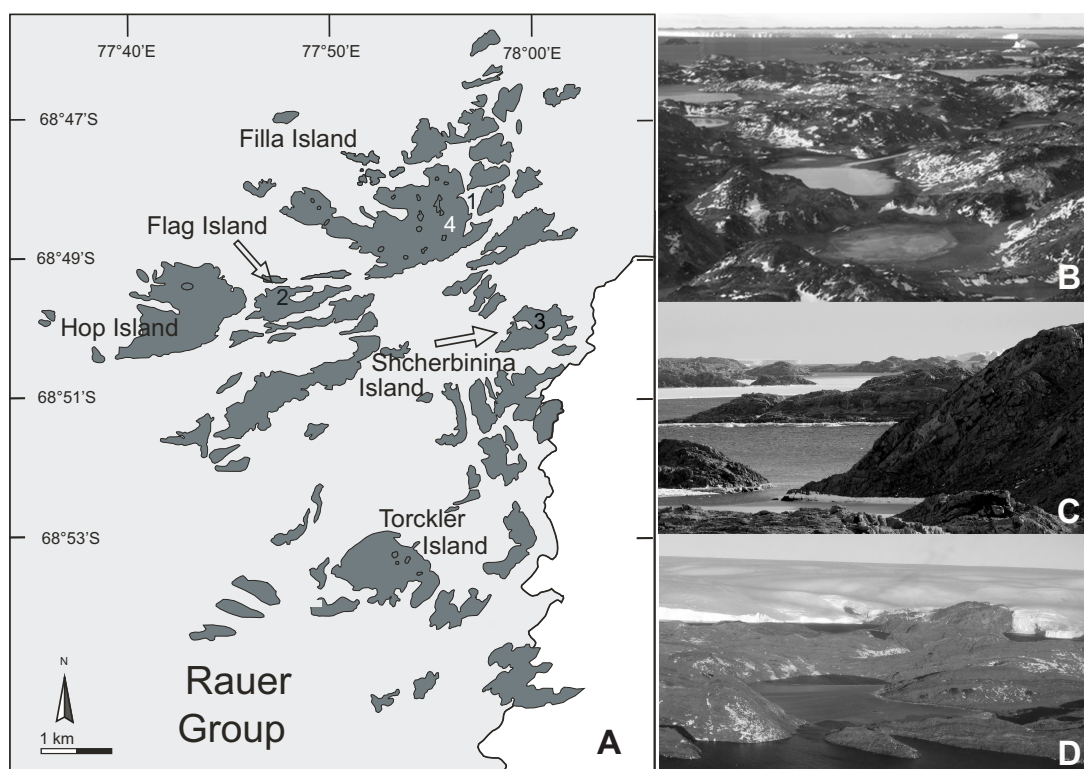
Figure 2.1 Map of Rauer Group, 1 Filla Island inlet, 2 Flag Island inlet, 3 Shcherbinina Island inlet, 4 Skua Lake A), Filla Island with lake basins, in the background floating ice tongue of Sørsdal Glacier and hilltops of Vestfold Hills; Photo by B. Wagner, 2007 B), View from Shcherbinina Island to the west C), Shcherbinina Island inlet and ice sheet margin in the background; Photo by B. Wagner, 2007 D).

2.1 Climate

Climate conditions in Rauer Group are affected by maritime as well as by continental influences. North-westerly oceanic winds provide moisture to the islands. Katabatic winds from the adjacent ice sheet, however, dominate and cause a relatively dry climate. No climate data from Rauer Group exist; however, temperature and precipitation are probably very similar to the nearby Vestfold Hills. A 53-year time series of temperature and precipitation was recorded at the Australian Davis Station, Vestfold Hills (Figure 1.3).

Mean monthly maximum temperatures at Davis Station exceed 0°C in the summer months (December and January). Minimum temperatures recorded during the observation period (1957-2009) are as low as -44°C in winter with mean minimum temperatures around -20°C in July and August (Figure 2.2).
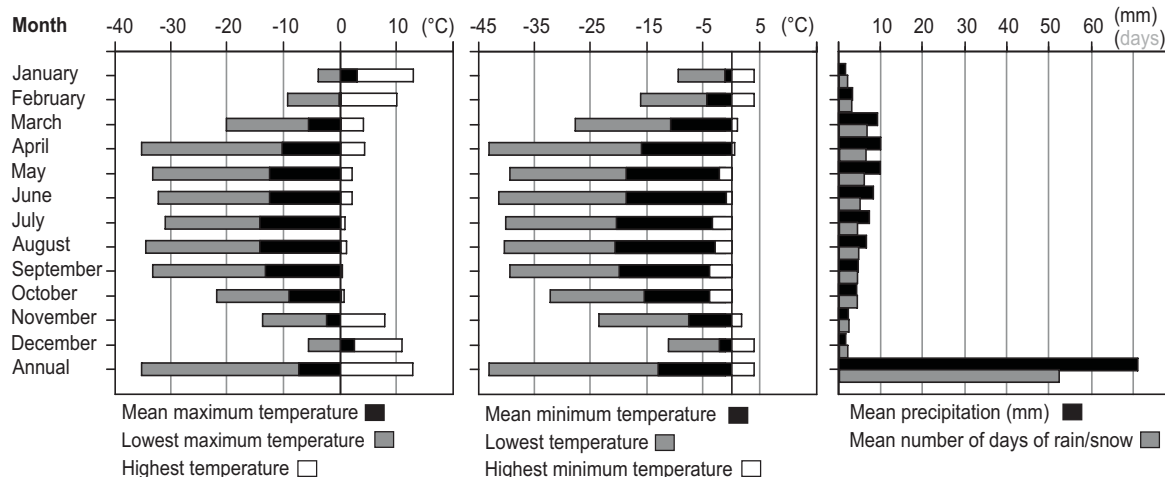
Figure 2.2 Temperature and precipitation recorded at Davis Station, Vestfold Hills; Observation period for temperature 1957-2009, and for precipitation 1960-2009; data from Australian Bureau of Meteorology (2010).

On the islands of Rauer Group, no permanent snowfields have been observed. Ablation and melting keep the islands snow-free in summer. During the field campaign, light snowfall occurred several times, but faded in the following days. Mean monthly precipitation recorded at Davis Station indicates snowfall throughout the year, with maximum precipitation in autumn and early winter (March-May; Figure 2.2). A low mean annual precipitation of 70.9 mm is given for Davis Station (Figure 2.2). The dry conditions in the area become more evident when the annual precipitation is compared to the annual evaporation of 928 mm which Bronge (1996) determined form the Druzhby drainage system in Vestfold Hills.

2.2 Biology

Due to the extreme conditions no soil formation is perceivable on the islands (Ganzert et al., 2008) but algae and bacterial mats can be found in littoral places of depressions that are temporally moist from melting snow. Some lichens sporadically colonize rock surfaces (Figure 2.3C). In rarely abundant brackish lakes, mosses have been observed (Wagner et al., 2008) and Hodgson et al. (2001b) describe colonization by benthic diatoms and cyanobacteria. Several bird species inhabit the islands: Snow petrels (*Pagodroma nivea*) and Wilson's storm petrel (*Oceanites oceanicus*) nest in rock caves (Norman and Ward, 1990) and Adèlie penguins (*Pygoscelis adeliae*) occupy rookeries to the north-west of Filla Island and on Hop Island (Bhikhardas et al., 1992). Antarctic petrel (*Thalassoica antarctica*), cape petrel (*Daption capense*), and the southern fulmar (*Fulmaris*

8

glacialoides) are abundant on several islands (Norman and Ward, 1990). During the field campaign, individuals of the south polar skua (*Catharacta maccormicki*; Figure 2.3B) have been observed, hunting for penguins in the interior of Filla Island. Seals and sea leopards visited Filla and Hop islands during the field campaign.

Figure 2.3 Adèlie penguins on Hop Island A), South polar skua B), Lichens on bedrock at Filla Island C), Snow petrel on Shcherbinina Island D); Photos by O. Bennike, 2007.

Diatoms are highly abundant in Antarctic coastal marine waters (McMinn et al., 2000). Since they contain preservable frustules, diatoms are a main contributor to the biogenic proportion of marine sediments and are a valuable proxy for paleoenvironmental reconstructions (e.g., McMinn et al., 2001; Cremer et al., 2003a).

2.3 Geology and geomorphology

The bedrock of the islands consists of an orthogneiss-dominated granulite terrain (Harley, 1998). The Archaean and Proterozoic rocks consist of felsic and mafic ortho- and paragneisses and metapelites. Several studies on the structure and metamorphism of the rocks of Rauer Group have been conducted in order to clarify their genesis and provenance in the context of plate tectonic reconstruction (e.g., Kinny et al., 1993; Harley et al., 1998; Kelsey et al., 2003; Wilson et al., 2007).

The islands have a smooth morphology with rounded hills and incised valleys (Figure 2.2B-D). The low-lying islands have mean elevations around 30-50 m above sea level (a.s.l) and barely exceed 100 m a.s.l. (Australian Antarctic Division, 2002). Physical

weathering is the main process for producing minerogenic detritus in the cold and dry conditions prevailing in coastal East Antarctica. Bedrock as well as overlying glacial sediment is strongly weathered at distances exceeding several hundred metres from the ice sheet margin. Surfaces show tafoni and honeycomb like weathering styles as well as iron staining and salt efflorescence. Unconsolidated sediments cover parts of the islands. Sediment is redistributed by wind documented by dunes of different sizes on the lee sides of hills and of single rocks as well as by stone pavements on wind-exposed sites (White et al., 2009). Moraine sediments of terrestrial origin are rare, yet erratics are distributed across all islands (White et al., 2009). Evidence for a higher than present relative sea-level comes from beach sediments up to 8.5 m above present high tide mark and a distinct fossil terrace and platform system at 6 m a.s.l. (White et al., 2009). On Filla Island, marine fossils in sediments from low-lying basins also point to a former transgression into the interior of the island (Wagner et al., 2008).

2.4 Lakes

One characteristic feature of Rauer Group is its shallow lakes and ephemeral ponds that occupy low-lying basins on several islands. On Filla Island 14 lakes were investigated during the field campaign in March 2007. Many of the lakes are hypersaline and salt encrusts lake bottoms and shorelines (Wagner et al., 2008). Some of the lakes were even completely desiccated. Hodgson et al. (2001b) proposed that the lakes of Rauer Group have evolved from trapped seawater, following post-glacial isostatic uplift. This mechanism has also been suggested for the formation of lakes in Vestfold and Bunger hills (Kaup et al., 1993; Hodgson et al., 2001b). Nevertheless, water chemistry data of the lakes of Rauer Group is distinct from other lakes of Prydz Bay region (Hodgson et al., 2001b). Sensitivity of the lakes towards precipitation is reflected by an increase in lake levels of several centimetres, which was observed after one day of snowfall (Wagner et al., 2008). In some lake basins watermarks above the present lake level indicate seasonal lake level fluctuations up to 20-30 cm (Wagner et al., 2008). It is worth mentioning that several lakes on Filla Island had much higher lake levels in late December 1997 (Hodgson et al., 2001b) than during our field campaign in March 2007. Furthermore, Hodgson et al. (2001b) cites earlier maps, where water bodies were even larger.

The deepest lake on Filla Island is Skua Lake (Figures 2.1A and 2.4). In the deep central part a water depth of 120 cm was determined. The littoral areas are as deep as 30 cm and their bottom is covered with red microbial mats (Figure 2.4C). Seasonal lake level fluctuations are very likely, since watermarks can be found 20-30 cm above the present lake level. Measurement of the water conductivity indicates brackish to saline conditions and ice of about 8.5 cm in thickness covered the lake in March 2007. The basin, in which the lake is located, is enclosed by higher elevations except for the southern side, where a connection to a valley system exists, which leads to the sea (Figure 2.4A). For determining

the precise elevation of the lake and the sills between the lake basin and the sea, levelling was carried out along a profile from the sea to Skua Lake (Wagner et al., 2008). The water surface of Skua Lake was determined to 9.5 m a.s.l. The threshold connecting the basin with the sea was determined to 11.5 m a.s.l. (Figure 2.4A).
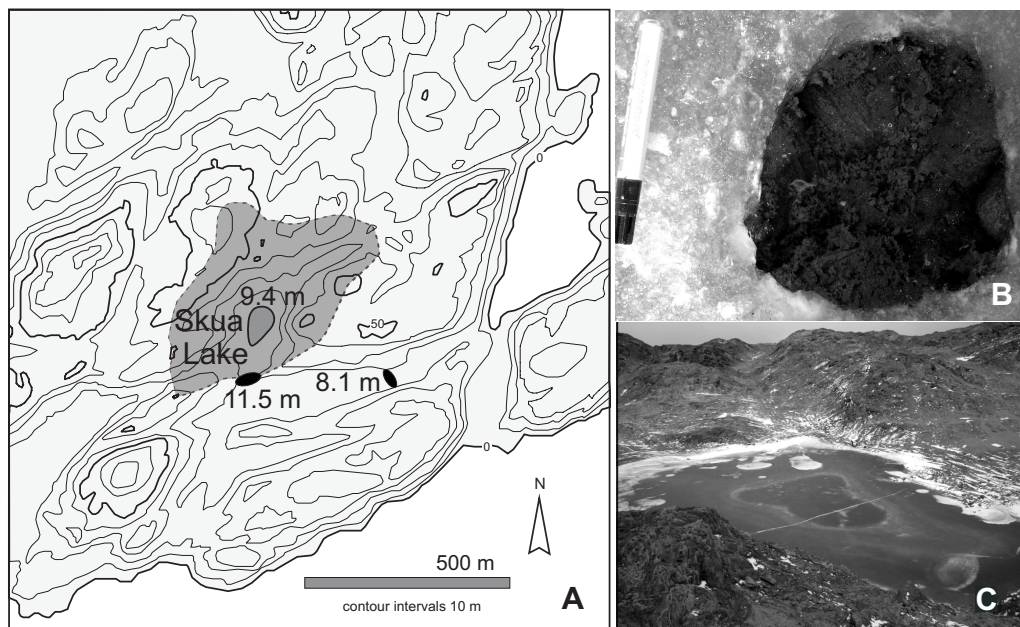
Figure 2.4 Map of the Skua Lake and surroundings, approximated catchment area shaded in dark grey, numbers indicate altitude of lake level above sea level (a.s.l.) in m, black ellipses indicate the sill heights in m a.s.l. A). Moss layer in the shallow littoral zone, picture taken through a hole in the ice B), Ice-covered Skua Lake; core Co1008 was taken in the deep central part of the lake C); Photos by S. Ortlepp, 2007.

2.5 Marine inlets

The relatively shallow marine inlets in Rauer Group can provide long and undisturbed sediment sequences. Sedimentation in this near shore marine environment is influenced by terrigenous input via aeolian, fluvial and ice rafting transport, as well as by autochthonous biogenic sedimentation (McMinn et al., 1998). High sedimentation rates in the marine inlets provide records with a high resolution for paleoenvironmental reconstructions. For this study, three marine inlets were selected, with different distances to the ice sheet margin (Figure 2.5, Table 2.1). All of them have subaquatic sills toward the open ocean, but they differ in size and water depth. The inlets will be refered to as Filla Island inlet, Flag Island inlet, and Shcherbinina Island inlet, unofficially named after the sourrounding island.

2.5.1 Filla Island inlet

The inlet is located at the eastern side of Filla Island, in a distance of c. 4 km to the present ice-sheet margin. It is surrounded by relatively steep slopes and has a water depth of 38 m at the coring location in the centre (Figure 2.5A). The depths of the sills that separate the basin from the open ocean have been determined to 12 m in the north and to 18 m in the

11

south. During the field campaign the inlet was covered by c. 1 m of sea ice in the centre, with decreasing thickness towards the sills. Hydrological parameters were determined at the coring location (Figure 2.6). Oxygen depletion in the lower metres of the water column was detected, indicating restricted water exchange between the inlet and the sea (Wagner et al., 2008).
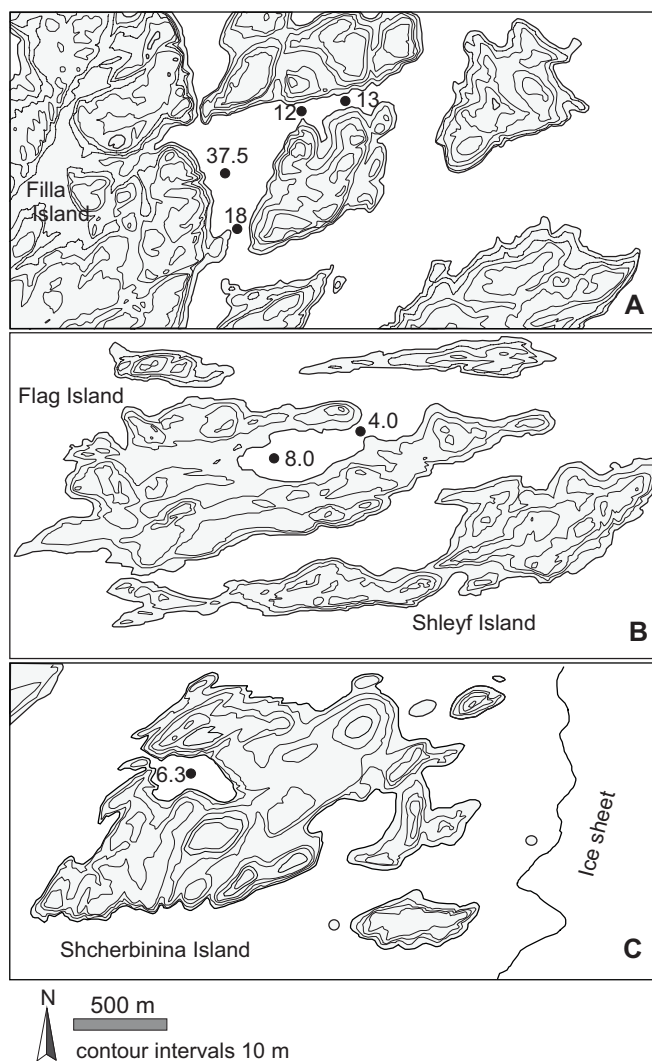
Figure 2.5 Topographic maps of the surroundings of Filla island inlet A), Flag Island inlet B) and Shcherbinina Island inlet C); Numbers indicate water depths (m) of subaquatic sills and at coring locations in the centres of the inlets; for position of the inlets see Figure 2.1.

2.5.2 Flag Island inlet

The Flag Island inlet is located at the north-eastern side of Flag Island, in a distance of c. 6 km to the ice sheet. A maximum water depth of 8 m at the coring location was determined. The depth of a subaquatic sill to the east of the inlet has a maximum depth of 4 m (Figure 2.5B). By the time of coring, the inlet was not covered by ice, however, by mid March sea ice formation increased.
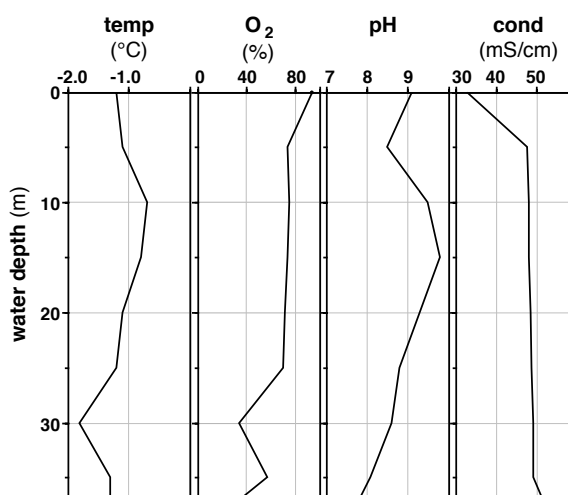
Figure 2.6 Hydrological profile of Filla Island inlet, Wagner et al. (2008).

2.5.3 Shcherbinina Island inlet

The Shcherbinina Island inlet is located at the western side of the island, c. 1.8 km away from the ice-sheet margin (Figures 2.1A and 2.5C). A water depth of 6.3 m was measured at the coring location in the centre of the inlet. A subaquatic sill between the inlet and the sea has a maximum depth of 2 m, with exposed rocks at low tide. The inlet was ice-free in the beginning of March and sea-ice formation advanced throughout the field campaign. The prevailing north-easterly wind enforced ice formation radiating from the western end of the inlet.

Table 2.1 Cored inlets of Rauer Group; locations are indicated in Figures 2.1 and 2.5.

Inlet	Core no.	Water depth coring site	Sill depth	Tidal range	Distance to ice sheet	Sea ice cover (March 2007)
Filla Island inlet	Co1010	38 m	12 and 18 m	< 0.5 m	4 km	1 m
Flag Island inlet	Co1011	7.8 m	4 m	< 1 m	6 km	No ice cover
Shcherbinina Island inlet	Co1014	6.3 m	2 m	< 1 m	1.8 km	No ice cover

3. Materials and Methods

3.1 Fieldwork

3.1.1 Lake coring

Sediment sequences from Skua Lake have been recovered with a 2 m long Eijkelkamp piston corer, operating from the ice cover of the lake. Levelling of the lake water surface and thresholds was conducted using a surveying instrument (Leica Corp.) and a staff of 5 m height. Measurements were performed along a profile starting at sea level at high tide level. For evaluation of limnological properties, conductivity and temperature measurement of the lake water was conducted with a WTW multi 197 probe (WTW Corp., Germany; Wagner et al., 2008).

3.1.2 Coring of marine inlets

Water depths of sills and coring locations was determined prior to coring. At the ice-covered Filla Island inlet holes were drilled in the ice and determination of water depth was conducted with echo sounder and rope, respectively. At the other two inlets, water depths were measured with echo sounder from a floating platform. Coring of the marine inlets was conducted with UWITEC piston corer device (UWITEC Corp., Austria), either operated from the ice cover or from a floating platform. Core sections of maximal 3 m in length have been recovered with a depth overlap of 1 m. A more detailed description of the coring technique is also given in Melles et al. (1994a). For sampling of undisturbed surface sediments, an UWITEC gravity corer (UWITEC Corp., Austria) was used, producing cores of 1.2 m maximum length. To avoid severe disturbance of the sediments during transport, two gravity cores (Co1010-4 and -15) were sub-sampled in 2 cm steps in the field. After core recovery all sediment cores were stored at 4 °C.

In Table A1 (see Appendix) all core sections are listed with coordinates of coring sites and the type of coring equipment used.

3.2 Laboratory work

If not stated otherwise, sample preparation and analyses were conducted in the laboratories of the Institute of Geology and Mineralogy at the University of Cologne (Germany), by S. Berg and student co-workers. Data collection of each parameter, which was applied in this thesis, will be described briefly. The analysis of biogenic silica and the application of X-ray fluorescence (XRF) analysis will be discussed more in detail, since these methods have been particularly considered in the course of this thesis.

3.2.1 Core description and sub-sampling

Sediment cores have been split in two halves, photographically documented, and described. Correlation of core sections was made on half cores based on core description, geochemical parameters and water content. To visualise textural features of the sediments high-resolution radiographies with an image width of 2 cm were made with the ITRAX XRF-core-scanner (Croudace et al., 2006). Sediment cores were sub-sampled in 2 cm (Co1010, Co1011, and Co1008) and 1 cm (Co1014) steps. Water content was determined for each sample from weight loss after freeze-drying. For further analyses, aliquots were ground to < 63 μm.

3.2.2 Carbon (C), nitrogen (N), sulphur (S)

Elemental analyses for total carbon (TC), total nitrogen (TN) and total sulphur (TS) was conducted with a Vario Micro Cube combustion elemental analyzer (VARIO Corp.). For core Co1010, total organic carbon (TOC) was quantified with a Leco CS-225 carbon-sulphur detector (LECO Corp.) from samples pre-treated with hydrochloric acid (HCl, 10%) to remove carbonate. Total inorganic carbon (TIC) is derived from the difference of C and TOC. For the other cores, TOC was quantified from the difference between C and total inorganic carbon (TIC), which were measured with a DIMATOC 200 (DIMATEC Corp.).

3.2.3 Biogenic silica (BSi)

Biogenic silica (BSi) refers to SiO_2, which is derived from organisms with siliceous skeletal elements like diatoms, silicoflagellates, radiolarians or siliceous sponges. For the quantification of BSi as a component of sediments, the separation of BSi and aluminous silicates derived from minerogenic material is required. In this study, the wet chemical extraction technique after DeMaster (1981) was applied in a slightly modified way. The extraction of BSi was made with 1 molar sodium hydroxide (NaOH). First 10-20 mg of ground sample was leached in 150 ml NaOH for 1.5 hours, keeping the temperature constantly at 85°C. In the meantime 12 sub-samples of 1 ml volume each have been taken in time intervals from 1 to 10 min. The detection of the dissolved silica ($Si_{(aq)}$) concentration was conducted photometrically (Photometer by SCALAR Corp.). For the photometric detection, the sample was acidified with sulphuric acid and mixed with ammonium molybdate solution. The reaction product molybdosilicic acid was then reduced by ascorbic acid to form a blue dye, which was finally measured at 810 nm.

The stepwise sampling produces sub-samples with increasing $Si_{(aq)}$ concentrations (Figure 3.1). Due to different dissolution rates of BSi compared to the non-biogenic compounds, the concentration increases rapidly in the first minutes, when BSi dissolves (Figure 3.1). Afterwards, dissolution progresses more slowly, when minerals are the only contributors to the increase in concentration (Figure 3.1).
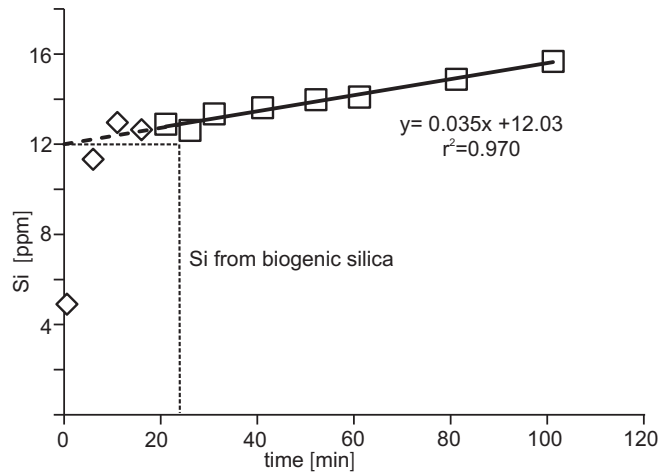
Figure 3.1 Time/concentration curve obtained from a sediment sample of core Co1014; Extrapolation of biogenic silica concentration in the alkaline solution is made from linear regression of the time dependent increase in concentration of the minerogenic fraction (squares).

In the evaluation, BSi is considered as the "background" concentration of silica in the solution. This value is determined by linear regression for the mineral dissolution line from the time/concentration diagram: the intercept with the concentration axes (Si(t0)) marks the concentration of BSi in the solution (Figure 3.1, DeMaster, 1981). From this value the content of BSi in the sample can be extrapolated by the following equation (1):

$$(1) \; SiO_2[wt\%] = \frac{Si_{(t0)}[ppm] * 0.001 * V_{(NaOH)}[ml]}{m_{(sample)}[mg]} * 100 * \frac{60.09}{28.09}$$

$Si_{(t0)}$: graphically determined interception of regression line with y-axes

V(NaOH)	volume NaOH (100 ml)
m (sample)	weight of sample (mg)
60.09/28.09	molar ratio of SiO_2/Si

With this method the SiO_2 component bound to biogenic silica structures is determined, which is not synonymous with the opal content of a sediment, since opal contains a proportion of chemically combined water within the molecular structure.

Several alternative methods have been employed to determine the biogenic silica content of sediments. Besides digestion with NaOH solution (DeMaster, 1981), a sodium carbonate (Na_2CO_3) solution can be utilised (Mortlock and Froelich, 1989) for alkaline digestion of silicates. Both methods are effectively dissolving the BSi components (Kamatani and Oku, 2000) but equally face the problem of a need for correction of aluminous silicate dissolution. Dissolution experiments by Kamatani and Oku (2000) indicate that a parallel measurement of dissolved aluminium offers another possibility for the determination of BSi contents. In addition to the wet chemical applications X-ray diffraction (Bareille et al., 1990) and infrared spectroscopy (Vogel et al., 2008) provide non-destructive methods for analysis of biogenic silica in sediments. An interlaboratory

comparison for the measurement of biogenic silica in sediments showed, however, that there are significant differences in the determined concentrations between methods and laboratories, especially when BSi concentration in the measured sample is low (Conley, 1998).

3.2.4 Oxygen isotopes of diatom silica

Prior to oxygen isotopic measurement samples have been cleaned to separate the diatoms from the minerogenic components of the sediment. A four-step cleaning procedure, following the method by Moreley et al. (2004), was applied to receive pure diatom samples. In the first step treatment with hydrogen peroxide (H_2O_2) and HCl removed organic matter and carbonates and dispersed the sediment. Secondly, the grain-size fraction 75-10 μm was separated for further processing by wet sieving. The final separation of diatoms from minerogenic particles was made by heavy liquid separation, with sodium polytungstate (PST). In a last step, the purified sample was washed over a 10 μm sieve with distilled water. Some of the dried samples were checked for contaminations under light microscope and scanning electron microscope (SEM). Diatom silica samples were analysed for d^{18}O at the NERC Isotope Geosciences Laboratory, British Geological Survey (UK) by Melanie J. Leng, using the stepped fluorination technique to extract oxygen isotopes described by Leng and Barker (2006) and Leng and Sloane (2008). The precision of the $\delta^{18}O_{diatom}$ technique is c. 0.3‰. The oxygen isotope results are expressed as 'd' values, representing deviations in per mille (‰) from VSMOW.

3.2.5 Diatoms

Diatom assemblages of 60 samples from cores Co1010 and Co1011 were specified. For the preparation of diatom slides, 0.5 g of freeze-dried sediment was treated with HCl (10%) to remove carbonates and with H_2O_2 to oxidise organic matter. Permanent slides have been made by the sedimentation tray method (Battarby et al., 1973) and embedded afterwards in high-refraction mountant Naphrax®. The analysis of diatom species was made with a Zeiss microscope with a 1000-fold magnification (Figure 3.2). For diatom analyses at least 300 individuals were counted from each sample. A detailed description of diatom sample preparation is given in Cremer et al. (2001). Preparation of slides, counting and identification of diatoms was made by Holger Cremer (TNO Built Environment and Geosciences, Utrecht, NL).

3.2.6 Salt content

For the determination of salts, 0.1 g of ground sample was leached in 10 ml deionised water for one hour and afterwards the salinity of the solution was measured with a WTW multi 197 probe (WTW Corp., Germany). The salt content is given as weight percent of dry sediments.
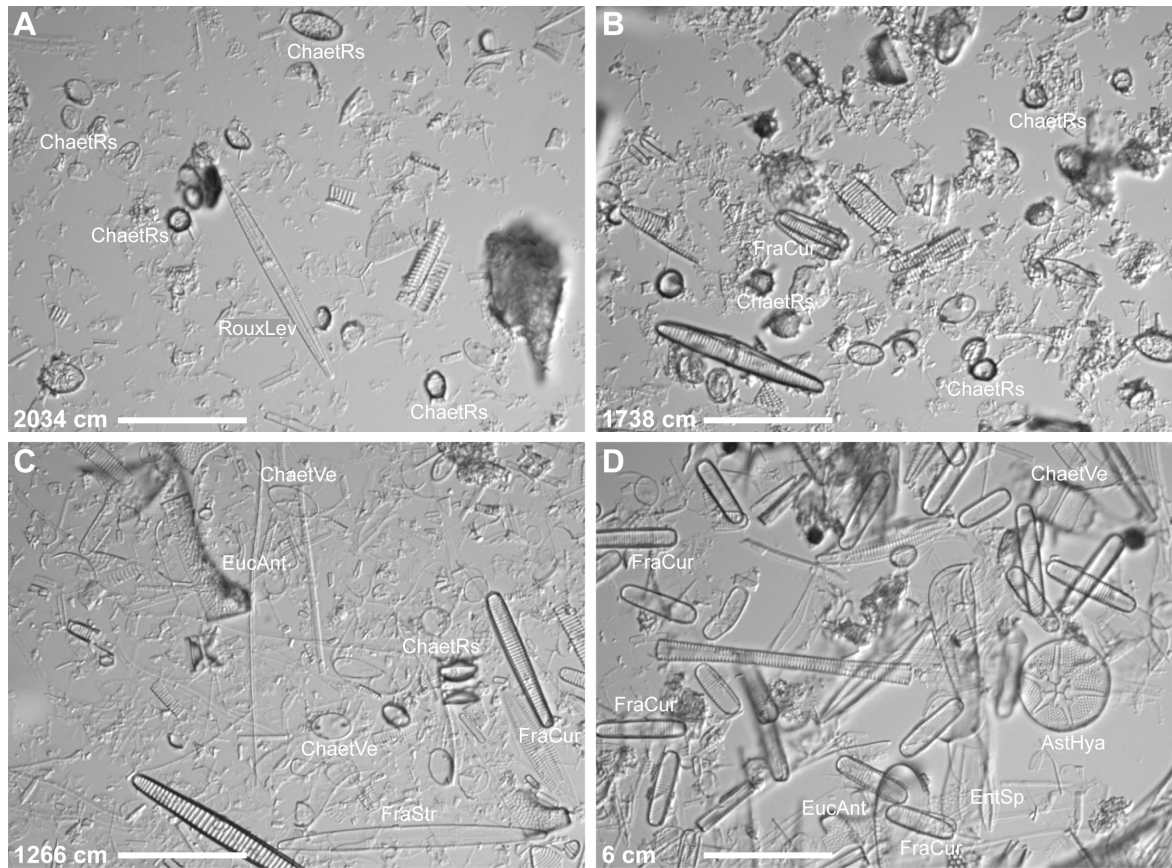
Figure 3.2 Light microscopic images of permanent diatom slides from different depths of core Co1010 A)-D); Abbreviations of the most significant taxa: AstHya *Asteromphalus hyalinus*; ChaetRs *Chaetoceros* resting stages; ChaetVe *Chaetoceros* vegetative stages; EucAnt *Eucampia antarctica*; FraStr *Fragilaria striatula*; FraCur *Fragilariopsis curta*; RouxLev *Rouxia leventerae*n; Scale bars 40 µm; Photos by H. Cremer, 2008.

3.2.7 Inorganic elemental analyses

Quantitative inorganic composition of sediments was determined by XRF spectrometry, with a wavelength dispersive sequential X-ray spectrometer (Philips PW2400) on fused discs. For the preparation of the fused disks ground sample material was oven dried at 105°C for four hours and then mixed with lithium tetraborate (1:6) and c. 0.5 g of NH_3NO_4. The mixture was then heated stepwise to 1000°C and fused to a glass disk. Elemental analysis was performed for 20 and 23 samples from cores Co1010 and Co1011, respectively.

For semi-quantitative analyses of the element composition, cores were analyzed by an ITRAX XRF core scanner (Cox Ltd.). The measurement was performed on split core halves with a molybdenum X-ray tube, set to 30 mA and 30 kV. Exposure time and resolution vary between the cores depending on sediment properties (Table 3.1). Prior to the measurement the sediment surface was flattened to provide an even surface. Furthermore, the sediment surface was covered with a 1.5 µm thick Ultrapolyester™ (Chemplex) foil, which is nearly transparent for X-rays, to prevent desiccation of the sediments during measurement and to protect the scanner device.

18

Table 3.1 Exposure times and step sizes applied for ITRAX XRF core scanner measurement.

Core	Exposure time	Step size
Co1010 (Filla Island inlet)	5 sec	1 mm
Co1011 (Flag Island inlet)	20 sec	2 mm
Co1014 (Shcherbinina Island inlet)	20 sec	2 mm
Co1008 (Skua Lake)	20 sec	2 mm

Excursus: Application of the ITRAX XRF core scanner; calibration and water correction

Inorganic elemental composition of sediments and the down-core variation of chemical properties can give valuable information about sedimentological and diagenetic processes, which have to be considered for paleoenvironmental reconstructions. The ITRAX XRF core scanner provides high-resolution data (down to 200 µm measuring intervals) of the elemental composition of sediments. It is constructed to analyse split sediment cores, what minimises the preparation effort and has the advantage of being non-destructive. The relatively fast measurement makes the scanning approach more time efficient than classical methods. Croudace et al. (2006) provide a detailed description of the instrument and the scanning procedure. The system is equipped with a Si-drift (SDD) EDXRF (energy dispersive) detector. The measured energy spectra are converted with Q-spec spectral analysis software to produce elemental intensities (Croudace et al., 2006). The fit of the modelled intensities to the measured spectra is optimised for each core, depending on the respective composition and physical properties of the sediments analyzed. Elemental intensities, expressed as counts per second (cps) or total counts (counts), are considered to be proportional to elemental concentrations. Scanner data is semi-quantitative since a calibration of elemental intensities into absolute concentrations is not possible straightforwardly (e.g., Tjallingii et al., 2007; Weltje and Tjallingii, 2008).

XRF data obtained from scanning whole sediment cores are affected by the physical properties of the sediment measured. Roughness and heterogeneity of the sampled surface as well as grain size can cause attenuation and scattering of XRF radiation. To provide a homogenous sample for XRF analysis particle size should not exceed 70 µm (Jansen et al., 1998). Therefore clay and silt sized sediments may provide more reliable results than sandy sediments (Jansen et al., 1998). Elements are not all affected to the same extent, since emission of XRF radiation differs in energy and wavelength for individual elements. Escape depth of XRF radiation emitted from a sediment sample depends on the respective element. Light elements like Al and Si have a escape depth of a few micrometres, whereas fluorescence emitted by Ca or Fe atoms originates from a depth of tenth to hundreds µm (Jansen et al., 1998). In wet sediments water is a main factor influencing the intensities of the detected XRF-radiation, since it is strongly absorbed when passing through the wet

material (e.g., Ge et al., 2005). Several approaches have been made to quantify the impact of water contents and physical properties (Ge et al., 2005) and to work out applicable correction methods (Tjallingii et al., 2007; Weltje and Tjallingi, 2008) for XRF measurements of original sediment samples.

The attenuation of the XRF-radiation theoretically follows an exponential function, when passing through a medium. The Beer-Lambert law quantifies the transmitted XRF-radiation, Transmission (T), dependent on the path length (x) radiation travelled through a medium: $T(x) = I_x/I_0 = e^{-(\alpha x)}$ (I_0 is the initial intensity of XRF-radiation, I_x is the residual intensity after passing through a medium, and α describes the mass attenuation coefficient, which is characteristic for each medium). The XRF analysis of a dry and homogenous sample is supposed to be not biased by differences in physical properties and water content between individual samples (Tjallingii et al., 2007), and therefore corresponds to I_0 of Beer-Lambert law. The ratio of the original wet intensity to the intensity of the dry sample is equivalent to I_x/I_0 of Beer-Lambert law and provides a measurement for the attenuation of XRF-radiation by the physical properties of the original, wet sample (Tjallingii et al., 2007). Tjallingii et al. (2007) use this relation for the determination of a function to correct scanner data of original wet sediments for water content and physical properties. In this way they achieve better down-core comparability of the data and improve the calibration of the scanner data into concentrations.

In the course of this thesis several experiments were made in order to evaluate the data set obtained from the ITRAX XRF core scanner. Our implementation of the methods proposed by Tjallingii et al. (2007) for water correction and calibration of semiquantitative, whole-sediments XRF data is described and discussed in the following sections.

Methods

Split halves of cores Co1010 and Co1011 have been scanned with the ITRAX XRF core scanner (see above). Conversion of raw XRF data into element intensities was made with the Q-spec software provided with the ITRAX system. To optimise the results of the modelled intensities conversion was fitted each core. The element intensities (counts) were averaged on 2 cm slices according to sub-samples used for non-whole core analyses and normalised to the exposure time (counts per second; cps). These original sediment samples will be referred to as "wet samples". Absolute element concentrations were determined by classical XRF from a total of 43 samples as described above.

Aliquots of 43 sub-samples were dried and pulverised (Co1010 n= 20; Co1011 n= 23). The powder was then packed into plastic slides and scanned according the alignment listed in Table 3.1. Values for each homogenised dried sample (dry sample) were averaged from valid data points and normalised to the exposure time (cps). Water content of the same

sub-samples was determined as stated above. Statistical data evaluation was performed with the programme Microsoft Excel.

Results and discussion

A complete description of the sediment cores Co1010 and Co1011 is given in chapter 4.4 Sediments are generally fine grained and have high water contents (65-95%) and high proportions of biogenic silica (20-45%). From the set of elements provided by the ITRAX XRF core scanner Si, Ti, Fe, and K will be discussed. The four elements are very different in their fluorescence properties as well as in their absolute abundance in the sediments considered in this study. Whereas SiO_2 makes up c. 42-47%, TiO_2 is present in concentrations of less than 0.5%. Mean elemental concentrations and down core variability are very similar in both cores with respect to the four elements (Table 3.2).

Table 3.2 Averaged concentrations of major elements (oxides and elements as weight percent of dry sediment) of Si, Ti, Fe, and K with standard deviations of cores Co1010 and Co1011; n indicates the number of samples.

core	SiO_2%	Si%	TiO_2%	Ti%	Fe_2O_3%	Fe%	K_2O%	K%
Co1010 (n=20)	47.2±8.5	22.05±3.99	0.40±0.18	0.24±0.11	3.29±1.45	2.30±1.04	1.23±0.31	0.88±0.22
Co1011 (n=23)	42.1±6.8	19.68±3.18	0.37±0.16	0.22±0.09	3.08±1.36	2.16±0.95	1.5±0.37	1.07±0.26
Detection limit[1]		*9000 ppm*		*60 ppm*		*25 ppm*		*150 ppm*

[1]Detection limit for ITRAX XRF core scanner for Mo tube (30 kV and 40 mA) and 100 sec exposure time (Croudace et al., 2006).

The sensitivity of the ITRAX XRF detection system was evaluated by Croudace et al. (2006) by measuring dry, pelletised briquettes of standard materials. Detection limits are very variable for the different elements (Table 3.2) and are expected to be significantly poorer in wet and organic-rich sediments and for exposure times less than 100 seconds (Croudace et al., 2006). Element intensities and corresponding concentrations are shown in scatter-plots in Figure 3.3. Correlation coefficients (r^2) of linear regressions are given for each core and element respectively (Table 3.3). Regression lines do not pass through the origin, a fact that was also noted by Weltje and Tjallingii (2008). This implies that a linear regression is not applicable outside the range of concentrations provided by the samples used for calibration. Probably a non-linear relation between concentration and intensity better describes the data, since inter element matrix effects do not take linear effect (Weltje and Tjallingii, 2008). When comparing the slopes of regression lines of a certain element for the two cores no parallelism is achieved, even if the concentration ranges are very similar. This probably results from the different setting files used for fitting element intensities to raw XRF spectra. A simple linear calibration of the scanner data has to be established for each core in particular, or data has to be normalised to achieve comparability. Scatter plots of dry samples versus concentrations correlate much better (Table 3.3), indicating that water content and sample heterogeneity have a significant influence on the measurement.
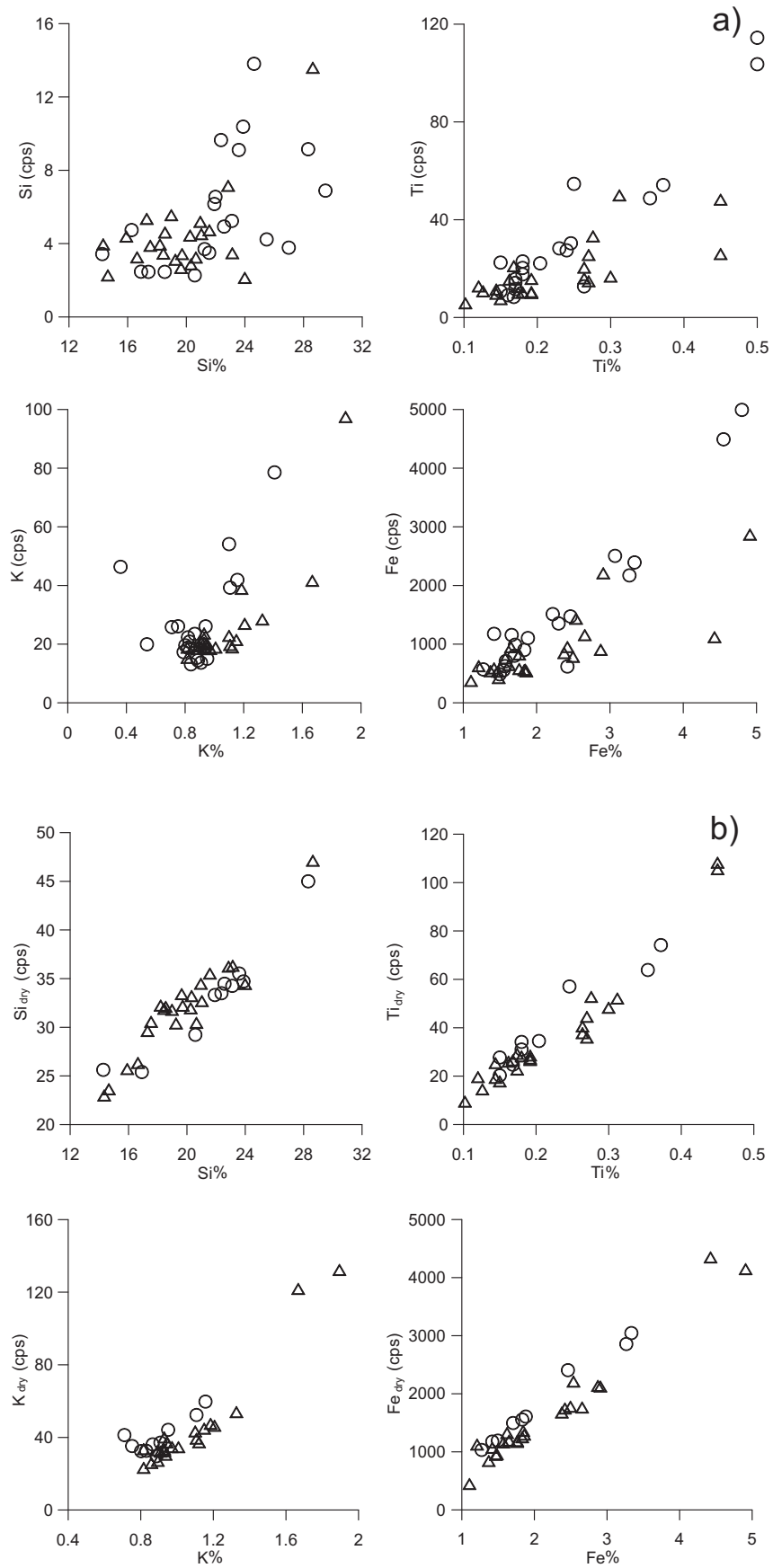
Figure 3.3 (previous page). Scatter plot of element intensities (cps) a) and element intensities (dry) b) from ITRAX core scanner vs. element concentrations from classical XRF for elements Ti, Si, K, and Fe. Plots show the results for cores Co1010 (circles) and Co1011 (triangles). Correlation coefficients (r^2) have been obtained from linear regressions for each element and each core and are listed in Table 3.3.

The dataset of core Co1010 for the evaluation of dry samples versus concentrations (Figure 3.3b) comprises a subset of data, since the values for both, dry sample and concentration, are only available for a total of 9 samples from core Co1010 (Table 3.3).

Although Si concentrations are high in all samples, a very low correlation of concentration versus wet samples is achieved. Low correlation coefficients in both cores probably indicate that the detection limit of Si in the water and organic rich sediments is above the concentrations provided by the samples, independently from the different exposure times (5 and 20 sec) for measurement. Correlation of concentration versus dry samples is much better pointing to lower absorption of XRF radiation in the dry material. Water content of the sediments is particularly influencing Si intensities, due to the low response depth of the XRF radiation and attenuation by the adhesive water film between the sediment surface and the cover foil (Tjallingii et al., 2007).

Results for K are different between the cores. While correlation of concentration versus wet sample is good for Co1011, data of Co1010 show significant scatter (Figure 3.3b, Table 3.3). Comparison of dry sample versus concentration only slightly improves the correlation for Co1010 and Co1011. This indicates that the K intensities of are probably affected by matrix effects as they have been described for Cl (Croudace et al., 2006) and are very likely in marine sediments with high Cl concentrations.

Table 3.3 Correlation coefficient r^2 for corresponding element pairs from conventional XRF and ITRAX XRF core scanner from Co1010 and Co1011 for wet and dry samples, respectively.

Element	Co1010 Filla Wet (n = 20)	Co1010 Filla Dry (n = 9)	Co1011 Flag Wet (n = 23)	Co1011 Flag Dry (n = 23)
Si	0.27	0.91	0.34	0.90
K	0.25	0.63	0.74	0.78
Ti	0.89	0.92	0.58	0.92
Fe	0.91	0.99	0.64	0.92

n gives number of samples, which are included in the calculation of r^2

A good correlation for Ti is achieved in core Co1010, while a much lower r^2 is achieved for the samples from Co1011, especially for the wet samples. Element intensities are significantly higher for Ti than for the lighter element Si, although the mean concentration is about an order of magnitude higher. Attenuation of XRF radiation from Ti is less influenced by water content of the sediment (Kido et al., 2006). A reason for the weaker correlation of the wet sample compared to the dry samples in core Co1011 probably originates from sample heterogeneity, since Ti is mainly associated with heavy minerals and biotite in the larger grain size fraction (Croudace et al., 2006).

Best correlations are achieved for Fe. Although Fe is mainly unaffected by water contents, inter-element effects are known with Ca (Böning et al., 2007), which might cause poorer correlation in carbonaceous sediments.

In order to estimate the water content of a sampled interval, Tjallingii et al. (2007) use Cl intensities measured by the XRF scanner. They assume that Cl intensities are proportional to the water content in marine sediments. However, in the marine sediments of cores Co1010 and Co1011 water content and Cl intensities are not proportional, pointing to down-core changes in pore water salinity. Therefore the water content was used directly to determine the effect of attenuation by water. The proposed exponential relation between the wet/dry ratio and the water content could not be observed for any of the elements studied (Figure 3.4). The range of water contents within the cores is rather small, probably limiting the effect.
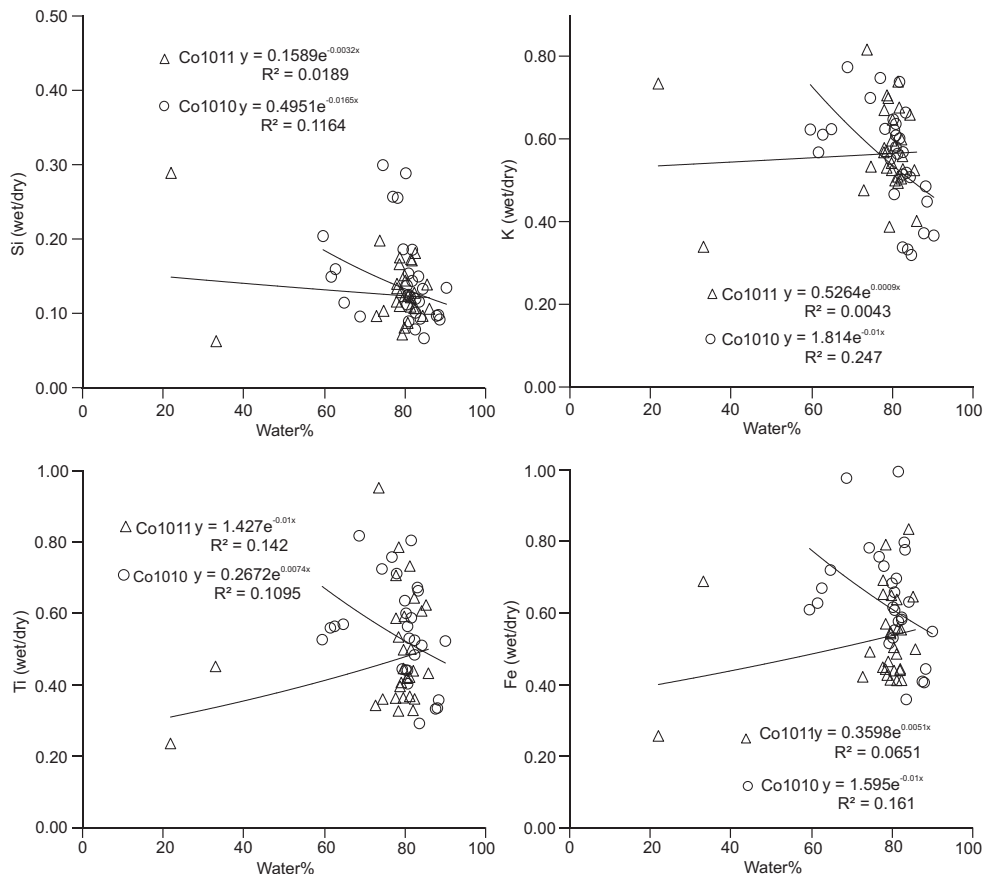
Figure 3.4 Ratio wet/dry intensities vs. water content for the elements Si, K, Ti and Fe. An exponential fit was calculated for data of cores Co1010 and Co1011, equation and correlation coefficient are given in each graph.

Two samples from core Co1011, however, with comparatively low water contents of c. 25% plot away from the other samples (Figure 3.4). Since these samples also differ from the others in their coarser grain size, in-homogeneities of the original sediment probably

have a more pronounced impact on the measurement than the water content. Due to the poor correlation of water content and the ratio of wet/dry intensities for all elements considered, a factor for the correction of the wet samples cannot be worked out in this way.

Conclusion and constraints

Comparison of ITRAX XRF scanner data to absolute concentrations indicate that element intensities are proportional to element concentrations. Element intensities provided by the ITRAX core scanner can be used to highlight relative changes in down core element concentration and composition. However, due to the very high water contents of the sediments investigated in this study a linear correlation of the scanner data to absolute concentrations is relatively low. Therefore a linear calibration of element intensities into concentrations was not made for the cores presented in this study. A correction for physical properties and water content based on the comparison of original wet samples with homogenised dry samples was inconclusive. Further studies should be carried out to better constrain the interaction between sediment properties and the XRF core scanner measurement.

3.2.8 Radiocarbon dating

Accelerator mass spectrometry (AMS) radiocarbon dating was applied to obtain chronologies of sediment sequences studied. One lake sediment sample was dated at the AMS facility of the Swiss Federal Institute of Technology (ETH) Zurich, Switzerland. The carbonate fraction (TIC) and total organic carbon (TOC) fraction were dated from this sample (ETH-38771, ETH-38772). All other radiocarbon ages were determined from bulk sediment samples at the AMS facility of the Leibniz Laboratory for Radiometric Dating and Isotope Research in Kiel, Germany. Dating of organic carbon in the sediments was performed on two separate fractions: the alkali residue or humic acid free fraction (HAF) and the humic acid fraction (HA). The extraction was performed with 1% NaOH to remove the humic acid fraction from the alkali residue (HAF). Acidification of the alkali extract with 1% HCl then precipitated the humic acid fraction (HA). Radiocarbon ages from the two separate fractions often differ significantly (Table A2 Appendix). In the marine diatomaceous oozes from Antarctica, the ^{14}C-dating of the HAF fraction of bulk sediment is considered to give reliable ages (e.g., Hillenbrand et al., 2009). Chronologies presented in this study are therefore mainly based on HAF ages. The HA fraction is more mobile and remobilization after deposition is more likely than for the HAF fraction.

The radiocarbon ages were converted into calendar years (cal yr BP) using the Calib 5.1 rev programme (Stuiver et al., 2005). Marine samples were calibrated with the Marine04 data set (Hughen et al., 2004) with a Southern Hemisphere offset of 362 years (Stuiver and Braziunas, 1993) and ΔR calculated from surface age of each core. Since Antarctic marine samples are subjected to a marine reservoir effect, which is usually higher than the global

average (Stuiver and Braziunas, 1993), a local reservoir effect was estimated from the uppermost dated sample of each core. Changes in the reservoir effect over time cannot be determined and therefore the modern reservoir effect is taken as constant over time. The SHCal data set (McCormac et al., 2004) was used for lacustrine/terrestrial samples. Radiocarbon ages older than the range of the Marine04 and SHCal calibration data sets have been calibrated with CalPal-2007 online (Danzeglocke et al., 2008) with the calibration data set CalPal2007Hulu (Weninger and Jöris, 2008). In the absence of a suitable model for a marine reservoir effect during the last glacial, no such correction has been applied.

A list of all radiocarbon ages and calibrated ages that have been obtained for this study is given in Table A2 in the appendix.

4. Rauer Group - Glacial and climatic history

4.1 Chapter contributions

Chapter 4.2 Geomorphology and glacial history of Rauer Group, East Antarctica

The text was written by Duanne White (Macquarie University, Sydney, AUS) with contributions of the co-authors Ole Bennike, Simon Harley, David Fink, Kevin Kiernan, Anne McConnell and Bernd Wagner. S. Berg assisted in the fieldwork and contributed to the discussion and interpretation of the results. S. Berg's contribution to chapter 4.2 is < 10%.

Chapter 4.3 Short Note: New marine core record from Rauer Group, East Antarctica

S. Berg participated in the field campaign and assisted in core recovery. She conducted the analytical work at the Institute of Geology and Mineralogy, University of Cologne, except for the preparation and analysis of diatom samples, which was conducted by Holger Cremer. Evaluation and interpretation of data as well as writing of the text was mainly conducted by S. Berg, with contributing discussions by B.Wagner, O. Bennike, H. Cremer, D. White, and Martin Melles. S. Berg's overall contribution to Chapter 4.3 is > 80%.

Chapter 4.4 Late Quaternary environmental and climatic history of Rauer Group, East Antarctica

S. Berg participated in the field campaign and assisted in core recovery. S. Berg and student co-workers conducted the analytical work at the Institute of Geology and Mineralogy, University of Cologne, except for oxygen isotope measurement, which was conducted by Melanie Leng and preparation and analysis of diatom samples, which was conducted by H. Cremer. Evaluation and interpretation of data as well as writing of the text was mainly conducted by S. Berg, with contributing discussion by B. Wagner, H. Cremer, M. Leng, and M. Melles. S. Berg's overall contribution to Chapter 4.4 is > 90%.

Chapter 4.5 No significant ice sheet expansion beyond present ice margins during the past 4500 yr at Rauer Group, East Antarctica

S. Berg participated in the field campaign and assisted in core recovery. S. Berg and student co-workers conducted the analytical work at the Institute of Geology and Mineralogy, University of Cologne. Evaluation and interpretation of data was mainly conducted by S. Berg, with contributing discussion by B. Wagner, D. White and M. Melles. The text was written by S. Berg with minor contribution of B. Wagner, D. White, and M. Melles. S. Berg's overall contribution to Chapter 4.5 is > 90%.

Chapter 4.6 Late Pleistocene configuration of the East Antarctic Ice Sheet - evidence from coastal ice-free areas

S. Berg participated in the field campaign and assisted in core recovery. O. Bennike collected and described the sediment samples from the unnamed lake and of recent marine mud. S. Berg conducted the analytical work, made the evaluation and interpretation of data and wrote the text.

4.2 Geomorphology and glacial history of Rauer Group, East Antarctica

Abstract

The presence of glacial sediments across the Rauer Group indicates that the East Antarctic ice sheet formerly covered the entire archipelago and has since retreated at least 15 km from its maximum extent. The degree of weathering of these glacial sediments suggests that ice retreat from this maximum position occurred sometime during the latter half of the last glacial cycle. Following this phase of retreat, the ice sheet margin has not expanded more than c. 1 km seaward of its present position. This pattern of ice sheet change matches that recorded in Vestfold Hills, providing further evidence that the diminutive Marine Isotope Stage 2 ice sheet advance in the nearby Larsemann Hills may have been influenced by local factors rather than a regional ice-sheet response to climate and sea-level change.

4.2.1. Introduction

A detailed paleoenvironmental reconstruction during the recent geological past is a precondition for a thorough understanding of ice sheet stability during future climate changes. Paleoenvironmental investigations in oases and other currently ice-free coastal areas of Antarctica form a crucial link between investigations of ice cores from adjacent ice sheets and sediment cores from the Southern Ocean. From the oases, detailed information can be obtained on the past long-term natural variability of the local ice sheet extension (e.g., Fabel et al., 1997), ice sheet altitude (e.g., Mackintosh et al., 2007), climate (e.g., Kulbe et al., 2001), and relative sea level (e.g., Zwartz et al., 1998; Hodgson et al., 2001a; Verleyen et al., 2005).

Dating of the timing and extent of the last deglaciation, and the subsequent relative sea-level changes has been completed at a number of widely separated sites scattered around East Antarctica. Results from these studies indicate that in some areas, the ice sheet has retreated by as little as c. 5 km since c. 20 ka (Hodgson et al., 2001a; Verleyen et al., 2005; Gore et al., 2001), while in others it was grounded out to the middle (Fabel et al., 1997; Domack et al., 1998; Zwartz et al., 1998) or near the edge (Harris and O'Brien 1998; Leventer et al., 2006) of the continental shelf prior to 10 ka. Since the results from each of these studies constrain the position of the ice sheet on only limited portions of the East Antarctic coast, it is difficult to determine which of these quite disparate reconstructions are regionally applicable, and which have been strongly affected by local glaciological conditions.
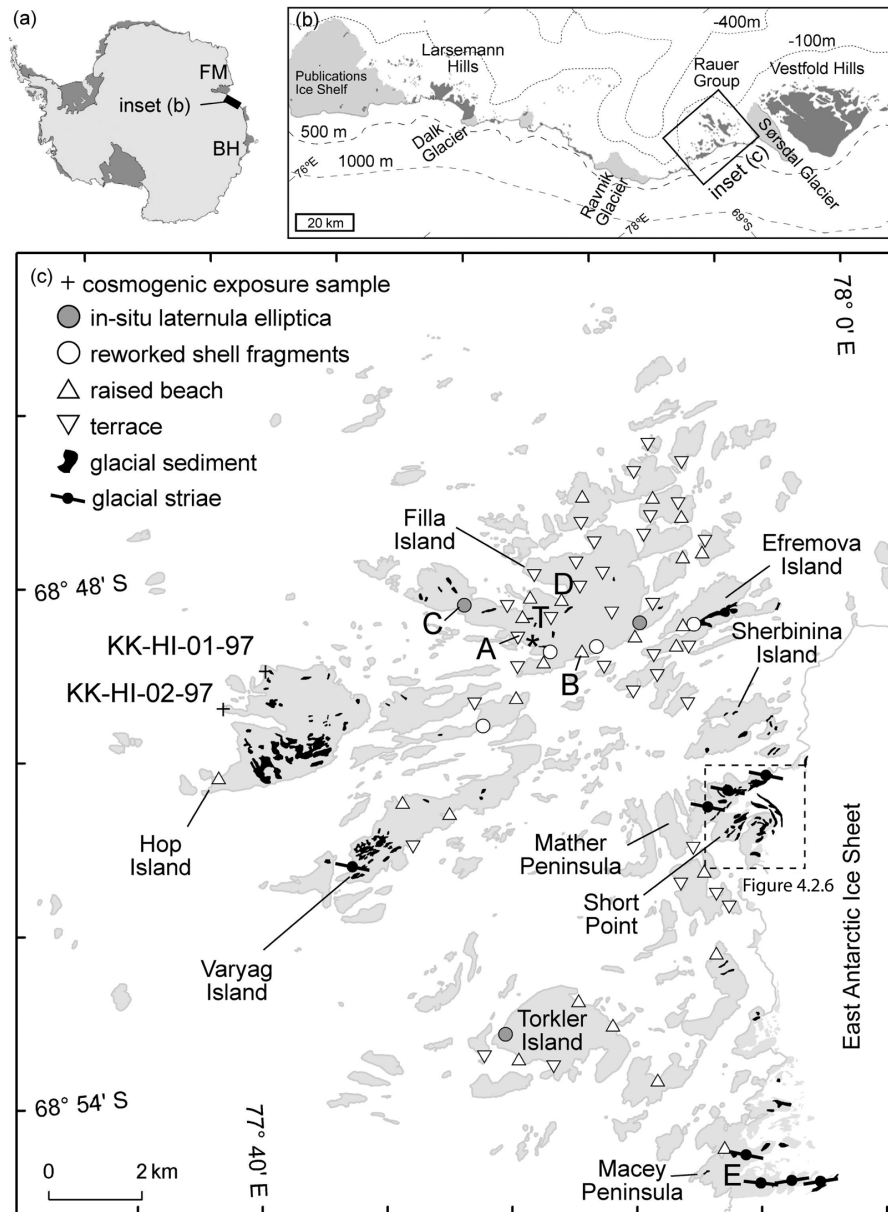
Figure 4.2.1 Map of Antarctica, with the position of the study region in eastern Prydz Bay indicated by the black rectangle. FM Framnes Mountains, BH Bunger Hills (a). Map of eastern Prydz Bay indicating the position of the Rauer Group (b). Map of the Rauer Group, where letters A-E indicate the location of photos in Figure 4.2.2, and T indicates the weakly defined terrace-beach system at c. 30 m a.s.l. that presumably formed during the presence of an ice-marginal lake (c).

The south-eastern margin of Prydz Bay (Figure 4.2.1) provides one of few regions on the East Antarctic coast where enough outcrop is exposed that a detailed regional picture of ice-sheet change can be reconstructed. The two well-studied sites in this area provide quite different ice-sheet reconstructions, as there is strong evidence for a relatively minor advance at Larsemann Hills during MIS 2 (e.g., Hodgson et al., 2001a), while the ice sheet likely overran and extended by c. 30-40 km offshore from Vestfold Hills during this time (Zwartz et al., 1998). The Rauer Group is a collection of over 400 islands and peninsulas located between Vestfold Hills and Larsemann Hills and provides a good site to determine which of the extant reconstructions best reflects the history of the ice sheet in this region during the late Quaternary. In this study, we identify the relative age of glacial deposits in

30

the Rauer Group to reconstruct the spatial extent of the ice sheet during former ice advances. Where possible, we also determine the timing of these events and determine if these advances are comparable to the magnitude and timing of ice-sheet retreat in Vestfold or Larsemann Hills.

4.2.2 Study area

The Rauer Group is a coastal archipelago of ice-free islands, skerries and peninsulas which cover an area of c. 300 km². The topography is characterised by low, rounded hills with a maximum altitude of 137 m a.s.l. The Precambrian gneiss bedrock is partly overlain by Quaternary glacial, marine, and aeolian sediments (Harley, 1987). Modern-day climate records do not exist fromRauer Group, but the climate is broadly similar to that recorded at Davis Station, 30 km to the north, where monthly mean temperatures range from 0.5 to -18°C (Streten, 1986) and precipitation averages 72 mm/yr water equivalent (Australian Bureau of Meteorology, 2007). Snowfall occurs throughout the year, but ablation keeps the islands essentially snowfree in summer.

Previous investigations of the geomorphology and Quaternary sediments of Rauer Group are limited. Adamson and Pickard (1986a and b) indicate the overall geomorphology is similar to that in the nearby Vestfold Hills, Pickard (1986) noted the presence of abundant aeolian deposits, and Yevteyev (1962) and Hodgson et al. (2001b) noted the presence of raised deposits with marine shells a few meters above sea level.

4.2.3 Methods

The islands in the northern part of the archipelago and the two major peninsulas (Mather and Macey) were investigated and mapped during land-based traverses undertaken during a 3-week field campaign between 25 February and 16 March 2007, with a traverse spacing of 0.5 to 1 km. The majority of the observations in the southern section were conducted from boat and helicopter. These data are supported by observations collected by SLH during investigations of the bedrock geology of the region since 1980, and field observations by KK and AM during a brief visit to Hop Island in January 1997. A map of the glacial deposits was created from field observations and the aid of vertical aerial photographs from 1980 and 1998, and oblique images from 1947 and 1959. The map is displayed in Figure 4.2.1, and the ArcGIS shapefiles used to create this image are also available from the Australian Antarctic Data Centre at the Australian Antarctic Division. The former ice extent was reconstructed by evaluating the distribution and character of erratics, glacial diamicts, and smallscale glacial bedforms such as striae, grooves, and chattermarks. The marine highstand was determined from raised beaches, marine terraces, wave-cut platforms and muddy sediments with *in situ* shells of *Laternula elliptica*. The altitude of lake sills and marine terraces was measured from above the modern high tide mark using an automatic level (Leica Corp.) and staff, or where close to the seashore, a

measuring tape and clinometer accurate to 0.2 degrees. Elevations determined using these two techniques are accurate to within 0.5 vertical meters.

The weathering characteristics of glacial sediments deposited above the marine limit were mapped using the Moriwaki index (Moriwaki et al., 1994), and Schmidt Hammer rebounds (e.g., Shakesby et al., 2006) to constrain the extent and relative timing of former glacial advances. Previous workers (e.g., Moriwaki et al., 1994; Augustinus, 2002) have used the original version of the Moriwaki index, whereby the largest 100 clasts on the surface of a 10x10 m quadrangle are individually assigned a Degree of Weathering (DW) value, according to the following scheme:

DW_0: a fresh clast

DW_1: a stained clast without cavernous weathering, ventifact and crumbling

DW_2: a stained, cavernously weathered and/or wind-faceted, not crumbled clast

DW_3: a distinctly stained and somewhat crumbled clast

DW_4: a strongly stained and crumbled clast

The Moriwaki Degree of Weathering (MDoW) is then assigned to each deposit using the following formula: **MDoW = N0 · 0 + N1 · 1 + N2 · 2 + N3 · 3 + N4 · 4**, where N_x is equal to the number of DW_X clasts in each count. In this study, we used a slightly modified version of the technique whereby the proportion of clasts in each weathering category was visually estimated, allowing a much more rapid assessment of the degree of weathering at each site. At each site, all boulders greater than 30 cm diameter, within a 20-m radius, were included, resulting in an assessment of at least 50 (but more commonly 100-200) boulders at each site. Previous work comparing these methods in the Prince Charles Mountains (White, 2007) indicates that this method produces MDoW values within 15-20% of those derived by counting individual boulders, with no obvious bias. This discrepancy is less than the variance found between sites recorded on synchronously deposited moraines using the original method (e.g., Augustinus, 2002), which is likely caused by local variations in the weathering rate. It is also significantly less than the variation between the three weathering zones identified in this study. Thus, we used the modified version in this study as the potential reduction in precision was justified by the increased number of sites measurable in the limited time available. This enabled us to better map out broad-scale variations in weathering across the study region, and lessened the impact of local variations in the weathering rate in our results. A single Schmidt Hammer rebound measurement was carried out on each of the 30 largest boulders present at each site, using a Proceq N-34 hammer in a vertical position. Rebounds were not collected if boulders > 25 cm in size were absent, and rebounds were only performed on flat faces away from edges, fractures or hollows that can cause anomalous results (e.g., Katz et al., 2000). Boulders with well-developed wind polish were avoided due the

potential for this feature to misleadingly raise the rebound value of weathered rocks (White, 2007). Boulders with exotic lithologies (e.g., iron formations or quartz veins) were avoided, but as many of the sites visited contained few suitable boulders, all four types of Precambrian granulite facies gneiss exposed as bedrock (and found as erratics) across the hills were used. Fortunately, factors known to affect hardness, such as grain size, texture and mineral composition, are broadly similar (Harley, 1988), and differences in average rebound values for these four gneisses are small, especially when compared to the variation between sites (Table 4.2.1).

Table 4.2.1 Schmidt Hammer rebound values from boulders with different lithologies on top of a highly weathered, former glacimarine deposit near the apple on Filla Island, 77.832º E; 68.819º S.

Lithology	mean	2σ
Felsic Gneiss	27.9	3.3
Quartz Gneiss	26.7	3.1
Orthogneiss	28.1	2.7
Garnet Gneiss	27.2	3.4

N = 30 for each lithology, 2s = standard error, at 2σ confidence level

Also, we noted the abundance of each of these gneiss types at the Schmidt hammer measurement sites (Table 4.2.2), which was broadly similar across the study area. Thus, the trends in rock hardness reduction due to weathering reported in this paper are robust. The effect of different styles of weathering and different weathering regimes on these data was estimated by recording whether characteristic markers of different weathering styles, namely whether surface features including tafoni, elongated pits, halite accumulations, glacial polish, striae, Fe staining, patterned ground, frost shattered debris, wind polish, sand accumulations and crumbled rock were absent, present or abundant at each site. The rate of weathering on Hop Island is constrained by the analysis of *in situ* produced cosmogenic [10]Be concentrations in two bedrock samples (Figure 4.2.1).

These samples were processed for [10]Be following standard procedures (Child et al., 2000), and Accelerator Mass Spectrometry (AMS) measurements were carried out at the ANTARES AMS Facility at ANSTO, Australia, using methods described previously (Fink et al., 2004; Fink and Smith, 2007). Sample thickness was restricted in all cases to < 5 cm surface slices. Measured [10]Be/[9]Be ratios were corrected by full chemistry procedural blanks with ratios of $< 10 \times 10^{-15}$, and background corrections amounted to < 5%. Independent repeat sample measurements (n=3) were combined as weighted means with the larger of the total statistical error or mean standard error. Final analytical error in concentrations (atom/g-quartz) are derived from a quadrature sum of the standard mean error in an AMS ratio, 2% for AMS standard reproducibility, 1% in Be spike assay and quartz mass.

Table 4.2.2 Weathering site details.

Locality	DT	Lat. °S	Long. °E	Alt. [m]	km to ice s.	Schmidt rebound[2]	MDoW	Lithology				
								Q	F	M	G	O
Macey Pen.	G	68.9214	77.9696	60	0.1	34.8±2.6	15	5	75	15	5	0
Macey Pen.	G	68.9200	77.9621	80	0.1	38.1±3.0	100	2	80	5	10	3
Macey Pen.	G	68.9215	77.9457	90	0.3	26.9±3.8	200	5	70	10	15	0
Macey Pen.	G	68.9147	77.9209	70	0.4	26.7±3.6	180	-	-	-	-	-
Macey Pen.	G	68.9199	77.9027	20	1.6	*	370	*	*	*	*	*
Macey Pen.	G	68.9162	77.9259	75	1.7	-	260	10	65	10	10	5
Mather Pen.	G	68.8453	77.9385	20	0.1	39.8±2.4	35	0	60	30	5	5
Mather Pen.	G	68.8489	77.9384	10	0.1	36.0±2.8	70	3	70	20	5	2
Mather Pen.	G	68.8486	77.9371	50	0.1	34.8±3.6	50	2	70	25	2	1
Mather Pen.	G	68.8443	77.9424	40	0.2	30.0±3.0	150	-	-	-	-	-
Mather Pen.	G	68.8475	77.9331	30	0.3	31.1±3.0	195	2	50	20	28	0
Mather Pen.	G	68.8452	77.9334	40	0.4	26.5±3.0	280	15	55	20	5	5
Mather Pen.	G	68.8488	77.9231	58	0.7	-	235	15	65	18	10	2
Mather Pen.	G	68.8508	77.9156	90	1.2	18.7±3.4	270	10	60	10	20	0
Mather Pen.	G	68.8544	77.8954	25	1.5	-	320	30	60	10	0	0
Shcherbinina	G	68.8300	77.9276	30	1.9	26.0±3.0	330	20	59	20	1	0
Shcherbinina	G	68.8333	77.9513	39	0.6	24.4±3.2	280	10	50	15	20	5
Efremova I.	G	68.8113	77.9339	40	2.6	27.0±2.8	360	40	40	10	10	0
Roadblock[1] I.	G	68.8220	77.8908	30	3.2	25.1±3.0	320	10	40	10	40	0
Filla Island	G	68.8089	77.8985	46	3.7	26.0±3.2	280	73	20	5	2	0
Sierra[1] Island	G	68.7981	77.9055	50	3.8	*	350	30	50	10	10	0
Romeo[1] Island	G	68.8021	77.9048	40	4.1	*	370	*	*	*	*	*
Filla Island	B	68.8169	77.8606	10	4.6	*	180	10	50	18	0	22
Mistake[1] I.	G	68.8316	77.8184	45	5.1	-	300	20	50	20	10	0
Filla Island	G	68.8041	77.8711	40	5.4	21.9±3.4	310	10	50	39	1	0
Filla Island	G	68.8129	77.8616	30	5.4	30.3±4.0	310	45	30	20	5	0
Echo[1] Island	G	68.7903	77.8955	27	5.4	*	340	10	60	10	20	0
Filla Island	Gm	68.8153	77.8498	15	5.4	35.5±3.2	250	10	50	20	20	0
Filla Island	G	68.8152	77.8335	70	5.8	*	350	20	40	20	20	0
Slon Island	G	68.7825	77.8951	30	6.1	*	350	30	60	5	5	0
Filla Island	G	68.8146	77.8161	35	6.3	*	320	-	-	-	-	-
Filla Island	Gm	68.8191	77.8317	10	6.6	23.4±2.6	320	-	-	-	-	-
Shleyf Island	G	68.8281	77.8068	35	6.7	26.6±3.8	300	10	60	10	10	10
Filla Island	G	68.8023	77.8313	45	7.1	27.3±14	360	40	40	20	0	0
Filla Island	Gm	68.8127	77.8308	8	7.4	30.7±3.0	300	-	-	-	-	-
Slon Island	G	68.7914	77.8600	30	7.4	*	350	40	30	20	10	0
Flag Island	Gm	68.8279	77.7595	10	7.4	30.3±3.0	260	-	-	-	-	-
Filla Island	G	68.8084	77.8045	25	8.0	24.8±3.2	320	10	60	20	10	0
Shleyf Island	G	68.8323	77.7741	30	8.5	29.0±3.4	320	40	40	10	10	0
Filla Island	G	68.8066	77.7783	42	9.3	25.7±3.8	300	30	40	20	10	0
Flag Island	G	68.8251	77.7552	20	9.4	26.0±3.6	320	20	40	20	10	10
Hop Island	G	68.8294	77.7137	40	9.5	26.4±3.0	280	20	50	20	10	0
Hop Island	Gm	68.8211	77.7094	10	10.6	-	280	30	30	20	5	15
Hop Island	G	68.8196	77.6884	32	10.7	27.6±3.2	280	0	40	20	20	20

DT deposit type (G Glacial deposit. Gm diamict below marine limit. B raised beach). *not enough boulders >30 cm diameter at site to conduct test (30 for Schmidt Hammer, 20 for lithology). - no data. Spatial coordinates are referenced to WGS 84 datum. MDoW Moriwaki Degree of Weathering (see text for definition). Q Quartz rich gneiss, F Felsic gneiss, M Mafic gneiss, G Garnet rich gneiss, O other. Schmidt rebound values are presented as the mean and standard error (95% confidence) of 30 measurements. [1]Unofficial name, [2]of erratics.

Absolute [10]Be concentrations are obtained following normalisation of AMS [10]Be ratios to the NIST standard reference materials, SRM-4325. We assign a [10]Be/[9]Be value of $30,200 \times 10^{-15}$ for SRM-4325 based on recalibrating the NIST certified value upwards by the ratio of 1.127, which is equivalent to the ratio of the NIST [10]Be half-life (1.34 Ma) to that commonly in use (1.51 Ma; see Fink and Smith, 2007 for further details). To ensure self-consistency with the above procedure, all AMS-derived [10]Be concentrations are converted to exposure ages using a [10]Be half-life of 1.51 Ma. The exposure age calculations presented in Table 4.2.3 are based on the scaling algorithms defined for Antarctic air pressures and temperatures with high-latitude sea-level production rates (Stone, 2000) of 5.1±0.3 atom/g-quartz/yr for [10]Be (a value calibrated to AMS standards that were referenced to a 1.5 Ma [10]Be half-life).

Table 4.2.3 Cosmogenic [10]Be exposure sample details.

Sample name	[10]Be conc. atoms/g-quarz x10[6]	Altitude [m]	Latitude (°S)	Production rate [at/g/yr]	Maximum erosion rate [mm/ka]
KK-HI-01-97	0.534±0.036	30	68.5	5.253	5.2
KK-HI-02-97	0.644±0.097	45	68.5	5.335	4.3

Samples were collected from sites with minimal shielding.

4.2.4 Results

4.2.4.1 Geomorphology and sedimentology

The summit heights of the islands and hills are largely controlled by their lithology. Areas of orthogneiss (Harley, 1987) form the highest summits and plateaus, with elevations above 100 m a.s.l., particularly when close to the ice sheet. Regions composed of layered gneiss generally have lower summits, with elevations of 30-50 m being common. The less resistant paragneisses is almost exclusively found in the valleys between the summits. Most of the islands with summits above 10 m a.s.l. have a roche moutonnée form consistent with significant modification by an overriding ice sheet. Erratics are found on all of the large, and most of the small, islands including the most distal island visited, c. 15 km from the present ice edge. Accumulations of diamict, in the form of small debris drapes in saddles or high basins, are scattered across the archipelago. There are two distinct, roughly N-S trending, zones where diamict accumulations are particularly common (Figure 4.2.1c). Firstly, relatively unweathered moraines, diamict sheets and glacio-fluvial debris are common within c. 1 km from the ice sheet, with well preserved ice-margin parallel moraine ridges present at Mather Peninsula. The second zone, which is found on the western portions of Hop, Varyag and Filla islands, is generally composed of degraded patches of diamict, with occasional N-S oriented debris ridges on Hop Island.

A distinct terrace and platform system similar in form to those near Watts Lake in the Vestfold Hills (Pickard et al., 1986) is developed in bedrock at c. 6 m a.s.l. in many places around the Rauer Group (Figure 4.2.1c), especially on Filla Island (Figure 4.2.2a).

Hodgson et al., (2001b) identified these terraces in closed lake basins that have their bases a few meters above sea level. We observed that these terraces are also relatively common on the coastline surrounding the islands, indicating that they were formed at a paleo-seashore rather than at a raised lake margin. In many places the terrace-platform system is accompanied by a distinct change in the form of bedrock weathering. Above the terrace height, the bedrock displays tafoni and other concave forms, while below this height bedrock incuts occur along joints and weak lithologies, and are more convex in form. Deposits of moderately sorted, angular to subangular pebbles with a sandy matrix are present on many places across the islands. These are identical to deposits formed in modern beach environments (Figure 4.2.2b), and former beaches in the Vestfold Hills (Blandford, 1975; Adamson and Pickard, 1986a; Gore et al., 1996) and are thus interpreted as raised littoral deposits that were formed along marine shorelines. These deposits are common in many of the bays adjacent to the terraced headlands and rock walls, and are particularly well-developed near where the terraces are formed. They are preserved up to 8.5 m above the modern high tide mark, although the decimeter- to meter-scale morphology of these beaches is better preserved within a few meters of the modern high tide level, suggesting an increase in age with altitude. Raised sea-ice pressure ridges were observed 1-2 m above the present high tide mark on southwest Filla Island. Muddy sediments, sometimes containing *in situ* or reworked *Laternula elliptica* shells are also present below the 8.5-m level (Figure 4.2.2c) but are restricted to protected sites. Other, less well-developed or preserved terraces and platforms are also found, including a moderately well-defined system at c. 14 m a.s.l., which is best developed on Filla Island and southern Efremova Island. There is also a very weakly developed terrace in a small basin at c. 30 m a.s.l. on western Filla Island (Figure 4.2.1c), coincident in altitude with some nearby sediment units with similar morphology, texture and geomorphic position to modern and raised beach deposits. However, these are isolated features and not well preserved. V-shaped valleys filled with cobble-rich, subrounded to rounded diamict lead away from the lower sills of this basin, suggesting that the terrace and the littoral units may have been formed by an ice-marginal lake when the ice sheet was more advanced, rather than a former sea-level highstand.

Well-sorted accumulations of aeolian sand (and in some places gravel) reaching up to 12 m in height are common in the lee of bedrock obstacles or downwind of narrow gaps in valleys (Figure 4.2.2d). These accumulations were particularly large and abundant on the downwind side of the islands, and also downwind of former marine basins. Ventifacts and other wind-polished clasts are also present in the sediment-filled valleys upwind of these deposits. Downwind of shell-rich former marine sediments, these deposits commonly contain reworked shell fragments.
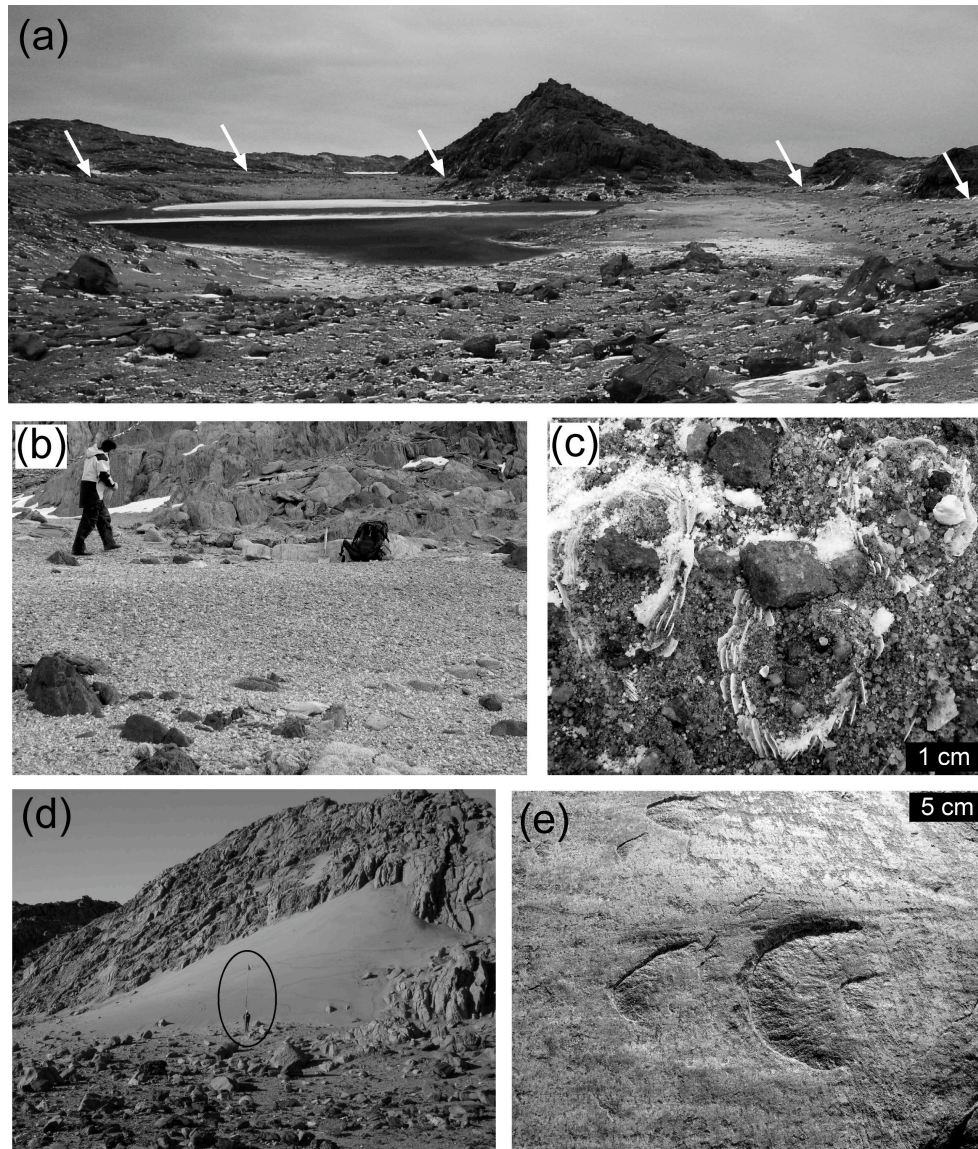
Figure 4.2.2 Geomorphology of the Rauer Group. Littoral terrace on eastern Filla Island, indicated by white arrows (a). Raised beach ridge on southern Filla Island c. 3 m a.s.l. at c. 0.5 m a.s.l. (b). *Laternula elliptica* **in growth position in marine sediment, northwest Filla Island (c). Large sand accumulation in lee of bluff on central Filla Island (d). Chattermarks and striae on summit on Macey Peninsula (e).**

4.2.4.2 Weathering and relative chronology of glacial deposits

Three distinct weathering zones were differentiated, based on general observations of glacial deposits in the field. The separation of these zones is also supported by clustering of measurements of erratic weathering when the Moriwaki index values are plotted against Schmidt Hammer rebound values (Figure 4.2.3).

The "least weathered" glacial deposits are within 200 m of the modern ice sheet margin (Figure 4.2.4) on Macey and Mather peninsulas. Boulders in these deposits have relatively little iron staining, rarely display tafoni development, and are largely intact, often retaining their glacial polish and coarser striae. Moriwaki index values are low (15-100) and average Schmidt Hammer rebounds relatively high (36-41). Moraines associated with these deposits are steep-sided (c. 34°) and have a sharp crest. Some of these moraines are ice-

cored, with only 20-50 cm of debris cover. Studies of aerial photographs from 1947 and field observations over the past 24 yr indicate that some of the debris in this weathering zone classification near Short Point have been released from the ice sheet since 1980 (Figure 4.2.5).
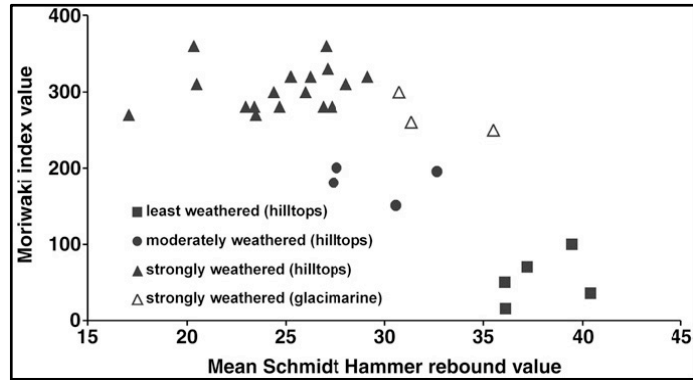
Figure 4.2.3 Schmidt Hammer rebound vs. Moriwaki Index results.

Next are a group of "moderately weathered" moraines and erratics within 0.5 km of the ice margin, again only observed on Macey and Mather peninsulas. Boulders on these deposits are moderately iron-stained and have a limited degree of crumbling. Tafoni cells are present in some boulders but rarely greater than 10 cm in diameter. Moriwaki index values for these deposits range between 150-200 and average Schmidt Hammer rebound values from 27-33. Moraines associated with these deposits have likely lost the majority of their former ice core and are flatter than the less weathered deposits, with moraine sides on Mather Peninsula sloping at c. 14°.
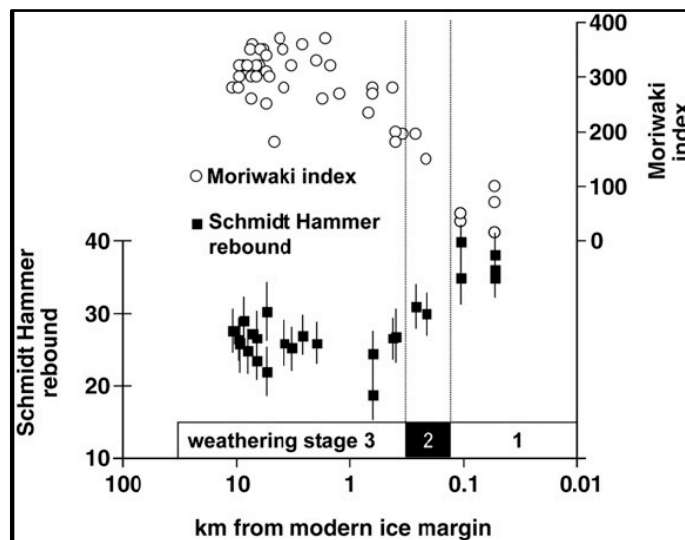
Figure 4.2.4 Weathering indices vs. distance from the modern ice margin. Note the lightly weathered deposits (high Schmidt Hammer rebound, low Moriwaki Index values) close to the ice sheet.

Lastly, "strongly weathered" diamict and erratics are present on the remainder of the islands and peninsulas. Distinct moraines are rare, but four moraines measured on Hop Island had moraine sides sloping at 5-16°, spanning that of the moderately weathered moraines. Large boulders on the surface of these deposits usually display extensive tafoni

or wind faceting, while the surfaces of the cobble-sized clasts are typically crumbly. Boulders with mafic lithologies have a moderate degree of iron staining. Moriwaki index values within this area range from 235 to 370, generally increasing toward the windward (northeast) side of the islands, corresponding with a reduction in the abundance of erratics and diamict. Mean Schmidt Hammer rebound values are 17-29, with lower (more weathered) values in the northeast sector. Importantly, the distinction between the three diamict and erratic weathering zones was quite clear. No erratics with a degree of weathering corresponding to that of the "least weathered" or "moderately weathered" deposits were found in areas of "strongly weathered" diamict and erratics (i.e., more than c. 0.5 km from the ice sheet).
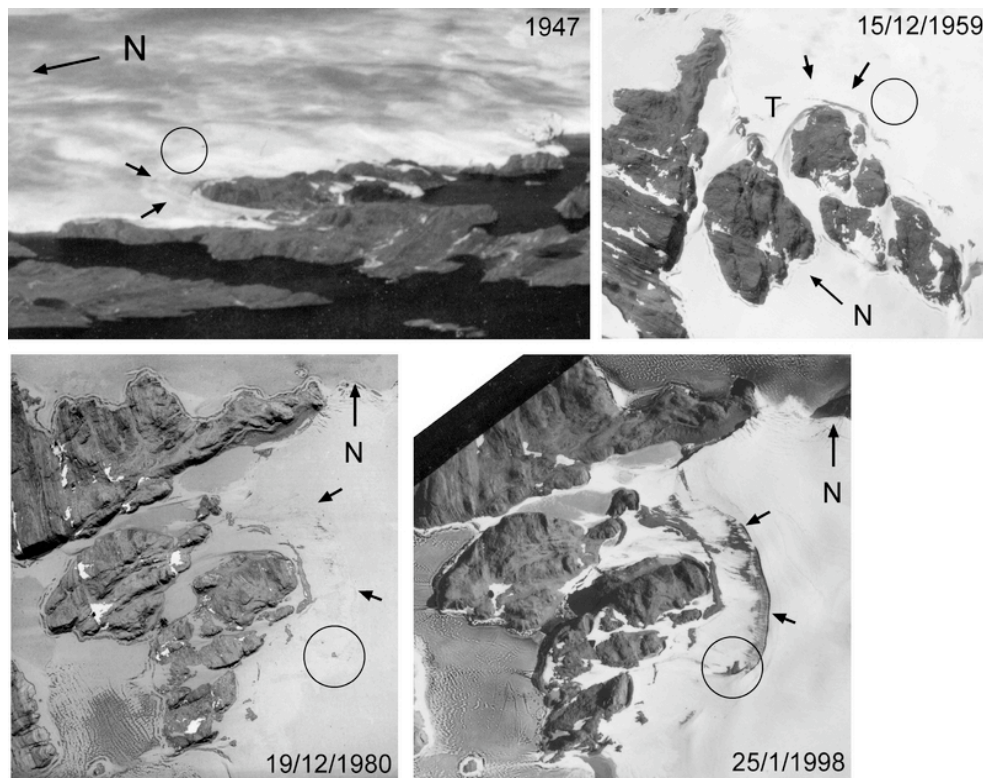
Figure 4.2.5 Changes in the ice sheet margin near Mather Peninsula. See Figure 4.2.1c for location. Prior to 1980, the only debris present on the ice surface was a single, linear, ice-margin parallel debris covered ridge close to the ice edge. By 1980 the upper (iceward) moraine lines (arrowed) became exposed, and had become a very visible feature by 1998. This corresponds with the emergence of a small nunatak from the ice sheet (circled). Also, the 'tongue' or frontal lobe where the ice gradient shows a marked change and sweeps into the area between Short Point and Mather Peninsula was covered in firn in 1980 and negotiable by walking in 1992, with no moraine exposed. The lobe area is now mostly exposed moraine (ice cored), and the wind scours which were formerly floored by ice are now flooded by water.

There were a few rare "strongly weathered" erratics mixed up with the "least weathered" and "moderately weathered" deposits, suggesting that the ice sheet may have overridden and recycled some of the strongly weathered debris during later advances. In the areas covered by the two younger sets of erratics, the degree of bedrock weathering was fairly limited, and in many places striae and glacial polish were preserved. However, the transition between these zones in the bedrock was not as well defined as for the erratics. In

the area covered by the strongly weathered diamict, the degree of bedrock weathering was dependant on the abundance of marine salts. On eastern Macey Peninsula and southern Mather Peninsula (Figure 4.2.6), where no source of marine salt was present directly upwind, most of the bedrock surface in these areas was strongly Fe-stained and crumbled, tafoni were present, grus was found in joints and non-marine salt efflorescences were found on bedrock and glacial boulders.
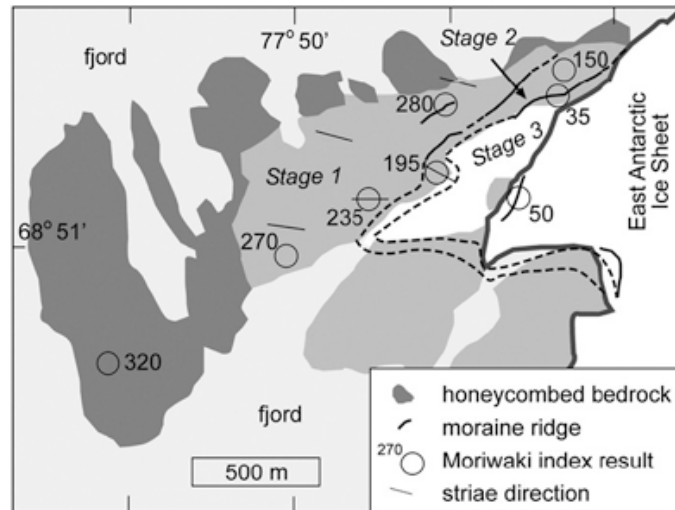
Figure 4.2.6 Weathering, moraines and striae directions on Mather Peninsula. Stage 3: "lightly weathered" glacial deposits, Stage 2: "moderately weathered" deposits, Stage 1: "highly weathered" deposits. Note that the areas of honeycomb weathering of bedrock are all downwind of marine salt sources.

However, patches of bedrock in this zone preserved glacial grooves, striae and polish, and the differential weathering was limited to c. 10 cm and honeycomb forms were largely absent. In areas covered by strongly weathered diamict, but downwind of a marine salt source, bedrock was strongly crumbled and large tafoni and honeycomb forms (Figure 4.2.7a) were very common. With the exception of a small occurrence on the western end of Varyag Island (where E-W-oriented striae are preserved), no striae or glacial polish were observed on bedrock. Marine salts such as halite (from taste) and gypsum (from crystal morphology) were present in almost all of the many small basins, but salt efflorescences were rarely found on bedrock or boulder surfaces in this area. Surface height variations between resistant (e.g., quartz veins, pegmatite dykes, felsic gneiss bands) and weak (e.g., pelites, ultramafic dykes and mafic gneiss bands) lithologies of up to 2 m were present across small lateral distances (c. 1-10 m, Figure 4.2.7b), although height variations of 30 cm to 1 m were more common. Differential weathering was less frequent in areas with relatively homogenous orthogneiss, but dykes and quartz veins in these areas were observed to protrude up to half a meter from the surrounding orthogneiss, although thin, fragile quartz veins were generally limited to < 10 cm in height (Figure 4.2.7c). Schmidt Hammer rebound values from erratics and bedrock at any one site generally agree within 20% (Figure 4.2.8), although there are two sites from the very outer limit of the smallest, least-weathered advance where fresh erratics were found on weathered bedrock,

presumably due to thin, cold-based ice at the ice margin. This suggests that in most places, either the ice that overrode the hills was erosive enough to remove any pre-existing weathered bedrock, or perhaps more likely that subsequent subaerial weathering and erosion of the bedrock and erratics has proceeded to a degree sufficient to mask prior weathering.
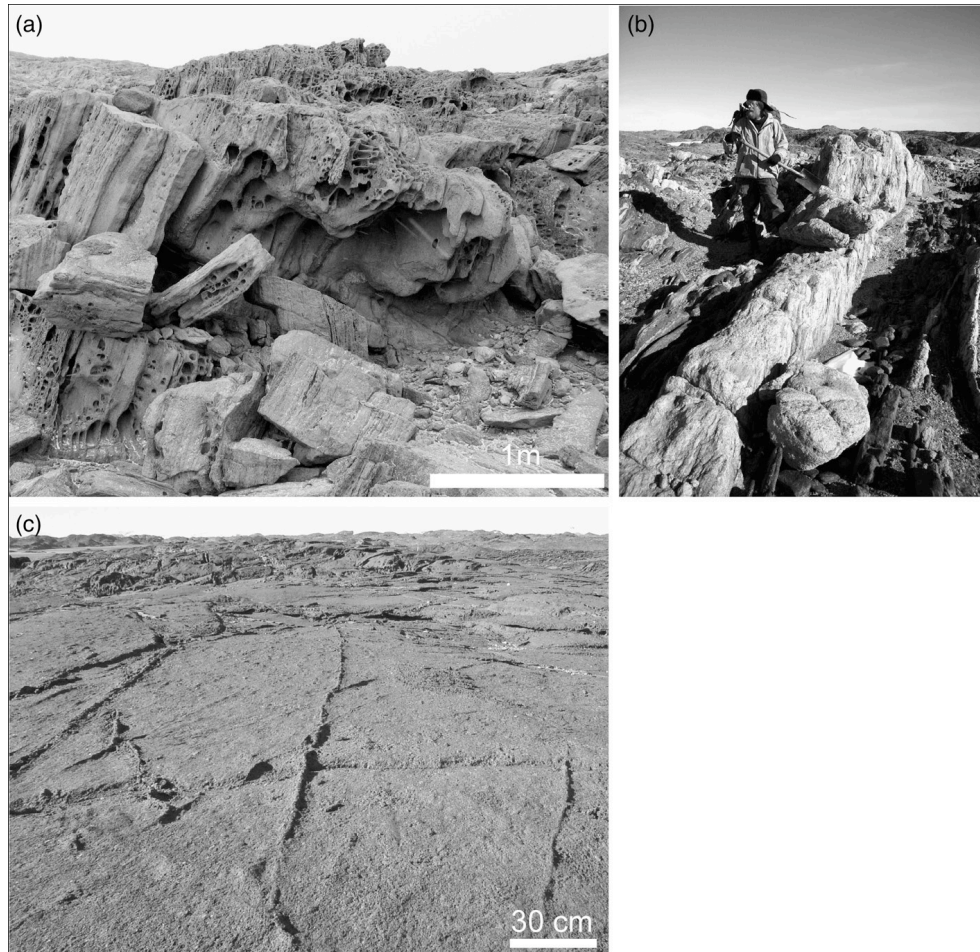
Figure 4.2.7 Honeycomb and tafoni forms on banded gneiss on western Mather Peninsula (a). Differential weathering of banded gneiss on an unnamed island directly west of Filla Island (b). Raised quartz veins produced by granular disintegration of the surrounding orthogneiss on Hop Island (c).

The two cosmogenic [10]Be samples from bedrock on Hop Island have apparent ages of 104 and 124 ka (Table 4.2.3). However, in most places in Antarctica where the exposure age of glacial erratics has been dated using cosmogenic isotopes, the ice sheet has not been erosive enough to remove weathering rinds formed prior to the last period of ice cover (e.g., Mackintosh et al., 2007). In other areas, such as the Vestfold Hills (Zwartz, 1995), northern Mt. Stinear in the Prince Charles Mountains (White, 2007) and Marie Byrd Land (Sugden et al., 2005), glacial erosion has removed evidence of subaerial weathering but has not been vigorous enough to reset the cosmogenic isotope concentration of the bedrock surface. Unless the Rauer Group was covered by unusually erosive ice during the last glaciation, it is unlikely that these surface [10]Be concentrations are solely controlled by (and thus can be used to calculate) the amount of time since the ice sheet retreated from these

sites. Instead, the [10]Be isotope concentration is likely affected by a combination of the subaerial erosion rate, the subglacial erosion rate (while ice-cored) and the timespan over which the sites have been covered by ice or subject to subaerial weathering. However, as [10]Be can only accumulate during periods when the site is ice-free, subaerial erosion will always limit the maximum [10]Be concentration that the rock surface can attain.
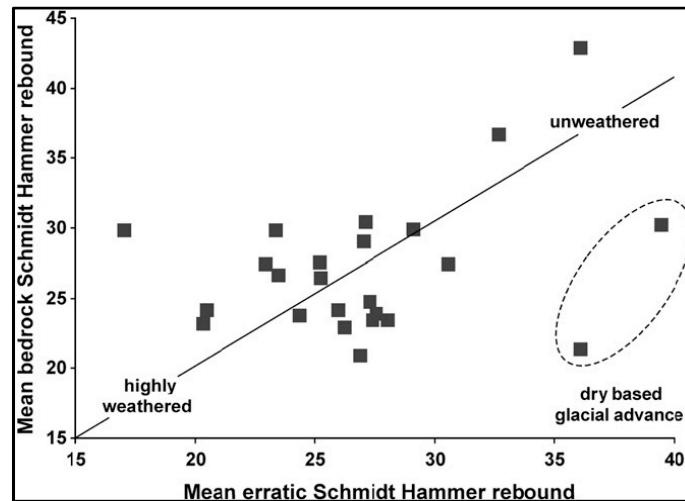
Figure 4.2.8 Mean bedrock vs. erratic Schmidt Hammer rebound values. Note the general coincidence of these two results at each site, with the exception of two sites near to the modern ice margin where fresh erratics sit on weathered bedrock (dashed ellipse), indicating a small cold-based glacial readvance. The diagonal line represents a 1:1 relationship, which would be expected if (a) both bedrock and erratic surfaces were stripped of weathered materials during glaciation, and (b) weathering rates for bedrock and erratics are similar.

This has the important implication that no matter what inheritance scenario is assumed, the rock surface [10]Be concentration will always be limited by subaerial erosion, so the rock surface [10]Be concentration can be used to constrain the subaerial erosion rate. Whether the erosion rate calculated from the [10]Be concentration reflects the actual subaerial erosion rate is dependant on if the exposure and/or glacial erosion history of the site can be constrained, as subglacial erosion or radioactive decay during periods of ice cover can also reduce the rock surface [10]Be concentration, and increase the apparent erosion rate deduced from the [10]Be measurement. If, as is the case for the samples in this study, these latter factors cannot be ruled out then the erosion rates calculated from the [10]Be concentration can only be used to calculate an upper limit on the subaerial erosion rate. For the two Hop Island samples the calculated maximum subaerial erosion rate is c. 5 mm/ka. These measurements are likely to be relevant for much of the orthogneiss on Hop Island, but it is feasible that erosion rates in the other areas of less resistant lithology within the Rauer Group have higher subaerial erosion rates. In particular, the areas of paragneiss are rich in foliae that contain fine sillimanite, which tend to break into 1-cm-thick plates that then flake off from cliffs. The potential for more rapid weathering in areas of paragneiss and marbles is evidenced by the lithological control the positions of some valleys on Mather Peninsula and Shcherbinina Islands, where these lithologies lie at much lower altitudes than the other rock types (e.g., orthogneiss).

4.2.5 Discussion

The presence of erratics, debris drapes and occasional moraines across almost every island and peninsula in the Rauer Group indicates the ice sheet has at some stage extended beyond the outermost islands. The degree of erratic weathering provides the basis for the identification of three distinct weathering zones, likely corresponding to three periods of ice sheet advance and retreat.

4.2.5.1 Stage 1

The advance that covered the entire Rauer Group, described as "strongly weathered" above. The N-S orientation of the individual debris ridges and the debris-rich zone on the outer islands, as well as the E-W trend of the striae on Varyag Island, indicate that this material was deposited by an expansion of ice sheet rather than an advance of the Sørsdal Glacier.

A minimum late Pleistocene/early Holocene age for the retreat of the ice sheet from this expanded position is indicated by the rate and degree of bedrock weathering on the north-eastern tip of Hop Island, and a dated sediment sequence from near Filla Island. The thin, 50 mm high, upstanding quartz veins shown in Figure 4.2.7c would very likely have been removed by any passage of ice across this area. As both the short-term erosion rate measurements from the nearby Vestfold and Larsemann Hills (Spate et al., 1995) and the long-term average rates derived from ^{10}Be concentrations in samples (KK-HI-01-97 and KK-HI-02-97) from the surrounding rock indicate that the orthogneiss is lowering at a rate slower than 5-20 mm/ka, we can use the height of these veins to provide an estimate of the time since ice last passed across this area. Assuming (conservatively) that these veins themselves have not been eroded by subaerial processes (e.g., by wind, freeze-thaw) since the last time that they were overridden by ice, the height of these veins suggests that northeast corner of Hop Island has been ice-free for many thousands of years. This timing is further constrained by sediments from a marine basin east of Filla Island (Figure 4.2.1), which contains an uninterrupted sequence of open-marine sedimentation dating to 10.88±0.04 (KIA34077) ^{14}C ka BP (Berg et al., 2009).

Removal of the large quantity of ice as indicated by the highly weathered erratics would have a significant effect on local relative sea level, so the timing of this phase of retreat is also constrained by the height of the local sea-level maxima. Assuming that this expansion had a similar ice-surface profile to the present ice sheet inland from the Rauer Group, an ice sheet with a margin located offshore from the most seaward island in the Rauer Group archipelago would have a thickness of > 600 m at Filla Island. The common presence of raised beaches and littoral terraces up to c. 8.5 m a.s.l. suggests that the most recent relative sea-level maxima at Filla Island was located near this elevation. As removal of > 600 m of ice would result in isostatic uplift of > 50 m (e.g., Zwartz 1995), ice retreat could

not have occurred during the Mid-late Holocene or any other period when eustatic sea level was within a few tens of meters of today's value, as the local marine highstand would be many tens of meters higher than that observed. Thus, it is clear that most of the Rauer Group has been ice-free throughout the Holocene. Identifying a precise maximum limiting age for deglaciation from the Stage 1 limits is difficult. However, comparison of the degree of preservation of these glacial deposits with those from other areas in the region provides a limited maximum age constraint, as follows. Glacial debris from this event in the Rauer Group has a similar degree of preservation to that of deposits scattered across the eastern Vestfold Hills, which deglaciated following an advance during the last glacial maximum (Zwartz et al., 1998). This widespread preservation of glacial deposits contrasts strongly with the northern part of Broknes in the Larsemann Hills, which was not glaciated during the latter part of the current glacial cycle (Hodgson et al, 2001a).

While the rate of boulder weathering in these areas is not well constrained, the lithologies of boulders and bedrock within each of these sites is similar, so it is probable that the two rates are broadly comparable. Modern bedrock lowering rates in Larsemann (20 mm/ ka) are slightly higher than those from Vestfold Hills (10 mm/ka; Spate et al., 1995), but the difference is not great enough to explain the lack of glacial deposits on northern Broknes. Maximum erosion rates calculated from cosmogenic isotope measurements at these two sites suggests that this assertion is also valid on longer timescales (up to 10's of ka), with values from various sites between 5 and 15 mm/ka in both regions (Zwartz, 1995; Kiernan et al., 2009). Furthermore, clasts deposited at the ice margin in these regions rarely have a radius greater than 1 meter, and at modern erosion rates such boulders (eroding from both sides) would be completely removed in c. 50 ka in Larsemann Hills, so it is indeed possible that glacial debris was deposited when the striae were produced but have since disintegrated. Thus, our knowledge of the erosion rates in these areas supports the notion that the deposition of the (now) highly weathered glacial debris across the Rauer Group likely occurred during the latter half of the present glacial cycle. The presence of *in situ*, open-marine sediments with radiocarbon ages ranging from 40-30 ka BP to the east from Filla Island (Berg et al., 2009) indicates that this ice retreat must have occurred either in the early part of MIS 3, or more likely during MIS 2 or the last few thousand years of MIS 3.

4.2.5.2 Stage 2

The "moderately weathered" erratics and moraines within 500 m of the ice sheet. The Schmidt Hammer rebound and Moriwaki index values lie mid-way between those of the highly weathered deposits and those presently being released at the ice margin. While it is tempting to suggest that their age should therefore be mid-way between these two events, the linearity of this relationship in these environments is not well established. Thus, no strong age constraints can be placed on this event at this stage.

4.2.5.3 Stage 3

"Fresh glacial deposits" close to the ice margin, indicating the ice sheet margin was a few hundred meters more advanced than at the present. The historically observed retreat of ice, depositing erratics with a similar degree of weathering as the deposits in this stage, indicates that this unit was deposited during the late Holocene.

4.2.6 Conclusions

The geomorphology and weathering of glacial deposits in the Rauer Group indicate that the ice sheet had advanced more than 15 km from its present margin during the last glacial cycle at this site. While a precise retreat chronology for the Rauer Group awaits the application of more accurate dating techniques, the magnitude and broad-scale timing of this advance is suggestive of the most recent ice-sheet reconstructions in the Vestfold Hills (Zwartz et al., 1998). Also, in the sense that the ice sheet expanded onto the shallow portions of the continental shelf (i.e., to at least the -100 m contour line relative to modern sea level) during the latter half of the last glacial cycle, the history of the ice sheet in the Rauer Group/Vestfold Hills region is similar to what occurred in the Framnes Mountains (Mackintosh et al., 2007) and the wider Mac.Robertson Land region (Harris and O'Brien, 1998; Leventer et al., 2006). Thus, it is probable that advance of ice in these regions represents the regional ice sheet response to climate and sea-level variations during this time, and that the very limited expansion of the ice sheet at the Larsemann Hills (Burgess et al., 1994; Hodgson et al., 2001a,b; Verleyen et al., 2005) is due to local factors, such as the drawdown of the ice sheet due to the nearby Dålk Glacier (Hodgson et al., 2001a).

The importance of local ice drawdown by large, fast-flowing outlet glaciers may have wider implications for ice sheet reconstructions both within and outside of Antarctica. The regions surrounding outlet glacier termini are favoured sites for ice sheet reconstructions due to relatively large ice-free areas that are often found near their outlets. They are also targeted through the notion that they may represent the state of the ice sheet throughout the ice catchment drained by the outlet glacier. Many of the ice-free sites investigated in East Antarctica that have thus far suggested minimal ice sheet expansion during the LGM, including the Larsemann Hills, the Bunger Hills (Gore et al., 2001), Amery Oasis (Fink et al., 2006) and Lützow-Holm Bay (Igarashi et al., 1995, 1998) lie adjacent or close to major outlet glaciers. Thus, it is feasible that these records provide a biased view on the extent of ice expansion at the LGM, and ice expansion along the wider Antarctic coastline is, on the whole, better represented by sites that are not affected by large outlet glaciers, such as the Framnes Mountains (Mackintosh et al., 2007) or the margin of Law Dome (Goodwin and Zweck, 2000). Conversely, the drawdown effect from these large glaciers may provide an excellent opportunity for those looking for sites that may have remained continuously ice-free for long periods of time, and thus formed biological refugia during previous glacial maxima.

4.3 Short Note: A new marine sediment core from Rauer Group, East Antarctica

4.3.1 Introduction

The evolution of the East Antarctic Ice Sheet (EAIS) during the Late Quaternary is poorly known, partly because some regions, such as the Prydz Bay vicinity, indicate significant variability in the glaciation patterns (e.g., Domack et al., 1998; Zwartz et al., 1998; Hodgson et al., 2005).

Refinement of glaciation in Prydz Bay vicinity could be obtained from a 2143 cm long sediment core (Co1010) from Rauer Group (77°54'E; 68°48'S), which is an ice-free archipelago between Vestfold and Larsemann Hills. Core Co1010 was recovered at 37 m water depth from a marine inlet. Visual description, geochemical parameters, and diatom assemblages in combination with radiocarbon age determinations of the sediment sequence provide a first interpretation of the ice sheet extent during the Late Quaternary for Rauer Group.
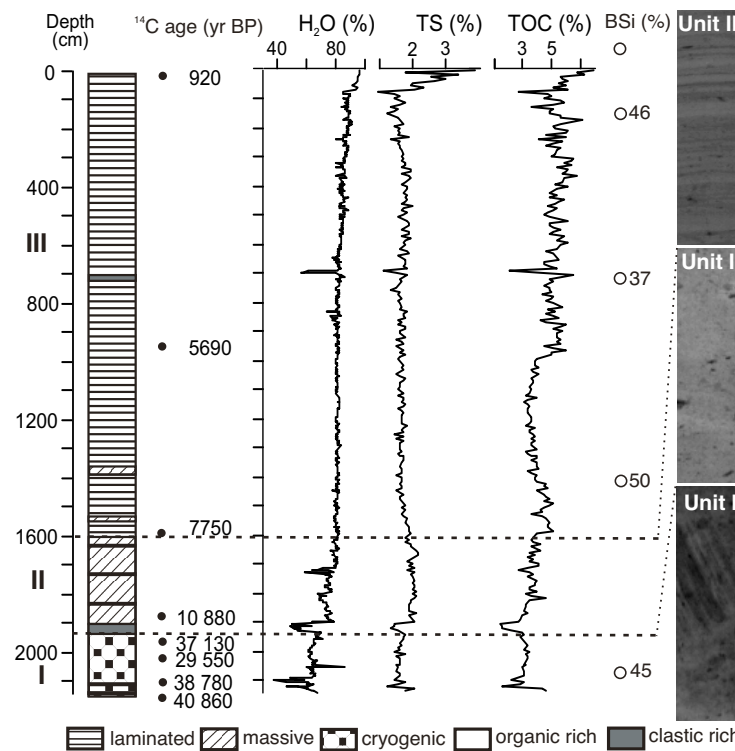
Figure 4.3.1 Lithological profile of Co1010: contents of water, total sulphur (TS), total organic carbon (TOC), and biogenic silica (BSi). Radiographic images were made by an ITRAX core scanner, image width 1 cm.

4.3.2 Results and discussion

Three major sedimentary units were defined in core Co1010.

Unit I (2143-1930 cm) is characterised by olive colour and a flaked structure (Figure 4.3.1). A low proportion of fine-grained minerogenic material, consisting of platy micas and unrounded grains (e.g., quartz, pyroxene) is associated with high contents of biogenic

46

silica (BSi) and total organic carbon (TOC) (Figure 4.3.1). BSi is mainly derived from diatom frustules whereas *Chaetoceros* resting spores are the main diatom components. Another abundant species, *Rouxia leventerae*, is reported to have a last occurrence date in marine isotope stage (MIS) 6 (Zielinski and Gersonde, 2002). Both diatom species show marine conditions. Four bulk sediment samples from unit I yielded radiocarbon ages between 42 to 29 ^{14}C ka, including one reversal (Table 4.3.1, Figure 4.3.1). These ages show that unit I was deposited prior to the LGM, during a period of ice-free, marine conditions. Marine conditions in the inlet around 40 to 30 ^{14}C ka would require an isostatic load that compensated the c. 100 m lower than present global sea level at that time (Huybrechts, 2002). However, a large-scale ice expansion at this period is unlikely, since the distance from the ice sheet margin to the inlet is only c. 6 km today. Local ice expansion, such as indicated in some records from Vestfold and Larsemann Hills (Aharon, 1988; Hodgson et al., 2005), might explain the isostatic load required. On the other hand, the presence of *Rouxia leventerae* indicates too young radiocarbon ages in unit I.

The flaked structure of unit I probably derives from postdepositional freezing of the marine sediments below a cold-based glacier. Similar structures have been described by Bird et al. (1991) from frozen fine-grained sediments. However, since overconsolidation is not observed, freezing occurred more likely at subaerial conditions, probably with subsequent glacial overriding. Both scenarios imply that marine sedimentation was interrupted in the inlet.

Unit II (1930-1600 cm) is characterised by greenish colour and a higher content of fine-grained minerogenic matter with some interspersed sandy horizons. The sporadic occurrence of pebbles and probably redeposited sediments with flaked structure in the lowermost 30 cm indicate glacial influence on sedimentation. From 1900 cm topwards, the structure of the sediment is massive, but some algal mats occur and are horizontally bedded. TOC and TS contents are slightly higher than in unit I (Figure 4.3.1). Sample KIA34077 from 1873 cm yielded an age of 10,880 ^{14}C yr BP (Table 4.3.1). The diatom taxa in unit II indicate marine conditions, with abundant *Chaetoceros* resting spores. Marine conditions in the inlet match with relative sea-level reconstructions from Vestfold and Larsemann hills (Verleyen et al., 2005). The distinct change in structure and the radiocarbon ages imply that units I and II are separated by a hiatus. This hiatus could be due to glacial overriding. Low amounts of clastic material in the overriding ice could explain the absence of a till layer between units I and II. Similar observations have been made in lake sediments from Baffin Island, Canada (Miller et al., 2002). A widespread glaciation across Rauer Group at some stage during the Late Pleistocene is supported by glacial deposits and the degree of weathering of local bedrock and glacial boulders (D. White, unpublished data). Further support comes from a marine sediment sequence recovered c. 30 km off Rauer Group, where a glacial diamicton underlays sediments, which indicate open marine conditions prevailing since 11,100-10,800 cal yr BP (Leventer

et al., 2006). Deglaciation at that time matches with the age of sample KIA34077 at the base of unit II. The relatively high minerogenic content in this unit, particularly in its lowermost 30 cm, could be due to deglaciation and subsequent enhanced availability of detrital material on the islands or increased meltwater discharge from snowfields and residual ice masses in the catchment.

Unit III (1600-0 cm) is characterised by green to black, laminated sediments that contain relatively high proportions of organic matter (Figure 4.3.1). The diatom assemblage, with high abundances of *Fragilariopsis curta* and *Fragilariopsis cylindrus,* displays marine open water conditions in the inlet. A gradual decrease of radiocarbon ages topwards throughout unit III (Table 4.3.1) and relatively constant sedimentary characteristics suggest that these conditions prevailed until today.

Table 4.3.1 Radiocarbon ages of bulk organic carbon from core Co1010

Lab.no.	Material	Depth [cm]	^{14}C age [yr BP]	Age range
KIA34076	bulk	4	920	±80
KIA35017	bulk	957	5690	±55
KIA35021	bulk	1593	7750	+260/-250
KIA34077	bulk	1873	10,880	±40
KIA35023	bulk	1946	37,130	+1430/-1220
KIA35024	bulk	2001	29,550	+180/-170
KIA35025	bulk	2100	38,780	+920/-830
KIA34078	bulk	2143	40,860	+2080/-1650

In summary, Rauer Group was likely ice-covered during the LGM. Marine sediments at the base of the sequence, deposited prior to the LGM, and the lack of a till layer indicate low erosive energy of the overriding ice sheet. Deglaciation of the inlet likely occurred prior to 10,880 ^{14}C yr BP.

4.4 Late Quaternary environmental and climatic history of Rauer Group, East Antarctica

Abstract

Rauer Group is an ice-free archipelago in East Antarctica. Two sediment records from marine inlets of Rauer Group have been studied for their sedimentological, geochemical, and biological characteristics. Radiocarbon ages from one of the inlets indicate ice-free conditions within the last glacial cycle, probably during the second half of Marine Isotope Stage 3. Subsequent ice sheet coverage of Rauer Group during the LGM can be inferred from a till layer recovered in one of the basins. The inlets became ice-free prior to 11,200 cal yr BP, when biogenic sedimentation started. Deglacial processes in the catchments, however, influenced the inlets until c. 9200 cal yr BP as evidenced by the input of minerogenic material. Marine productivity under relatively open water conditions indicates an early Holocene climate optimum until 8200 cal yr BP, which is followed by a cooler period with increased sea ice. In the Mid-Holocene both basins experienced an input of freshwater between c. 5700-3500 cal yr BP. Probably warmer conditions caused ice-sheet melting and increased precipitation on the islands. Neoglacial cooling in the late Holocene is reflected by an increase in sea ice in both inlets.

4.4.1 Introduction

Reconstructions of Holocene climate variations in East Antarctica that improve the understanding of natural climate variability have been derived from diverse archives. Ice core records for example provide valuable information on temperature change in the interior of the continent (e.g., Masson et al., 2000), whereas marine sediment cores from the Southern Ocean give insights into oceanographic circulation change (e.g., Denis et al., 2009). Other sites in East Antarctica, which provide useful archives recording more regional and local effects of climatic variability, are located in ice-free coastal areas. Terrestrial and shallow marine records from these areas are used to reconstruct past ice sheet expansions and retreats as well as paleoenvironmental and climatic conditions during the Holocene (e.g., Björk et al., 1996; McMinn et al., 2001; Cremer et al., 2003a). Reconstructions of pre-Holocene environmental and climatic conditions are, however, limited due to the poor preservation of soft sediments from the terrestrial and shallow marine realm (Cremer et al., 2003a; Hodgson et al., 2005).

Rauer Group is an ice-free archipelago covering an area of approximately 300 km^2 in eastern Prydz Bay (77°54'E; 68°48'S). Its extent is confined by the East Antarctic Ice Sheet (EAIS) to the east and by the Sørsdal Glacier to the north (Figure 4.4.1). Recent studies have focused on the hydrology of the lakes in Rauer Group (Hodgson et al., 2001b) and on the glacial history of the region (Berg et al., 2009; White et al., 2009). Here we present a multidisciplinary study of the first detailed reconstruction of climatic and

environmental conditions from Rauer Group during the late Quaternary. Sediment cores were recovered from the centre of two marine inlets at Filla and Flag islands (Figure 4.4.1), where sedimentation is thought to be undisturbed and continuous. Submarine sills restrict water exchange and inhibit the intrusion of icebergs into the inlets which would disturb the sediments. The catchments of the inlets are free of glaciers or multi-year snowfields.
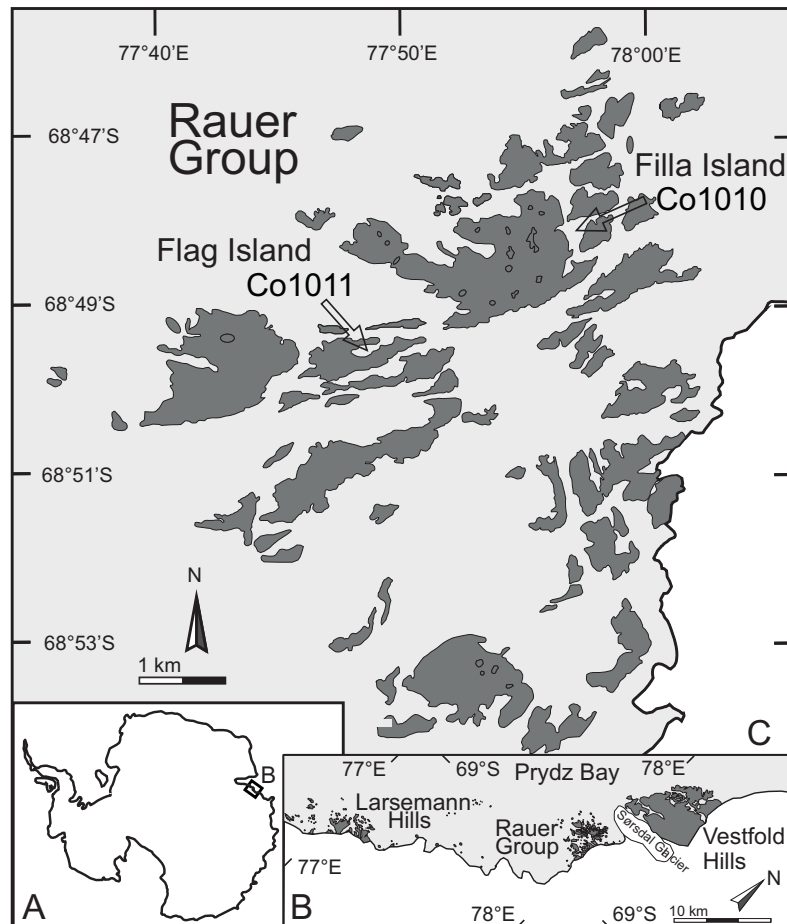
Figure 4.4.1 Map of Antarctica (A), and eastern Prydz Bay with ice-free coastal areas Larsemann Hills, Vestfold Hills and Rauer Group (B). Map of Rauer Group with the coring locations in Filla Island inlet and Flag Island inlet (C).

The core from Filla Island inlet (Co1010) was taken in a water depth of 38 m (Figure 4.4.1). Two sills to the south and to the east are 18 and 12 m below sea level, respectively. A third sill to the north is located in the intertidal zone. At the time of sampling in March 2007 the Filla Island inlet was covered by 1 m of sea ice and the bottom waters were oxygen depleted (Wagner et al., 2008). The depth of the Flag Island inlet (Figure 4.4.1) at the coring location of core Co1011 was 7.8 m. A sill to the east of the inlet is 4 m below sea level. The inlet was free of sea ice at the coring location. The tidal range in the inlets of Rauer Group is currently less than 1 m (Wagner et al., 2008).

4.4.2. Materials and methods

Coring was conducted with a gravity and piston corer (both UWITEC Corp. Austria). Gravity cores allowed the sampling of undisturbed surface sediments. For deeper penetration into the sediment the piston corer was employed for the recovery of 3 m long sections. Coring was conducted with 1 m overlap. The 3 m sections were cut into 1 m pieces in the field and stored at 4°C. To avoid disturbance of the water-rich surface sediments of core Co1010 during transport, the gravity core was sub-sampled in 2 cm intervals in the field. The correlation of the core sections was made on split half cores by macroscopic core description, geochemical parameters, and water content.

Semi-quantitative XRF elemental scans were obtained on core halves using an ITRAX XRF-core scanner (Cox Ltd., Croudace et al., 2006). The setting for the molybdenum X-ray tube during elemental analysis was chosen as to 30 mA and 30 kV. Exposure time and step size of measurement was 5 sec and 1 mm for Co1010, and 20 sec and 2 mm for Co1011. For better comparison between the cores elemental intensities were normalised for the exposure time and given as counts per second (cps). Data is averaged over 2 cm intervals matching with the sub-samples in order to reduce noise and to achieve comparability with other analyses. Quantitative inorganic sediment chemistry was determined by X-ray fluorescence (XRF) analysis for 20 samples of Co1010 and 23 samples of Co1011. For these analyses, 0.6 g of ground sediment was oven dried at 105°C for four hours and then mixed with lithium tetraborate (1:6) and c. 0.5 g of NH_3NO_4. The mixture was then heated stepwise to 1000°C and fused to a glass disk. Analysis on fused discs was carried out with a sequential X-ray spectrometer (Philips PW2400).

One core half of each sediment core was sub-sampled at 2 cm intervals. The water content was determined from weight loss after freeze-drying. For further analyses aliquots of the sub-samples were ground to < 63 μm. Elemental analyses for total carbon (TC), total nitrogen (TN) and total sulphur (TS) were conducted with a Vario Micro Cube combustion elemental analyzer (VARIO Corp.). For core Co1010 total organic carbon (TOC) was quantified with a Leco CS-225 (LECO Corp.) from samples, which were pre-treated with 10% hydrochloric acid (HCl) to remove carbonates. Total inorganic carbon (TIC) was derived from the difference of TC and TOC. For core Co1011, TOC was quantified from the difference between TC and TIC, which was measured with a DIMATOC 200 (DIMATEC Corp.). TIC is assumed to be mainly calcium carbonate in the sediments. Biogenic silica (BSi) concentrations were determined from 10-20 mg of ground aliquots, which were dissolved in 150 ml of 1 molar sodium hydroxide (NaOH) solution at 85°C. Over a period of 1.5 hours 12 aliquots of 1 ml were taken from the solution and analyzed for dissolved silica contents, in order to extrapolate the content of biogenic silica in the sediment sample according to DeMaster (1981).

For the determination of salts, 0.1 g of ground sample was leached in 10 ml deionised water for one hour. Subsequently, the salinity of the solution was measured with a WTW multi 197 probe (WTW Corp. Germany). The term salt in our study refers to the water-soluble fraction of the marine sediments, which should be mainly formed by sodium chloride (NaCl). Diatom assemblages were determined from 28 samples of core Co1010 and 19 samples of core Co1011. For the preparation of diatom slides 0.5 g of freeze-dried sediment was treated with HCl (10%) to remove carbonates and with hydrogen peroxide (30%) to oxidise organic matter. Permanent slides have been made with the high-refraction mountant Naphrax®. For diatom analyses at least 250 individuals were counted from each sample. For a more detailed description of diatom sample preparation see Cremer et al. (2001).

The oxygen isotope composition of diatom silica was analysed on 12 samples from Co1010. Samples were cleaned to separate diatoms from minerogenic components in the sediment following the method described by Morley et al. (2004). After organic and carbonate removal the samples were sieved using meshes to obtain a single fraction between 10 and 75 µm. To separate diatoms from minerogenic material, samples were centrifuged over a heavy liquid, i.e., sodium polytungstate, and checked using optical microscopy. A few samples were further checked using scanning electron microscopy to ensure that no visible minerogenic particles were included (e.g., Figure 4.4.2). Diatom silica samples were analysed for $\delta^{18}O$ at the NERC Isotope Geosciences Laboratory, British Geological Survey, UK, using the stepped fluorination technique to extract oxygen isotopes described by Leng and Barker (2006) and Leng and Sloane (2008). The precision of the $\delta^{18}O_{diatom}$ technique is c. 0.3‰. The oxygen isotope results are expressed as 'd' values, representing deviations in per mille (‰) from VSMOW.

For obtaining chronologies of the sediment records radiocarbon ages were measured at the Leibniz Laboratory for Radiometric Dating and Isotope Research in Kiel, Germany. Except for one sample (KIA 37748, Table 4.4.1), which is a moss fossil, radiocarbon dates were determined on the humic acid (HA) and humic acid free (HAF) fraction of bulk organic carbon. In the marine diatomaceous oozes from Antarctica ^{14}C-dating of the HAF fraction of bulk sediment is considered to provide more reliable ages (e.g., Hillenbrand et al., 2009) than the HA fraction, which is presumed to be more mobile. For core Co1010 the age/depth model has been established from solely HAF ^{14}C-ages. For the age/depth model of unit III from core Co1011 the radiocarbon ages of the HA fraction were used because the HAF fraction did not yield sufficient material for reliable dating of all the samples. The HA ages from this unit are assumed to be reliable, since two samples where both fractions were dated (i.e. KIA37742, KIA37745) show good agreement between the HA and HAF ^{14}C-ages.
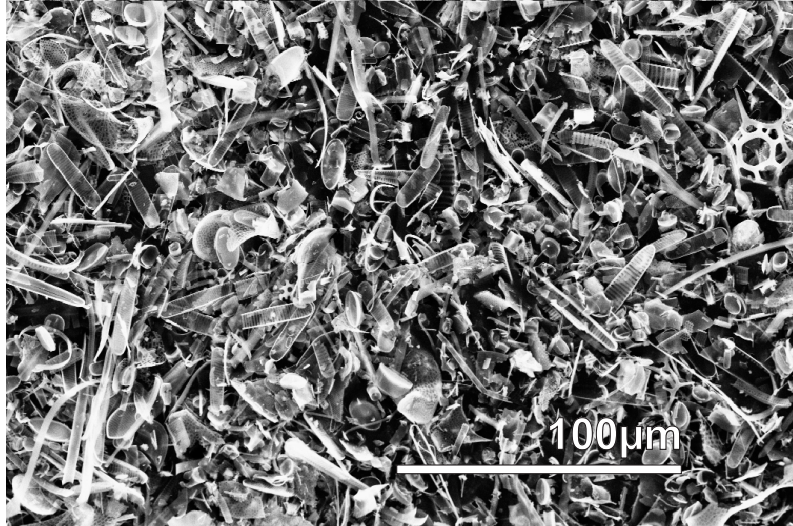
Figure 4.4.2 Scanning electron microscopy (SEM) image of purified diatoms (sample from Co1010, unit III). Image was taken to ensure that no visible minerogenic particles are included in the sample prior to δ^{18}O$_{diatom}$ measurement.

The radiocarbon ages were calibrated into calendar years using the Calib 5.1rev programme (Stuiver et al., 2005) and the Marine04 data set (Hughen et al., 2004) for marine samples, and the SHCal04.14c dataset (McCormac et al., 2004) for freshwater samples. For marine samples a local reservoir effect was estimated for each inlet from the uppermost dated sample, assuming that the sample is of recent age and its radiocarbon age represents the local marine reservoir effect. The reservoir effect of the two inlets are very similar and are c. 900 years (Table 4.4.1). This age was used to estimate the deviation of the general marine reservoir effect of the Southern Ocean (362 years for Southern Hemisphere; Stuiver and Braziunas, 1993; Table 4.4.1) from the local reservoir effect (ΔR). However, changes in the reservoir effect have likely occurred over time, although because they cannot be determined we have assumed that the reservoir effect is constant over time. Age/depth models were established by fitting the calibrated ages with a polynomial function. For better comparison with previous studies radiocarbon ages quoted in the text have been re-calibrated with the Marine04 data set (Hughen et al., 2004) or SHCal04.14c dataset (McCormac et al., 2004). The reservoir correction was retained as originally defined by the respective authors. The newly calibrated as well as the original radiocarbon ages are quoted in the text.

4.4.3. Results and discussion

4.4.3.1 Core Co1010, Filla Island

Sedimentology

The composite core Co1010 has a length of 2143 cm and was subdivided into three lithological units (Figure 4.4.3, Berg et al., 2009). Unit I (2143-1930 cm depth) consists of fine-grained sediments with a flaky texture and relatively low water content of about 55-

65%. The flakiness is thought to have been caused by post-depositional freezing indicating an interruption of marine conditions (Berg et al., 2009). The low water content is likely due to compaction of the sediments. Unit I also has a high proportion of organic matter (OM) and BSi, the latter mainly derived from diatoms. Relatively high C/N-ratios (c. 15) could either indicate a nitrogen limited or highly productive environment (McMinn, 2000) or represent a diagenetic signal due to the preferential decomposition of nitrogen rich OM (Middleburg, 1991). High sulphur content (1-2%) is possibly related to suboxic or anoxic conditions in the sediments or bottom waters during deposition and suggest considerable production. As Ti counts from the XRF scanner are in good correlation with quantitative data derived from classical XRF measurements (Figure 4.4.3), the XRF scanner data gives a good estimation of relative amounts of titanium-bearing minerals in the sediments. In the marine environment Ti is neither affected by diagenetic overprinting (Brumsack, 2006) nor involved in biological processes (Denis et al., 2006) and therefore Ti represents the allochthonous minerogenic input. The low Ti intensities as well as the macroscopic sediment description of Unit I indicate limited minerogenic input. Higher Ti intensities coincide with single interspersed sandy layers, which also contain poorly sorted and unrounded clasts, including fragments of shells and echinoids. The occurrence of marine macrofossils as well as salt content around 8-10% point to a marine origin of the sediments. Two samples from Unit I were analyzed for the oxygen isotope composition of BSi (Figure 4.4.3). It is assumed that the oxygen of diatom silica is in equilibrium with the surrounding water (Leng and Barker, 2006) and therefore reflects the isotopic composition of the water at a given temperature. The $\delta^{18}O$ values are the lowest from the core (32.7 and 32.3‰) and are therefore most likely to reflect a contribution of freshwater in the marine environment (i.e. input of meltwater from run-off from melting ice sheets in the area; cf. Meredith et al., 2008) or higher temperatures. Estimations of the temperature dependence of $\delta^{18}O_{diatom}$ range from -0.2°C/‰ to -0.5°C/‰ (review by Leng and Barker, 2006). If the $\delta^{18}O_{diatom}$ was solely explained by temperature effects, the difference between the average $\delta^{18}O_{diatom}$ of the whole core (38.0±3.1‰) and the values of Unit I could account a temperature difference of up to 28.5°C. Since such temperature shifts are not realistic, freshwater input probably has a much greater influence on the $\delta^{18}O_{diatom}$ than temperature.

Unit II (1930-1595 cm depth) has high water content (c. 75%), which suggests lower compaction and the possibility of a hiatus between this and the underlying unit (Berg et al., 2009). The greenish sediment appears massive except for several sandy layers and algae rich horizons. In general the sediments are fine grained but contain some sandy material as well as several interspersed gravels in the basal 30 cm. This minerogenic character is clearly reflected in the high Ti counts (Figure 4.4.3) and slightly lower proportions of OM. The C/N-ratio is the highest at the base (12.3) and decreases sharply (to 8.6) in the overlying 30 cm which probably indicates admixture of sediments from the underlying Unit I. Moreover, the low $\delta^{18}O$ value from the base of Unit II (1847 cm, Figure 4.4.3) is

close to the values in Unit I perhaps suggesting reworking of diatoms as the presence of soluble salts in the pore waters suggest a normal marine environment. The lack of bioturbation as well as relatively high sulphur content suggest oxygen depletion in the bottom water.

Unit III (1595-0 cm depth) is laminated and dark green to black colour. High salt contents of 40 to 60% suggest a marine origin of the sediments and are indicative of a high porosity of the sediments. High water content (> 80%) as well as high amounts of TOC (2-4%) and diatom-derived BSi (20-40%) indicate a high OM (Figure 4.4.3). Higher TOC content (>3%) above c. 1000 cm could be due to higher productivity or better preservation of OM. Although, as this change is not accompanied by a shift in BSi, or in diatom composition, it is more likely due to a change in the proportion of diatoms and non-skeletal algae and bacteria.
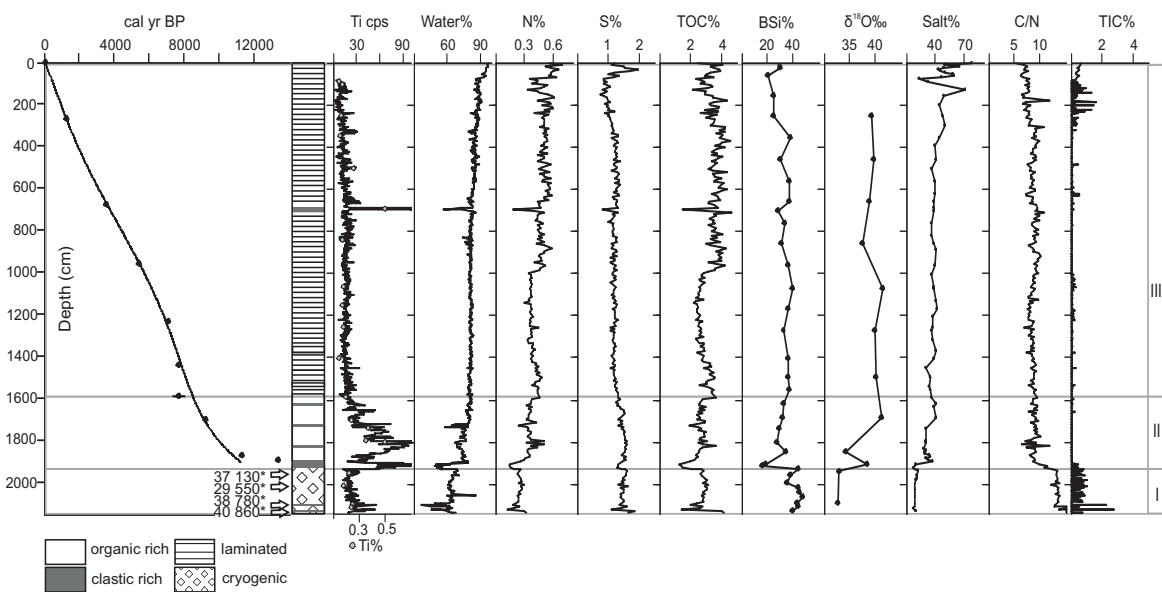
Figure 4.4.3 Chronology and lithology of core Co1010 from Filla Island inlet. All radiocarbon ages (^{14}C yr BP and cal yr BP) are listed in Table 4.4.1, Radiocarbon ages indicated with * are given as ^{14}C yr BP and are not corrected and not calibrated. Titanium (Ti) displayed as counts per second (cps) and weight percent (%), water content, nitrogen (N), sulphur (S), total organic carbon (TOC), biogenic silica (BSi), δ^{18}O values of diatom silica, salt content, total inorganic carbon (TIC) and atomic ratio of total organic carbon and nitrogen (C/N) versus depth.

Throughout Unit III the C/N-ratio shows only moderate variability (mean 8.4±0.8) with a decreasing trend in the uppermost 300 cm. This decrease could be due to a less nitrogen limited or less productive environment. Alternatively high sulphur content, and a strong smell of H₂S gas which occurred after the cores were opened, in the upper few meters suggests sulphate reduction in the sediments, anoxic conditions, and hence a good preservation of OM. Minor variations in sulphur content and the absence of marked redox horizons throughout Unit III indicate relatively stable redox conditions. The lack of variability in δ^{18}O values of diatom silica throughout Unit III (39.6±1.2‰) suggests a relatively stable marine environment, apart from a relatively low δ^{18}O value at 861 cm

(37.5‰) which could indicate a period of increased meltwater input (or less likely higher temperatures). The minerogenic proportion is fine-grained throughout Unit III. Sporadically interspersed sand grains are either subangular and unrounded or platy (as in the case of biotite) in shape. Transport of minerogenic particles into the inlet is probably mostly aeolian and by drifting sea ice. A sandy layer occurs at 700 cm, this sand is 5 cm thick and poorly sorted, and may originate from a single storm event which deposited larger amounts of sediment on the sea ice (McMinn et al., 1998). The decrease in Ti counts towards the top is probably due to lower compaction of the sediments and hence dilution by very high water and salt contents.

Diatom distribution

The sediments of core Co1010 contain a diverse diatom assemblage (Table 4.4.2). Preservation of diatoms is moderate in Unit I, where a lot of fragmented valves have been observed. Better preservation occurs in the upper two units. The diatom assemblage is dominated in all three units by *Chaetoceros* spp., *Fragilariopsis cylindrus* and *Fragilariopsis curta* and indicates a marine environment (e.g., Cremer et al., 2003a and b).
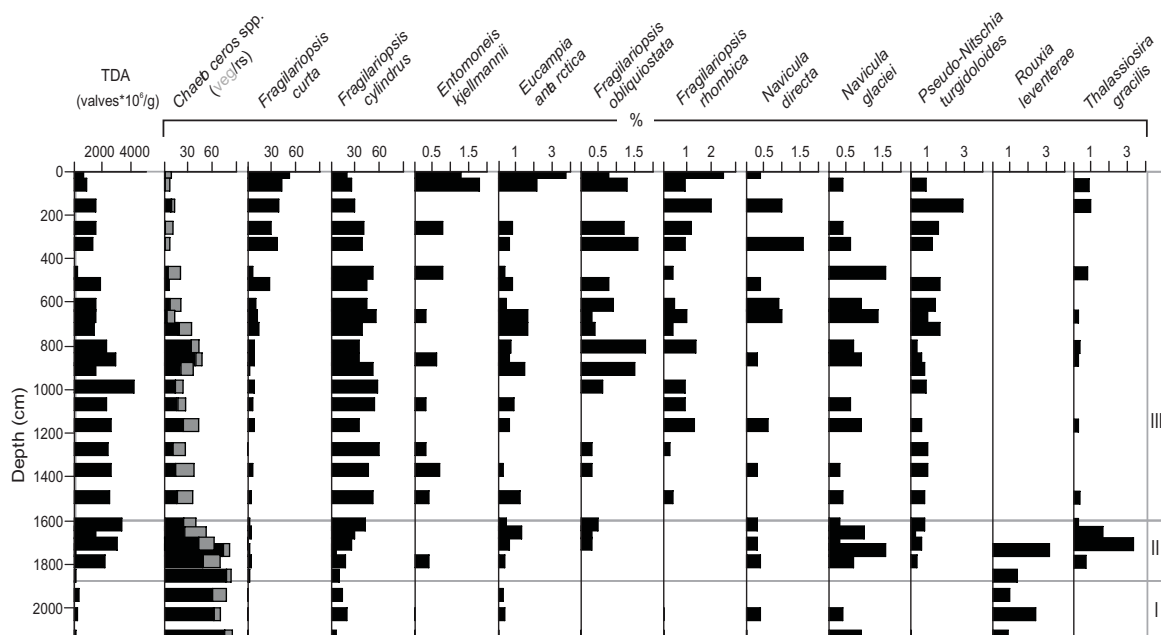
Figure 4.4.4 Total diatom abundance (TDA; million valves per g dry sediment) and proportion of selected diatom species of core Co1010 from Filla Island inlet, plotted versus depth; *Chaetoceros* spp. vegetative stages (veg) and resting spores (rs).

Total diatom abundance (TDA) in Unit I (2143-1930 cm depth) is rather low in comparison with the high BSi content. This might be an effect of preservation, since the sediments of Unit I contain a lot of fragmented valves, which are not taken into account for TDA estimation. The diatom assemblage in this unit is characterised by a relatively low number of taxa. The predominant species are *Chaetoceros* spp., including high proportions of resting spores (Figure 4.4.4). *Chaetoceros* spp. thrive in open-water (McMinn et al.,

2001) and are often interpreted as indicators of high productivity (e.g., McMinn 2000; Stickley et al., 2005; Leventer et al., 2006). Since *Chaetoceros* spp. resting spores are heavily silicified their predominance in the sediment could be a result of better preservation (Crosta et al., 1997). Ice related species like *Fragilariopsis cylindrus* and *Fragilariopsis curta, Eucampia antarctica* and *Navicula glaciei* were also found (Figure 4.4.4). *Rouxia leventerea* is thought to be extinct after the marine isotope stage (MIS) 6 (Zielinski et al., 2002), so its occurrence strongly suggests input of re-worked older material (Berg et al., 2009). In Unit II, between 1930 and 1738 cm core depth, diatom assemblage shows low diversity and high proportions of *Chaetoceros* spp. resting spores, indicating open water conditions and high productivity. Two samples from this section with very low TDA contain *Rouxia leventerea*. Since sedimentation was interrupted between Unit I and Unit II (Berg et al., 2009), the fossil diatom assemblage suggests at least episodical incorporation of re-sedimented material. Above 1738 cm in Unit II, TDA and diversity increase. Since *Chaetoceros* spp. and *Thalassiosira gracilis* are typical species of the open ocean assemblage in the Prydz Bay region (Taylor et al., 1997; McMinn, 2001), they indicate relatively open water conditions during summer and probably higher sea surface temperatures (Bohaty et al., 1998). High proportions of *Chaetoceros* spp. resting spores in the sediments may also indicate nutrient restrictions, e.g., due to high productivity during springtime blooms (Stickley et al., 2005; Leventer et al., 2006). However, open water species gradually decline above 1657 cm depth and the sea-ice related, cryophilic *F. cylindrus* increases. From 1595 cm depth (Unit III) upwards *F. cylindrus* makes up to c. 60% of total diatoms valves. Intense blooms of this cryophilic species have been observed in marine basins in the Vestfold Hills directly after ice break up and in summer, when winter sea-ice is melting and freshening the uppermost water column occurs (McMinn et al., 2000). Other species associated with sea ice (e.g., *F. curta, Navicula glaciei, Fragilariopsis rhombica, Pseudo-Nitzschia turgiduloides, Entomoneis kjellmannii* and *Eucampia antarctica*) are abundant, but do not show a marked trend.

Between 909 and 726 cm depth, *Chaetoceros* spp. reach a second maximum with higher proportions of resting spores. This points to more open conditions and stable water column stratification. Above 662 cm, *Chaetoceros* spp. and *F. cylindrus* show a marked decline, whereas *F. curta* becomes more important and thus the dominant species in the uppermost sample. Both species of *Fragiariopsis* are associated with sea ice and their occurrence has been encountered to reconstruct the presence of sea ice in the summer season (Cremer et al., 2003a; Crosta et al., 2008). Nevertheless, the divergent pattern shows that their ecology differs. In an open ocean setting *F. curta* was most abundant, when sea ice lasted for about 10 months per year, whereas *F. cylindrus* showed maximum abundance when sea ice lasted for about months 8.5 (Armand et al., 2005). Hence, the increase of *F. curta* could be related to an increasing annual sea ice presence in the inlets. Alternatively, sea ice diatoms (e.g., *E. kjellmannii, N. glaciei*) do not significantly increase, and McMinn (2000)

interpreted the occurrence of *F. curta* in near-coastal marine environments as an indicator for open water, rather than for extensive sea ice cover. The gradual increase of *F. curta* could also reflect a change in seasonality, since investigations from the marine inlets of Vestfold Hills demonstrate a seasonal succession of *F. curta* and *F. cylindrus,* with *F. curta* blooms later in the season (McMinn et al., 2000).

Table 4.4.1. Radiocarbon ages from humic acid free (HAF) and humic acid (HA) fraction of bulk organic matter. Correction of radiocarbon ages was made by subtracting the surface age from ages down-core. Corrected ages have been calibrated. For marine samples calibration was made with Marine04 dataset (Hughen et al., 2004) and with ΔR-values determined as described in Stuiver and Braziunas (1993). The age range of calibrated ages is within the 2σ confidence interval.

Core	Lab. No.	Dated material	Depth [cm]	^{14}C age [^{14}C yr BP]	ΔR	Calendar age [cal yr BP]	Mean+/- dev. [cal yr BP]
Co1010	KIA34076	HAF	4	920±80	558	-3-149	73±76
Co1010	KIA35015	HAF	273	2335±35	558	1257-1396	1326±70
Co1010	KIA35016	HAF	678	4230±70	558	3401-3779	3590±189
Co1010	KIA35017	HAF	957	5690±55	558	5329-5590	5459±130
Co1010	KIA35019	HAF	1237.7	7140±80	558	6896-7268	7082±186
Co1010	KIA35020	HAF	1441	7810±70	558	7575-7864	7719±145
Co1010	KIA35020	HA	1441	8130±40		-	-
Co1010	KIA35021	HAF	1593	7750±260	558	7176-8185	7680±505
Co1010	KIA37749	HAF	1700	9125±50	558	9058-9381	9219±162
Co1010	KIA37749	HA	1700	9445±55		-	-
Co1010	KIA34077	HAF	1873	10,880±40	558	11,193-11,417	11,305±112
Co1010	KIA34077	HA	1873	10,505±40		-	-
Co1010	KIA35022	HAF	1894	12,490±80	558	13,246-13,491	13,368±123
Co1010	KIA35023	HAF	1946	37,130±1300		-	-
Co1010	KIA35024	HAF	2001	29,550±180		-	-
Co1010	KIA35024	HA	2001	45,360±2000		-	-
Co1010	KIA35025	HAF	2103.5	38,780±900		-	-
Co1010	KIA35025	HA	2103.5	42,200±2000		-	-
Co1010	KIA34078	HAF	2143	40,860±2000		-	-
Co1010	KIA34078	HA	2143	34,840±360		-	-
Co1011	KIA37742	HAF	2	985±30		-	-
Co1011	KIA37742	HA	2	890±25	528	-3-66	32±35
Co1011	KIA37743	HA	147	3370±30	528	2483-2707	2595±112
Co1011	KIA37745	HAF	619	7265±45		-	-
Co1011	KIA37745	HA	619	7210±40	528	7134-7309	7222±88
Co1011	KIA37746	HA	900	8530±45	528	8369-8561	8465±96
Co1011	KIA37748	HAF	1087	9890±60	-	11,125-11,404	11,264±140

Radiocarbon dating

Overall, 14 samples from core Co1010 were used for radiocarbon dating. Radiocarbon ages of Unit I give a reliable age/depth relation showing increasing ages with depth, except for one reversal (KIA35024, Table 4.4.1, Figure 4.4.3). The age range between 40.8 and 29.5 ka (Table 4.4.1) indicates a pre-Holocene age of deposition, probably in MIS 3. However, as the fossil diatom *Rouxia leventerae* is supposed to have been extinct since the

end of MIS 6 (Zielinski et al., 2002), Unit I could also be older or the sediments in Unit I include older, reworked sediments. Two samples from the base of Unit II gave ages of 13,368±123 cal yr BP (KIA35022, 1894 cm) and 11,305±112 cal yr BP (KIA34077, 1873 cm; Table 4.4.1). Diatom data as well as oxygen isotopes indicate incorporation of older sediments in the section between 1900 and 1738 cm, which likely also affected radiocarbon ages. Too old ages could also derive from a high input of radiocarbon-depleted meltwater. The increase in sedimentation rate between 1900 and 1700 cm (Figure 4.4.3) is therefore likely to be due to a decrease in the reservoir effect or less incorporation of reworked sediments. Above 1700 cm depth, corresponding with an age of 9219±162 cal yr BP (KIA37749), there is no indication for reworked material or further decrease in the reservoir effect. The age/depth model therefore is presumed to be reliable. One sample from 1593 cm (KIA35021, Table 4.4.1) was removed from the age/depth model, due to the large error that resulted from very low organic carbon contents in the measured sample.

4.4.3.2 Core Co1011, Flag Island

Sedimentology

The composite core Co1011 has a length of 1099 cm and was subdivided in three main lithological units (Figure 4.4.5). Unit I (1099-1087 cm) comprises the basal 12 cm of the core and consists of a grey, dry, and compact diamict with clasts of up to 5 cm in diameter embedded in a silty matrix. OM content is very low, indicated by low TOC and BSi and high Ti counts. TIC content is probably due to fine-grained authigenic carbonate, since macroscopic carbonaceous fossils were not found. This sediment is interpreted as a till, deposited by an ice sheet formerly covering the coring location.

Unit II (1087-1051 cm) contains a high content of minerogenic material, and is not markedly compacted. The very fine grain size suggests deposition in a low energy environment. A poorly sorted sand package forms the top of Unit II (1066-1051 cm). The coarser grain size indicates deposition in a higher energy environment. The sand layer could have been deposited during a storm or by a distinct phase of meltwater flux. A 2 cm thick moss layer at the base of Unit II suggests a subaquatic environment and freshwater conditions (Kudoh et al., 2003). The colonisation of the basin by benthic organisms indicates substrate stability at the coring location with low current reworking and moderate sedimentation rates. Between 1085-1066 cm, the sediment is laminated at millimetre scale with alternating grey clastic layers and green organic layers. Low BSi and TOC content indicate low biogenic production, probably of algae, in the basin. A further indication for biogenic production is the occurrence of up to 1.9% of TIC, which could derive from carbonate precipitation due to photosynthetic activity of algae (Hodgson et al., 2005). The OM is characterised by C/N-ratios of above 10 (Figure 4.4.5). The upward decrease in the

C/N-ratio can be explained by a nutrient limited environment changing to a more replenished system or to changing preservation efficiency. Relatively high sulphur content indicates high availability of sulphur or efficient bacterial sulphur fixation in the sediments due to reducing conditions, such as promoted by a permanent ice cover. Very distinct sulphur enrichment in the sand layer at the top of Unit II could result from post depositional migration of sulphur (e.g., H_2S) into the porous layer, either from below or from the overlying sediments (Sternbeck et al., 2000).
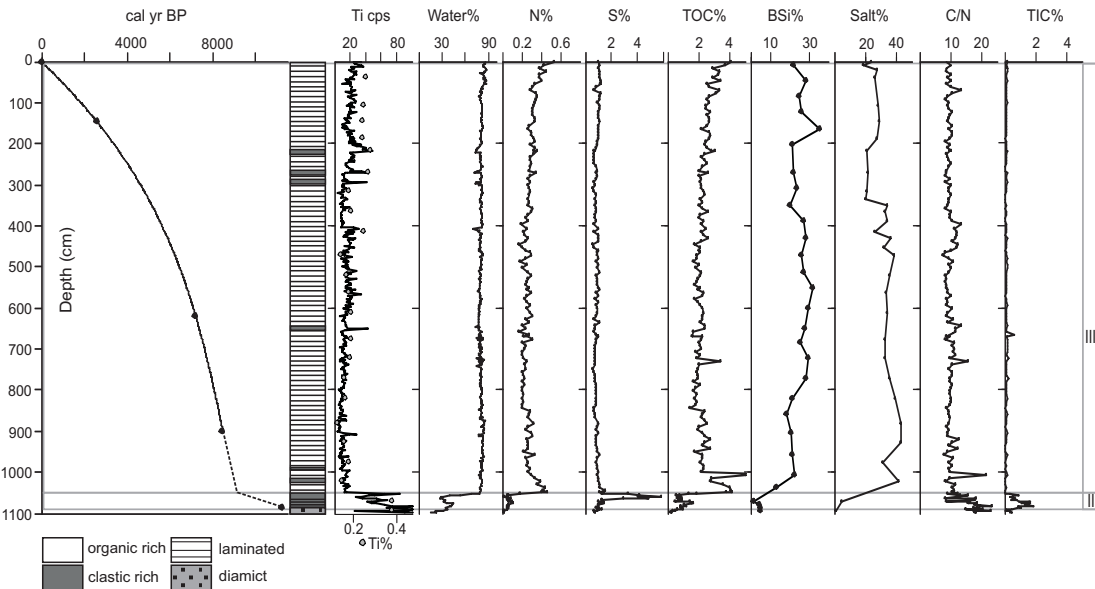
Figure 4.4.5 Chronology and lithology of core Co1011 from Flag Island inlet. Radiocarbon ages are listed in Table 4.4.1. Lithological units are indicated in Figure 4.4.5, except for Unit I (1099-1087 cm depth). Titanium (Ti) displayed as counts per second (cps) and weight percent (%), water content, nitrogen (N), sulphur (S), total organic carbon (TOC), biogenic silica (BSi), total inorganic carbon (TIC) and atomic ratio of total organic carbon and nitrogen (C/N) vs. depth.

Unit III (1051-0 cm) is a greenish to black colour and contains fine lamination of alternating OM rich and clastic rich layers. The thickest organic laminae ($\geq$ 0.3 cm) and high TOC content occur in the lower part of Unit III. The smell of H_2S in the same section points to anoxic bottom water conditions, possibly due to high productivity in the water column and intense bacterial decomposition in the surface sediment. High TOC (2-4%) and BSi (20-35%) content, as well as water content around 80%, indicates an overall high OM content (Figure 4.4.5). The C/N-ratio varies between 9 and 11. The variations could be caused by differing preservation of OM, however, TS indicates only minor variations and marked redox horizons were not observed in this unit. High salt content suggests a marine origin of the sediments (Figure 4.4.5). Decreasing salt content between 400 and 200 cm could be due to enhanced freshwater input or less sea ice and brine formation. The minerogenic component is fine grained, however, sand occurs sporadically as single grains or thin layers. Terrigenous matter is delivered to the basin either as IRD or by aeolian transport and exhibits some significant fluctuations, such as indicated in the Ti profile (Figure 4.4.5). Relatively fine-grained clastic rich layers between 400 and 200 cm core

depth probably originate from episodic input of fine-grained material. A gradual increase in Ti counts in the uppermost 250 cm corresponds with a visual increase in biotite throughout this sequence.

Diatom distribution

The sediments of core Co1011 contain a diverse diatom assemblage (Table 4.4.2). In Unit I, diatoms were not observed. The samples from Unit II contain very low TDA, which corresponds well with low BSi concentrations (Figure 4.4.6). Colonisation of the inlet by the epipelic and benthic *Amphora veneta* and *Craticula* cf. *molesta* (Wagner et al., 2004) is an indication of substrate availability and stability, either at the coring location or in the littoral part of the basin (Cremer et al., 2001).
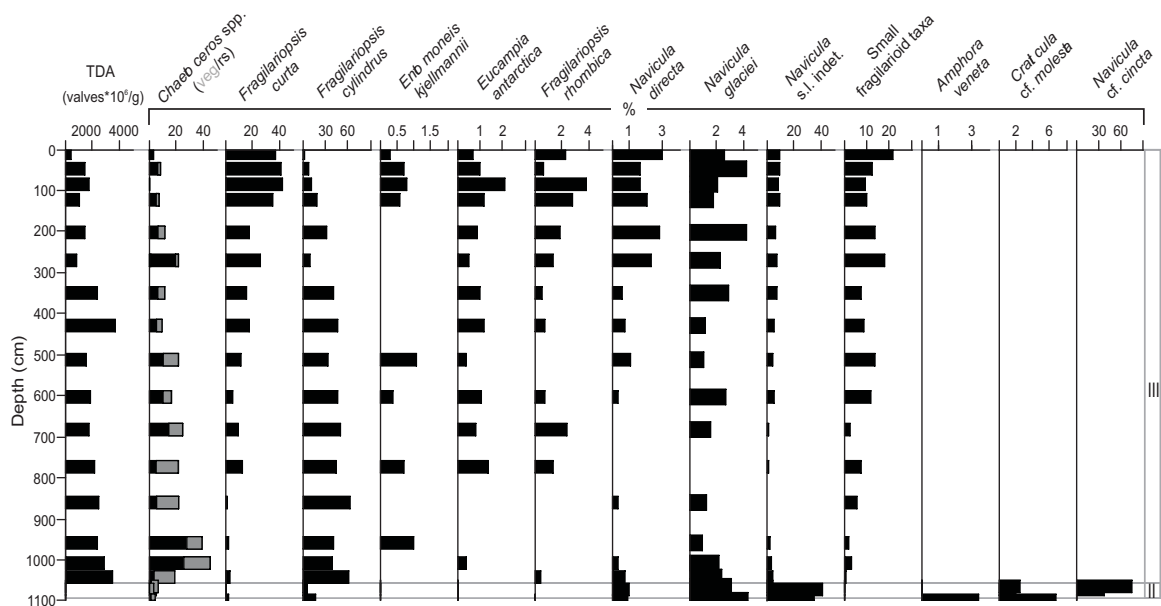
Figure 4.4.6 Total diatom abundance (TDA; million valves per g dry sediment) and proportions selected diatom species of core Co1011 from Flag Island inlet, plotted versus depth; *Chaetoceros* spp. vegetative stages (veg) and resting spores (rs). Lithological units are indicated in Figure 4.4.6, except for Unit I (1099-1087 cm depth).

Both species indicate a fresh to brackish habitat (Cremer et al., 2004), whilst the occurrence of *Navicula* cf. *cincta* points to clear brackish conditions. *Fragilariopsis cylindrus* and *Navicula glacei* are typical cryophilic diatoms, living in or near sea ice (Cremer et al., 2003b). The occurrence of different species, which occur in a broad range of fresh to marine conditions and which all have a broad salinity tolerance (Roberts and McMinn, 1999), could be a result of episodic influx of marine water into a freshwater filled basin.

Unit III has high TDA and contains a diatom assemblage which is typical of a coastal marine environment in Antarctica (Cremer et al., 2003b, Figure 4.4.6). Between 1051 and 950 cm depth high abundance of *Chaetoceros* spp. points to relatively open marine conditions and the high proportion of resting spores indicates high productivity.

Table 4.4.2 Diatom species identified in cores Co1011 and Co1010.

Specie	Co1011	Co1010	Remarks
Achnanthes breviceps Agardh	x	x	m/b
Amphora veneta Kützing	x	-	b/f
Chaetoceros spp. resting spores	x	x	m/b, u
Chaetoceros spp. vegetative stages	x	x	m/b, u
Corethron criophilum Castracane	-	x	m/b
Craticula sp. (cf. C. *molesta* (Krasske) Lange-Bertalot et Willmann	x	-	f/b
Diadesmis sp. (cf. *D. ingeae* Van de Vijver)	x	-	f/b
Diploenis sejuncta f. *constricta* Hustedt	-	x	m/b
Entomoneis kjellmannii (Cleve) Poulin et Cardinal	x	x	m/b
Eucampia antarctica (Castracane) Mangin	x	x	m/b
Fragilaria striatula Lyngbye	x	x	m/b
Fragilariopsis curta (Van Heurck) Hustedt	x	x	m/b
Fragilariopsis cylindrus (Grunow) Krieger	x	x	m/b
Fragilariopsis obliquecostata (Van Heurck) Heiden	x	x	m/b
Fragilariopsis peragallii (Hasle) Cremer	x	-	m/b
Fragilariopsis pseudonana (Hasle) Hasle	x	x	m/b
Fragilariopsis rhombica (O'Meara) Hustedt	x	x	m/b
Fragilariopsis separanda Hustedt	x	x	m/b
Fragilariopsis vanheurckii (Peragallo) Hustedt	x	x	m/b
Gomphonemopsis littoralis (Hendey) Medlin	-	x	m/b
Luticola mutica (Kützing) D.G. Mann	x	-	f/b
Muelleria peraustralis West et West	x	-	f/b
Navicula sp. (cf. N. *cincta* (Ehrenberg) Ralfs	x	-	f/b
Navicula directa (W. Smith) Ralfs	x	x	m/b
Navicula glaciei Van Heurck	x	x	m/b
Navicula perminuta Grunow	x	-	u
Nitzschia lecointei Van Heurck	x	-	m/b
Nitzschia medioconstricta Hustedt	x	-	m/b
Nitzschia palea (Kützing) W. Smith	x	-	m/b
Planothidium delicatulum (Kützing) Round et Bukhtiyarova	x	-	f/b
Pseudo-Nitzschia lineola (Cleve) Hasle	x	x	m/b
Pseudo-Nitzschia turgiduloides (Hasle) Hasle	x	x	m/b
Rouxia leventerae Bohaty, Scherer et Harwood	-	x	m/b, fo
Synedropsis laevis (Heiden) Hasle, Medlin et Syvertsen	x	x	m/b
Synedropsis recta Hasle, Medlin et Syvertsen	x	x	m/b
Thalassiosira gerloffii Rivera	-	x	m/b
Thalassiosira gracilis (Karsten) Hustedt	x	x	m/b
Thalassiosira gravida Cleve	-	x	m/b

m/b: marine to brackish environment, f/b: fresh to brackish environment, u: unidentifiable taxon, fo: fossil specie

The dominance of *F. cylindrus* above 950 cm (up to c. 60% of the total diatom valves) could be due to the presence of residual winter sea-ice and freshening of the uppermost water column due to melted sea ice (cf. McMinn et al., 2001). A high proportion of diatom valves are from *Navicula* s.l. and small fragilarioid taxa, which could not be identified to species level. Of the species with abundances < 2%, *Entomoneis kjellmannii* is an indicator for permanent ice cover during summer (McMinn, 2000). *Entomoneis kjellmannii* lives at the bottom of sea ice, which is attached to the coast ("fast ice") and is usually 1-2 m thick (McMinn, 2000).

No valves of the fast ice species were found between 500 and 150 cm depth, thus implying a period with less fast ice. In the same period benthic diatoms of the *Navicula* group (e.g., *Navicula directa* and *Navicula* indet.) became more abundant. The occurrence of benthic species could have been promoted by an increase in light availability and/or in oxic conditions in the bottom waters due to less summer sea ice and enhanced mixing (McMinn, 2000). In addition, the decrease of the relative sea level (RSL) during the Holocene (Zwartz et al., 1998; Verleyen et al., 2005) could also have favoured benthic species. *Fragilariopsis curta* as well as other small fragilarioid diatoms show a marked increase above 450 cm and 150 cm. This indicates increasing stability of freshened surface waters rather than an increase in sea ice (McMinn, 2000) or reflects a change in seasonality.

Radiocarbon dating

The chronology of core Co1011 is based on radiocarbon ages obtained from 5 samples throughout the profile (Table 4.4.1). A moss layer in Unit II, directly above the diamict of Unit I, gave an age of 11,264±140 cal yr BP (KIA37748). Although the occurrence of moss and the diatom assemblages indicate deposition in a fresh to brackish environment, the age is probably too old and should be regarded as a maximum age for the onset of biogenic production in the basin, since glacial meltwater supply and marine influence could have contributed to a significant reservoir effect. The basal age of Unit III was interpolated from two radiocarbon ages above, assuming a constant sedimentation rate (Figure 4.4.5). The samples dated from Unit III show a consistent age/depth relation, with decreasing ages with decreasing depth (Figure 4.4.5).

4.4.4 Late Quaternary environmental history

4.4.4.1 Pre-Holocene (> 11,200 cal yr BP)

In core Co1010 from Filla Island inlet radiocarbon ages as well as the diatom record, indicate a pre-Holocene age for the deposition of the basal sediments of Unit I (KIA35023-KIA35025, KIA34078, Table 4.4.1). Nevertheless, the timing of this ice-free and marine period on Rauer Group cannot be clearly determined due to the contrary evidence of the diatom data (suggesting deposition prior to MIS 6) and the radiocarbon ages (suggesting a MIS 3 age). At least partially ice-free conditions during the last glacial have been reported from several other coastal areas around East Antarctica. Sediment sequences from Larsemann Hills indicate a marine transgression into a near coastal lake basin around 32 ka (Hodgson et al., 2009). The Windmill Islands marine sediment cores contain marine sapropels dating back to 46-26 ka (Cremer et al., 2003a). Hence, ice-free conditions during MIS 3 might also have existed in Rauer Group. The high OM content of Unit I (core Co1010) suggests enhanced productivity in the water column and seasonally open water

conditions due to a relatively warm climate. Increased input of meltwater from an ice sheet margin nearby is suggested from the low $\delta^{18}O$ values of biogenic silica.

The subsequent glaciation history of East Antarctica is complex and equivocal. Marine records from Prydz Bay indicate an expansion of the Amery Ice Shelf (Domack et al., 1998) during the last glacial maximum (LGM). In contrast, only moderate EAIS thickening and expansion is inferred from exposure ages from nunataks in western Prydz Bay (Mackintosh et al., 2007). Likewise, lake sediment sequences from Larsemann Hills, to the south of Rauer Group, indicate only minor ice sheet advances throughout the LGM (Hodgson et al., 2001a). In the Vestfold Hills, 30 km north of Rauer Group, an ice sheet thickening of c. 600 m was inferred from relative sea level reconstructions (Zwartz et al., 1998). Another study from a lake sediment record from Vestfold Hills suggests continued existence of the lake during the LGM coevally with a very limited ice expansion (Gibson et al., 2009). Glaciation of Rauer Group prior to the Holocene, most likely during the LGM, can be inferred indirectly from the sediment cores discussed here. The occurrence of a pre-Holocene diamict in the basal part of core Co1011 from Flag Island inlet indicates former ice sheet coverage of the coring location. Glacial overriding is also indicated by a discontinuity in sedimentation in core Co1010 from Filla Island inlet (Berg et al., 2009), and by glacial deposits and geomorphological observations, which suggest glaciation of Rauer Group prior to the Holocene (White et al., 2009).

4.4.4.2 Late Pleistocene to early Holocene (11,200-9200 cal yr BP)

The radiocarbon age of c. 11,200 cal yr BP (KIA37748) from the base of Unit II in core Co1011 from Flag Island inlet provides a rough estimation of ice retreat in Flag Island inlet. The timing of the onset of biogenic sedimentation in the Filla Island inlet remains vague. The radiocarbon ages from the base of Unit II in core Co1010 (13,368 cal yr BP, KIA35022; 11,305 cal yr BP, KIA34077) are likely affected by re-deposition. It can be assumed that Filla Island became deglaciated slightly later than Flag Island, if the late Pleistocene/early Holocene ice retreat was parallel to the present ice-sheet margin. Therefore, the onset of biogenic sedimentation could have occurred in the Filla Island inlet shortly after c. 11,200 cal yr BP.

The diatom assemblage in Unit II of core Co1011 suggests a near shore freshwater to brackish environment in the Flag Island inlet shortly after deglaciation. Since RSL reconstructions from nearby Larsemann Hills (Verleyen et al., 2005) suggest 4-5 m higher sea level at this stage than at present, the input of marine waters must have been partly restricted. Possible explanations for the restriction would be dead ice or a partly damming ice sheet margin at the inlet mouth during ice retreat. A slow ice-sheet retreat from the inlet would allow sufficient freshwater supply and the establishment of brackish conditions and also would allow benthic diatom colonisation on relatively stable substrates. Some input of seawater is indicated by the presence of marine diatoms in Unit II and could have occurred

either by temporary storm surges or by a permanent but very small connection to the sea. The base of Unit III in core Co1011 marks the onset of full marine conditions in the Flag Island inlet around 9100 cal yr BP (Figure 4.4.7). Since the input of terrigenous material decreases significantly at this time, it also implies the end of direct glacial influence in the vicinity of the inlet. In contrast to the Flag Island inlet, Unit II of core Co1010 does not contain any fresh water diatoms. A possible explanation for the direct establishment of marine conditions in the Filla Island inlet could be that marine waters entered the basin from the north, or from the south, where the sill is deeper, while the retreating ice sheet was blocking the eastern sill (Figure 4.4.1). Relatively high terrigenous input indicates that deglacial processes were ongoing in the catchment of Filla Island inlet until c. 9200 cal yr BP (Figure 4.4.7).

Ice retreat and the onset of biogenic production in Rauer Group starting around 11.2 ka cal BP is in good accordance with other records from the eastern Prydz Bay region. Marine sediment sequences recovered c. 30 km off Rauer Group indicate open marine conditions since c. 11,100-10,800 cal yr BP, following the accumulation of a glacial diamict (Leventer et al., 2006). Another marine record indicates open marine conditions in the eastern Prydz Bay since c. 11,400±250 cal yr BP (10,700 corrected ^{14}C yr BP, Domack et al., 1991a). However, the glaciation and deglaciation of eastern Prydz Bay may have been discontinuous, such as indicated by the onset of biogenic sedimentation in Ace Lake in Vestfold Hills around 13,250±180 cal yr BP (11,380 corrected ^{14}C yr BP, Roberts and McMinn, 1999) or in the continuous sedimentation in lacustrine basins of the Vestfold Hills and Larsemann Hills since the LGM (Hodgson et al., 2001a; Gibson et al., 2009).

4.4.4.3 Early to Mid-Holocene (< 9200-5700 cal yr BP)

Decreased minerogenic input since c. 9200 cal yr BP points to negligible deglacial and paraglacial processes (*sensu* Fitzsimons, 1996) in the catchments of both inlets (Figure 4.4.7). However, the inlets apparently differ partly in local environmental conditions throughout the Holocene, as indicated by differences in some of the proxy data. The regional environmental conditions throughout the Holocene are probably best displayed in the evolution of the diatom assemblages, which are very similar in both inlets (Figure 4.4.7).

Paleoceanographic conditions in the inlets of Rauer Group after 9200 cal yr BP were characterised by high productivity in the water column, such as indicated in the deposition of organic rich or sapropelic sediments in both inlets following the onset of marine conditions. The high proportions of open water diatoms (*Chaetoceros* spp. and *Thalassiosira gracilis*) in the records from both inlets imply seasonal ice-free conditions and a good water exchange with the open ocean. Particularly *Chaetoceros* spp. are known to bloom in spring (Stickley et al., 2005). Their high proportions around 9000 cal yr BP probably correlate with an insolation-controlled maximum in spring temperatures, such as

modelled by Renssen et al. (2005). A gradual decline of open water species and an increase in sea-ice related species (e.g., *F. cylindrus*, *F. curta*, *Navicula glacei*, and *Fragilariopsis rhombica*) implies an increasing annual duration of sea ice since c. 8200 cal yr BP. The presence of relict ice floes on the inlets in summer and a freshening of the uppermost water column due to melt-out is particularly indicated by the relatively high proportions of *F. cylindrus* and *F. curta*. The increase in sea ice, however, seems to have not restricted diatom productivity and nutrient availability, as it is indicated by high TDA and BSi contents. Colder conditions after c. 8200 cal yr BP can also be inferred from increasing terrigenous input into the Flag Island inlet (Figure 4.4.7), which is probably related to an increase in aeolian deflation of sediments on land. In addition, cooler conditions are indicated by high (marine) $\delta^{18}O$ values of diatom silica in core Co1010 which suggest comparably low input of water from meteoric sources or meltwater influx from the ice sheet.
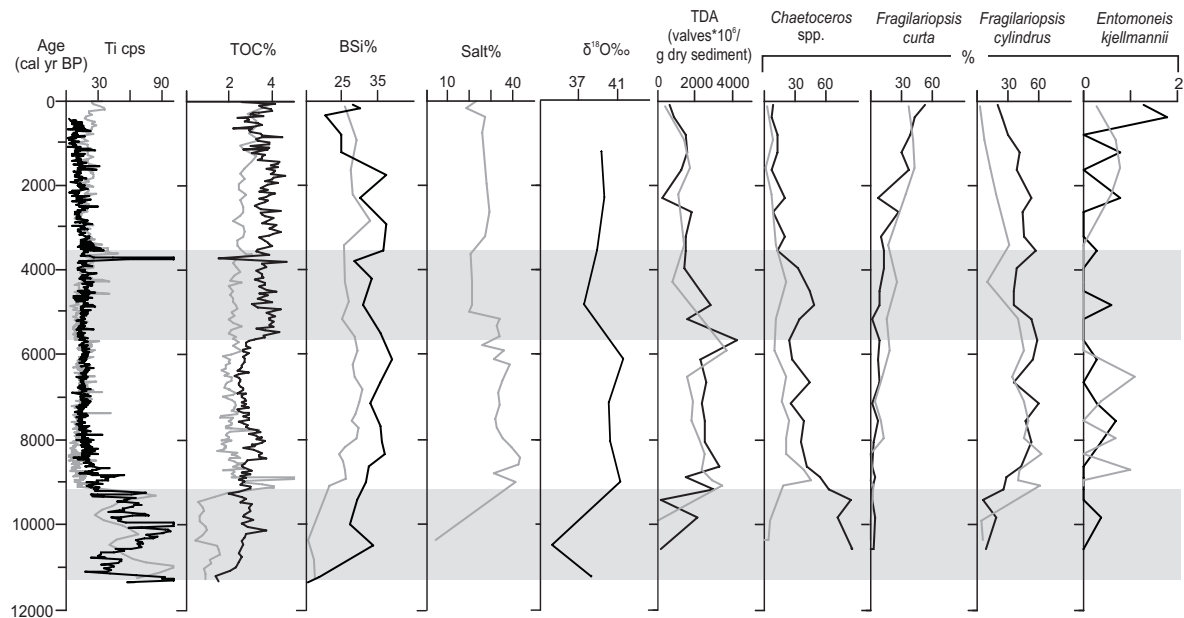
Figure 4.4.7 Holocene trend of Ti counts per second (cps), total organic carbon (TOC), biogenic silica (BSi), salt content, $\delta^{18}O$ values of diatom silica, total diatom abundance (TDA) and selected diatom species of cores Co1010 (black) and Co1011 (grey); grey rectangles underlie time slices described in the text.

An early Holocene temperature optimum and subsequent cooling around 8200 cal yr BP in Rauer Group, as suggested from the sediment records from Filla and Flag Island inlets, is in good accordance with other records from East Antarctica. Ice core records indicate warmer conditions for the period between 11,500 and 9000 yr BP and a subsequent cooling until 8000 yr BP (Masson et al., 2000). A diatom record from a marine sediment sequence from Prydz Bay indicates maximum summer ice-edge retreat between 10,700 and 7600 ^{14}C yr BP (Taylor and McMinn, 2001). Further inland, a sediment record from Lake Terrasovoje, Amery Oasis, suggests an early Holocene temperature optimum around 8500 cal, yr BP (Wagner et al., 2004; Cremer et al., 2007). Regional climate reconstructions

from Larsemann and Vestfold hills spanning the time period after the early Holocene are limited. The only existing records from these areas are from low-lying lake basins. The effects of climate change in these basins are overprinted by marine/lacustrine transitions coupled to RSL change (Roberts and McMinn, 1999; Verleyen et al., 2005).

4.4.4.4 Mid-Holocene (c. 5700-3500 cal yr BP)

In the Filla Island inlet an increase in TOC around 5700 cal yr BP suggests higher productivity. This is, however, not supported by BSi contents and diatom assemblage. It may be speculated that OM is better preserved in the sediments at this time due to a shift in the hydrological conditions and more stratification of the water column. A minimum in δ^{18}O of BSi indicates increased meltwater input around 4800 cal yr BP and implies warmer summers around this time. Less sea ice in summer between 5200 and 3700 cal yr BP is also indicated by an increase in *Chaetoceros* spp. resting spores, and a decrease of *F. cylindrus* (Figure 4.4.7).

In Flag Island inlet evidence for less sea ice between c. 5900 and 3000 cal yr BP comes from the absence of *Entomoneis kjellmannii*, an indicator for permanent sea ice cover (McMinn, 2000). A freshening of the water column due to less extensive brine exclusion from sea ice formation or due to freshwater input can be deduced from lower salt content in the pore water of the sediments. The more open conditions, however, seem not to be accompanied by increased diatom production, since BSi content is lower between 5600 and 3500 cal yr BP. The simultaneous increase in benthic diatoms, such as *Navicula directa* (McMinn, 2001) could result from less sea ice, but might be also related to a decrease of the RSL (Zwartz et al., 1998; Verleyen et al., 2005; Figure 4.4.7). The slightly changing climate conditions apparently also affected the catchment of Flag Island inlet. Some clastic rich and fine-grained layers between c. 4600 and 3500 cal yr BP were probably episodically brought into the basin by increased meltwater inflow. On the other hand, an overall decline of clastic input into the inlet after c. 5600 cal yr BP indicates less aeolian transport, which might be due to snow-covered or wetter soils in the catchment or reduced wind speed (Figure 4.4.7). Slightly warmer conditions, with less sea ice and increased meltwater inflow, are perceivable in both inlets between c. 5700 and 3000 cal yr BP. The apparent stronger imprint of changes in the catchment onto the record from Flag Island inlet is due to its smaller size and shallower water depths compared to Filla Island inlet. Intense meltwater supply from a locally expanded ice sheet margin in Rauer Group in the Mid-Holocene is rather unlikely. A marine sediment core, recovered 1.8 km in front of the present ice sheet margin, provides no evidence for a significant ice sheet expansion during the past 4500 years (Berg et al., in press). A potential source for meltwater could be the Sørsdal Glacier to the north of Rauer Group. However, there is no indication for an expanded glacier during the Mid-Holocene around c. 4000 cal yr BP (3770 corrected ^{14}C yr, Fitzsimons, 1997). In contrast, there is some evidence for ongoing deglacial processes

in the Prydz Bay region in the Mid-Holocene. Intensified ice retreat from Stornes Peninsula, western Larsemann Hills, has been reconstructed from lake sediments for the past 4000 years (Hodgson et al., 2001a). Hemer and Harris (2003) report a retreat of the Amery Ice Shelf since 5800-5600 cal yr BP (corrected 5700 ^{14}C yr BP). Increased melting and open water conditions inferred from Rauer Group as well as from other sites could be related to a climate optimum, which is suggested from ice core data between 6 and 3 ka for East Antarctica (Masson et al., 2000). Evidence for a Mid-Holocene climate optimum also comes from sediment records of Pup Lagoon, Larsemann Hills, where open water and stratified conditions were present until 4770-4440 cal yr BP (corrected 4785±45 ^{14}C yr; Verleyen et al., 2004). A climate optimum between 4700 and 2400 cal yr BP was also inferred from the presence of plentiful food for penguins at Gardner Island off Vestfold Hills (Huang et al., 2009). Further inland, the record from Lake Terrasovoje, Amery Oasis, indicates increased ice and snow cover of the lake between 6200 and 3700 cal yr BP (Wagner et al., 2004), which is probably correlated with the inferred reduced aeolian clastic matter supply from the catchment around Flag Island inlet. It seems, however, that environmental change of Rauer Group were only marginal, as we have only found slight changes in the proxies investigated.

4.4.4.5 Late Holocene (> 3500 cal yr BP)

RSL in eastern Prydz Bay gradually decreased in the late Holocene (Zwartz et al., 1998; Verleyen et al., 2005). The divergent trend of terrigenous input into Rauer Group basins (Figure 4.4.7) is probably a result of this RSL decrease, as clastic matter supply may have had a stronger impact on the smaller inlet of Flag Island. The RSL change apparently also affected the hydrology of the basins. Decreasing RSL might have had an influence on the ecology of the basins in Rauer Group, as it has changed, for example, habitat availability for benthic diatoms. Decreasing RSL also could have favoured the persistence of sea ice in summer, as water exchange and wind fetch in the basins became reduced. A gradual increase in sea ice after the Mid-Holocene is reflected by the increase in *F. curta* and *F. cylindrus* compared to *Chaetoceros* spp. (Figure 4.4.7). The longer persistence of sea ice in summer promoted density stratification (Gibson, 1999) and reducing conditions, such as reflected by high sulphur contents and lamination of the sediments. The marked increase of *F. curta* in both records since c. 2000 cal yr BP is not accompanied by a marked increase in fast ice diatoms, arguing against a further increase in the duration of sea ice cover during summer. Evidence for lower productivity since c. 1700 cal yr BP, however, is provided by lower TOC and BSi content in Co1010 and by a decrease in TDA in both cores (Figure 4.4.7), indicating less favourable conditions for diatoms in the inlets e.g., due to restricted nutrient availability. The diatom assemblage in the inlets of Rauer Group is probably not solely controlled by the absolute annual duration of sea ice cover, but also by the timing of its formation. A shift of sea ice formation to later in the season would agree with the

ecology of *F. curta* (McMinn et al., 2000) and with an insolation controlled late Holocene maximum in autumn temperatures (Renssen et al., 2005).

Late Holocene cooling and ice advances have been observed in several records from coastal regions in East Antarctica (e.g., Cremer et al., 2003a; Ingólfsson, 2004; Hall, 2009). In the open marine realm of Prydz Bay a late Holocene cooling and increased sea ice duration since 2020-1670 cal yr BP (2600 corrected ^{14}C years) was inferred from an increase in ice related diatom species (Taylor and McMinn, 2002). An increase in fast ice diatoms in sediment cores from marine inlets in Vestfold Hills provide evidence for a late Holocene cooling since 1590-1860 cal yr BP (2500 corrected ^{14}C years, McMinn, 2000; McMinn et al., 2001).

4.4.5 Conclusions

Two sediment cores from marine inlets in Rauer Group have been investigated in a multi-proxy study. While biogeochemical proxies provided evidence for changes in production and preservation of organic material, analysis of diatom assemblages gave valuable insights into salinity and sea ice evolution in the inlets. Late Pleistocene radiocarbon ages, derived from marine sediments in core Co1010 from Filla Island inlet are probably biased by older reworked sediments, while chronologies obtained for the Holocene period are supposed to be reliable, since radiocarbon ages show no reversals. Marine sediments of pre-Holocene age, preserved in Filla Island inlet, indicate ice-free conditions in Rauer Group sometime within the last glacial cycle, probably during the second half of MIS 3. The two core records provide evidence for subsequent ice sheet coverage of Rauer Group during the LGM. Our reconstructions confirm the non-uniform expansion of the EAIS during the LGM. The proximity of areas, which were glaciated, to areas which were not, points to a strong influence of local features (e.g., topography) on ice sheet movement.

Deglaciation of Rauer Group around the Pleistocene/Holocene transition can be inferred from the onset of biogenic sedimentation in the inlets around c. 11,200 cal yr BP. Ongoing ice retreat from the islands and marine production under relatively open water conditions indicate an early Holocene optimum until 8200 cal yr BP, which is followed by a period with increased sea ice. In the Mid-Holocene both basins experienced an input of freshwater between c. 5700-3500 cal yr BP. Probably warmer conditions caused ice-sheet melting and increased precipitation on the islands. In late Holocene sea ice increased in both inlets, however, neoglacial cooling, which has widely been inferred from sedimentary records in East Antarctica, is not very pronounced in the inlets of Rauer Group. Changes in climate conditions seem to cause only slight changes in environmental conditions in the marine inlets. Response to Holocene changes proceeded relatively slowly and the diatom records point to changing seasonality, suggesting insolation-induced changes in Rauer Group.

4.5 No significant ice sheet expansion beyond present ice margins during the past 4500 yr at the Rauer Group, East Antarctica

Abstract

The history of glacial advances and retreats of the East Antarctic ice sheet during the Holocene is not well known, due to limited field evidence in both the marine and terrestrial realm. A 257 cm-long sediment core was recovered from a marine inlet in the Rauer Group, East Antarctica, 1.8 km in front of the present ice sheet margin. Radiocarbon dating and lithological characteristics reveal that the core comprises a complete marine record of the past 4500 yr. A significant ice sheet expansion beyond present ice margins therefore did not occur during this period.

4.5.1 Introduction

The East Antarctic Ice Sheet (EAIS) currently holds c. 79% of global ice masses, which equals about 52 m of sea level equivalent (Lythe et al., 2001). Mass balance changes of the EAIS could thus have a significant impact on global sea level. However, mass balance estimations for the EAIS indicate that only minor changes have occurred in recent decades (Mayewski et al., 2009); whilst the West Antarctic Ice Sheet (WIAS) is showing dynamic and large ice volume fluctuations (Wingham et al., 2006), and the smaller ice areas on the Antarctic Peninsula (AP) are affected by the fast warming of the region (Vaughan et al., 2003).

The reconstruction of past glacial advances and retreats is difficult because of the complex reactions of glacial systems on changes in accumulation rates and temperature (Goodwin, 1998). Advances of East Antarctic alpine glaciers, ice sheet margins and outlet glaciers during the mid and late Holocene have been reconstructed from glaciological and geomorphological field evidence (e.g., see review by Hall, 2009). Yet, the extent of such advances is difficult to assess because robust chronological constraints are often lacking. Records, which allow precise dating and recognition of small-scale changes are needed to improve the understanding of past changes of the EAIS under different climatic conditions, and to help measure the regional variability of these changes and to gain a holistic view of the whole ice sheet. This is a major precondition to substantially improve future predictions about the impact of the recent global warming on ice sheets.

The Prydz Bay region is a crucial site for reconstructing past developments of the EAIS, because it encompasses the largest drainage system in Antarctica (O'Brien et al., 2007). Field evidence for glacier and ice sheet advances in the Prydz Bay region during the Holocene is rather sparse. A marine record from eastern Prydz Bay indicates a re-advance of floating glacial ice between c. 7300 and 3800 ^{14}C yr BP (Domack et al., 1991b), this observation is however not confirmed by another record from the same area (Taylor and McMinn, 2002). In the Vestfold Hills, eastern Prydz Bay, Holocene ice retreat was

interrupted by the so-called Chelnock Glaciation within the last 2000 ^{14}C yr BP, when the northern margin of the Sørsdal outlet glacier expanded (Adamson and Pickard, 1983). A limited extent of Holocene glacial re-advances was proposed by Fitzsimons and Colhoun, (1995), with ice advances of less than 500 m in the Vestfold Hills. A local glacier re-advance of unknown extent around c. 2600 cal yr BP has been reconstructed from relative sea-level observations in nearby Larsemann Hills (Verleyen et al., 2005).
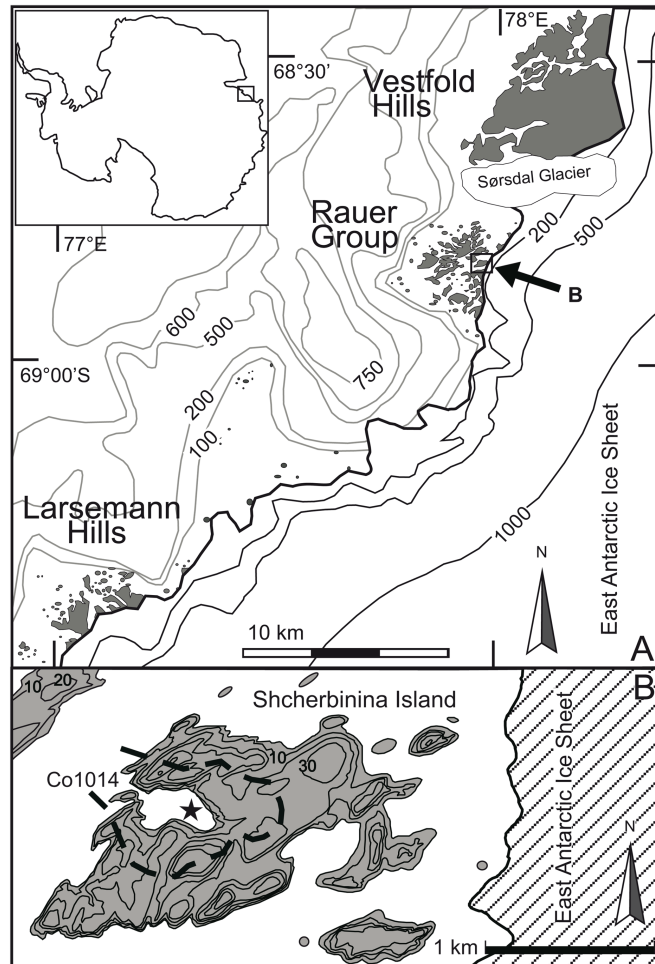
Figure 4.5.1 Eastern Prydz Bay, Antarctica, with presently ice-free coastal areas (dark grey). Rectangle in Rauer Group indicates the location of Shcherbinina Island and core Co1014 (A). Topographic map of Shcherbinina Island with hydrological catchment of the cored inlet (dashed line) and coring location Co1014 (star) (B).

The Rauer Group, located between Larsemann Hills and Vestfold Hills, consists of several ice-free and low-lying islands (Figure 4.5.1A) and is delimited by the EAIS to the east and bordered by outlet glaciers to the north and south. A rather stable ice sheet margin, with maximum ice expansion of less than 500 m throughout the Holocene, is inferred from the degree of weathering of glacial deposits (White et al., 2009). However, precise dating of the deposition of the glacial erratics and moraines deposited on Rauer Group is difficult.

A sediment core was recovered from a 6.3 m deep marine inlet located at Shcherbinina Island in the northern Rauer Group (Figure 4.5.1A). The distance from the coring location

to the present ice sheet margin measures c. 1.8 km (Figure 4.5.1B), and the hydrological catchment of the inlet comes as close as 1.3 km to the ice margin. The close distance of the core to the present ice sheet margin in combination with relatively well dateable coastal marine sediments make the record an important contribution to better understand the timing and extent of past ice sheet movements.

4.5.2 Results and discussion

The sediment core (Co1014) recovered from the marine inlet has a length of 257 cm. The sediments are of black colour and show faint lamination throughout. Low compaction is indicated by the high water content (Figure 4.5.2). The high proportion of organic material is reflected by TOC (1.6-5.0%) and particularly by biogenic silica (BSi) (16-27%). Microscopic inspection of some samples showed that diatoms form the main source of BSi. The terrigenous fraction of the sediments is in general fine grained, but some angular sand and gravel grains occur sporadically. Whilst the sand could originate from aeolian transport, the gravel clearly indicates ice-related transport, most likely due to drifting ice floes. The relatively uniform lithology of core Co1014 provides no evidence for a change in sedimentation processes.
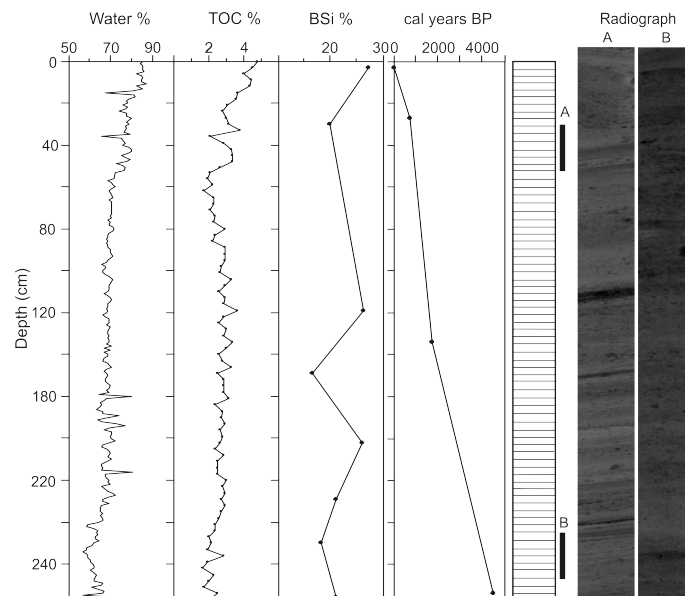
Figure 4.5.2 Water content, TOC (total organic carbon), BSi (biogenic silica), and calibrated radiocarbon ages of core Co1014. Lithological profile and radiographic images (2 cm in width) illustrate the laminated and monotonous appearance of core Co1014.

The age-depth model of core Co1014 (Figure 4.5.2) is based on four AMS radiocarbon ages. The ages were determined on the humic acid free (HAF) fraction of bulk organic carbon samples at the Leibniz Laboratory for Radiometric Dating and Isotope Research in Kiel, Germany (Table 4.5.1). A local reservoir effect of 1000 yr was estimated from the uppermost dated sample KIA 38366 (Table 4.5.1) and matches closely with that from 2 other marine inlets in the Rauer Group, where a reservoir effect of 920±80 and 890±25 ^{14}C yr was measured (Berg et al., 2009). It is likely that changes in the reservoir effect over

time occurred. However, since these changes cannot be determined, the modern reservoir effect is taken as constant over time. The radiocarbon ages were calibrated into calendar years (cal yr BP) using the Calib 5.1 rev programme (Stuiver et al., 2005) and the Marine04 data set (Hughen et al., 2004) with a deviation of 362 yr for the Southern Hemisphere (Stuiver and Braziunas, 1993) and a ΔR of 638 yr for the local reservoir effect. The radiocarbon ages of core Co1014 indicate a succession of increasing ages with increasing depths. The sample from the base of the core has an age of 4400-4615 cal yr BP (KIA38369; Table 4.5.1). Since major changes in sedimentation rates do not exist, core Co1014 likely contains a complete mid to late-Holocene record.

Table 4.5.1 Radiocarbon ages of the humic acid free fraction (HAF) of bulk organic matter in core Co1014. For calibration an ΔR of 638 yr was applied to correct for local reservoir effect, calibrated ages are given as 2 σ range.

Lab. No.	Depth [cm]	^{14}C age [^{14}C yr BP]	Calendar age [cal yr BP]	Mean [cal yr BP]
KIA38366	3-4	1000±25	-3 to 66	31±34
KIA38367	27-28	1815±30	656-785	720±64
KIA38368	134-135	2785±30	1630-1828	1729±99
KIA38369	254-255	5000±35	4400-4615	4507±107

4.5.3 Interpretation

The expanded ice sheet covered the Rauer Group region during the latter half of the last glacial cycle (White et al., 2009), and probably throughout the LGM. The onset of marine conditions after deglaciation was dated to the early Holocene in a marine basin located c. 6 km off the present ice sheet margin, 5 km to the northwest of coring location Co1014 (Berg et al., 2009). The basal age of core Co1014 from the inlet at Shcherbinina Island implies that the ice margin had reached a position comparable to the present prior to c. 4500 cal yr BP and deglaciation of the islands was virtually complete. Moreover, the presumed continuous marine sedimentation preserved in the sediment record indicates that the coring location was not overriden by an advancing ice sheet during the past c. 4500 yr. It is even unlikely that the ice margin reached the catchment of the inlet in Shcherbinina Island during the past c. 4500 yr, since significant changes in the sediment composition are absent. Also, taken in concert with the weathering data presented by White et al. (2009) it can be argued that the ice sheet has not advanced more than 500 m beyond its present position during this time. Hence, mid to late Holocene advances of the ice sheet margin must have been less than 1.8 km compared to the present ice sheet margin, and likely did not exceed 0.5 km.

Furthermore, continuous marine sedimentation within the core during the past 4500 yr indicates that the site, and likely the shallow sill (2 m below sea level), have remained below sea level during this time, precluding the possibility of significant isostatic uplift

during this period. Thus, it is unlikely that the regional or local ice load has altered significantly during this period - either by ice advance or retreat.

The well-dated record from Shcherbinina Island suggests relatively stable environmental conditions in the Rauer Group during the mid and late Holocene. This implies that the mid to late Holocene warm periods observed in the neighbouring ice-free regions (e.g., McMinn et al., 2001; Verleyen et al., 2004a) either did not or only slightly affect the Rauer Group, or that the mid to late Holocene temperature did not exceed the present temperature regime. Also, the relative sea level changes observed in Larsemann Hills are not necessarily replicated throughout the Prydz Bay region, or indeed throughout East Antarctica, providing further evidence that the East Antarctic Ice Sheet can behave quite heterogeneously, even on relatively small spatial scales. Thus, care must be taken to ensure that events recorded at high resolution sites such as the relative sea level curve at the Larsemann Hills are replicated across multiple sites before they are interpreted as representing the behaviour of large sectors of the continent, or of entire drainage basins such as the Lambert Glacier-Amery Ice Shelf System.

Lastly, our results confirm that the post-glacial rebound model (Ivins and James, 2005) used by satellite remote-sensing data of ice elevations and ice motion are a reasonable approximation. Thus, the evidence of stability up until recent years is reasonable (e.g., Rignot et al., 2008). On the other hand, modelling suggests an increased ice loss since the year 2006 (Chen et al., 2009), which might be an indication that the recent temperature increase indeed exceeds the mid to late Holocene warm periods reconstructed for East Antarctica.

4.6 Late Pleistocene configuration of the East Antarctic Ice Sheet - evidence from coastal ice-free areas

Abstract

Radiocarbon ages from a lake sediment core from Rauer Group, East Antarctica, provide evidence for a lacustrine environment on Filla Island around 37-30 ^{14}C ka BP (41-34 cal ka BP). Ice-free conditions are further supported by a further radiocarbon age of 35.6 ^{14}C ka BP (40.4 cal ka BP) from a marine shell (*Laternula elliptica*), which was collected from re-deposited marine sediments in a lake basin on Filla Island. Radiocarbon ages from Rauer Group as well as from other coastal areas around East Antarctica strongly suggest that the East Antarctic Ice Sheet (EAIS) did reach only insignificantly beyond its present margins in the second half of Marine Isotope Stage (MIS) 3. In Rauer Group and Vestfold Hills in eastern Prydz Bay as well as in Sôya Coast (Lützow-Holm Bay), relative sea level (RSL) reconstructions point to increased ice load in the vicinity of the coast. Since higher ice load is not accompanied by a significant lateral expansion, a steeper than present ice sheet profile during the last glacial can be inferred.

4.6.1 Introduction

During the last glacial the growth of continental ice sheets, mainly in Northern Hemisphere, resulted in a significant draw down of global sea level of several tens of meters, reaching a minimum of -120 m during the Last Glacial Maximum (LGM) between 30 and 19 ka (Bard et al., 1990; Huybrechts, 2002; Lambeck et al., 2002a; Lambeck et al., 2002b). In MIS (Marine Isotope Stage) 3 (59-29 thousand years BP; Voelker et al., 2002) millennial scale sea level fluctuations with amplitudes of 10-15 m occurred, reflecting changes in global ice volume (Lambeck et al., 2002b; Yokoyama et al., 2007). There is some indication for instability of the Antarctic ice sheet from millennial-scale pulses of ice rafted detritus (IRD) in the Southern Ocean during the same period (Kanfoush et al., 2002). However, relatively little is known about ice sheet configuration during the last glacial in East Antarctica. Evidence on ice sheet configuration and environmental conditions around East Antarctica during the last glacial comes from coastal ice-free areas, which comprise less than of 0,4% of the area of Antarctica today (SCAR, 2007; Figure 4.6.1). Although, erosion by glacial processes usually limits the preservation of soft sediments in these so-called Antarctic oases, lacustrine and coastal marine records provide sediment sequences, which are of late Pleistocene age (Igarashi et al., 1995; Miura et al., 1998; Schwab, 1998; Hodgson et al., 2001a; Cremer et al., 2003a). Radiocarbon ages point to biogenic production and a less expanded ice sheet during the second half of MIS 3. In this study we will present new data from Rauer Group, which reinforce the assumption of ice-free coastal areas in East Antarctica within the last glacial. Furthermore a review of previous

results from coastal East Antarctica will be given, to provide a base for a discussion on EAIS configuration during this period.
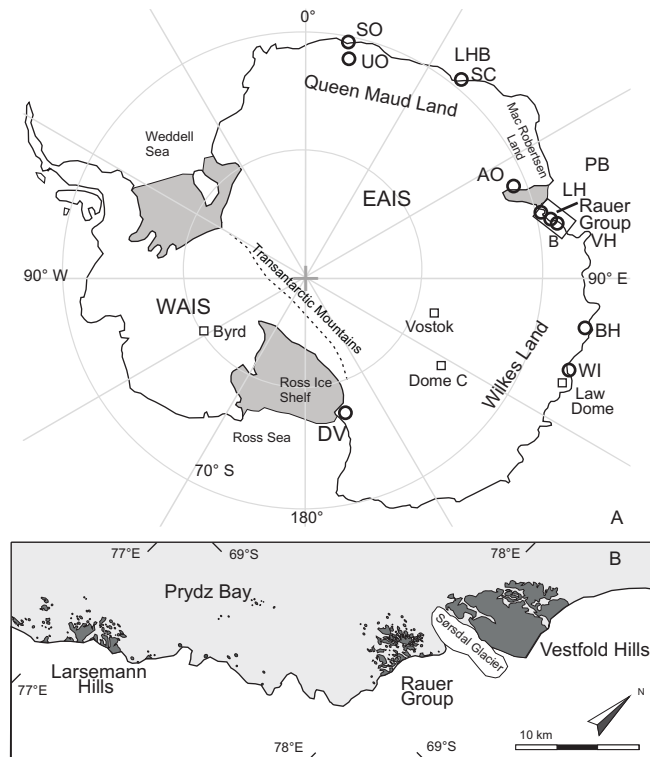
Figure 4.6.1 Map of Antarctica with the geographic sites mentioned in the text; EAIS East Antarctic Ice Sheet, WAIS West Antarctic Ice Sheet, SO Schirmacher Oasis, UO Untersee Oasis, LHB Lützow-Holm Bay, SC Sôya Coast, AO Amery Oasis, PB Prydz Bay, LH Larsemann Hills, VH Vestfold Hills, BH Bunger Hills, WI Windmill Islands, DV Dry Valleys A). Eastern Prydz Bay with Rauer Group and other ice-free sites B).

4.6.2 Rauer Group

Rauer Group is an ice-free archipelago in eastern Prydz Bay (Figure 4.6.1). On the larger islands several shallow lakes and ponds can be found, which are mostly saline due to the dry conditions in the region (Hodgson et al., 2001b). Skua Lake (unofficial name) located at 9.5 m a.s.l. on Filla Island is an exception, since its water is brackish to saline and water depth reaches a maximum of 120 cm (Wagner et al., 2008; Figure 4.6.2). Seasonal lake level fluctuations in Skua Lake are very likely, since watermarks are present 20-30 cm above the lake level at the time of field work.

4.6.2.1 Materials and methods

Two overlapping sediment cores were recovered from Skua Lake from the 8.5 cm thick ice cover at the same coring location with an Eijkelkamp piston corer (Co1008-5 and -6). Additionally, sediment samples were collected from a very shallow un-named lake basin close to Skua Lake (68°48.758' S; 77°56.055' E; Figure 4.6.2) and from recent marine mud, which were microscopically investigated for their fossil content (Table 4.6.1). A

large shell fragment (*Laternula elliptica*) was selected from the sample from the un-named lake for radiocarbon dating.

From the sediment cores of Skua Lake semi-quantitative XRF elemental scans were obtained on core halves using an ITRAX XRF core scanner (Cox Ltd.; Croudace et al., 2006). For elemental analysis with a molybdenum X-ray tube settings for measurement were chosen as to 30 mA and 30 kV, an exposure time of 20 sec, and a step-size of 2 mm. The cores were sub-sampled in 2 cm slices, freeze-dried, and aliquots were ground to < 63 µm for further analyses. Elemental analyses for total nitrogen (N) and total sulphur (S) was conducted with a Vario Micro Cube combustion elemental analyzer (VARIO Corp.) and total organic carbon (TOC) was quantified with a DIMATOC 200 (DIMATEC Corp.).
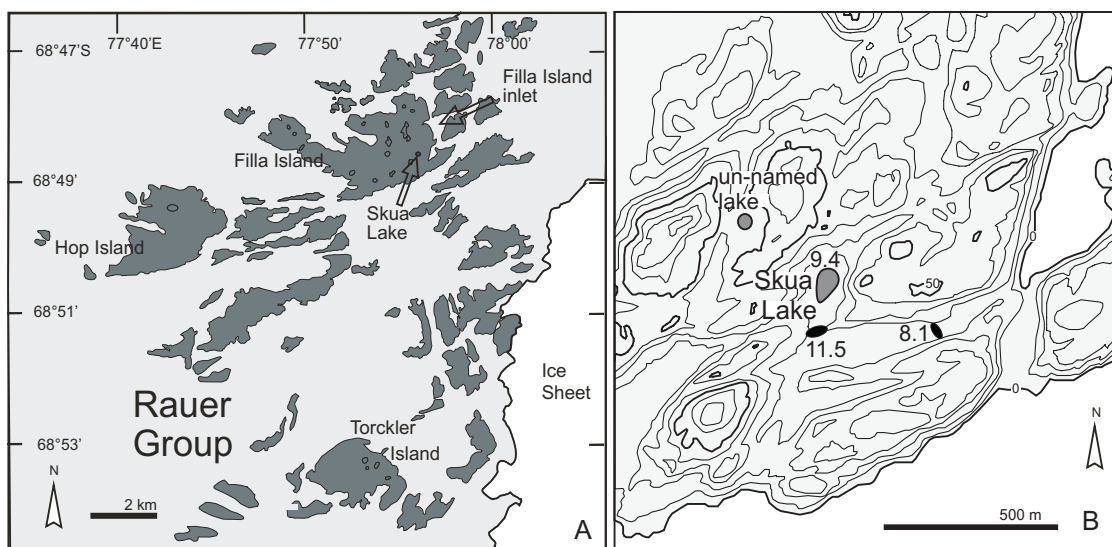
Figure 4.6.2 Map of Rauer Group with the location of Skua Lake on Filla Island and Filla Island inlet (A). Topographic map of the surroundings of Skua Lake and the location of un-named lake, numbers indicate altitude of lake level and topographic heights in m above sea level (B).

Radiocarbon dating of the carbonate of the shell fragment from the un-named lake (KIA33455) was conducted at the AMS facility of the Leibniz Laboratory for Radiometric Dating and Isotope Research in Kiel, Germany (Table 4.6.2). One sediment sample from the Skua Lake record was dated at the Swiss Federal Institute of Technology (ETH) Zurich, Switzerland. The carbonate fraction (TIC) and total organic carbon (TOC) fraction were dated separately from this sample (ETH-38772, ETH-38771). Radiocarbon ages cited within this study have been calibrated with CalPal-2007 online (Danzeglocke et al., 2008) with the calibration data set CalPal2007Hulu (Weninger and Jöris, 2008, Table 4.6.2). In the absence of a suitable model for a marine reservoir effect during the last glacial, no such correction has been applied. A calibration of radiocarbon ages, however, is necessary to achieve better comparability to other time scales since the offset between the radiocarbon age and calendar age is up to several thousand years in the time period considered in this study (e.g., Table 4.6.2).

4.6.2.2 Results and discussion

The sediment sample from the un-named lake on Filla Island (Figure 4.6.2) contains numerous shell fragments, most likely of *Laternula elliptica*. Remains of other marine organisms like echinoidea indet. and *spirorbis* sp. could be identified, which are also abundant in recent marine mud (Table 4.6.1). Fossils indicate a marine origin, but probably they are not *in situ*. Redeposition of marine sediments by glacial overriding and subsequent outwash from glacial deposits into the basin probably occurred (Gore et al., 1994). Nevertheless, the size and preservation of the fossils indicate no intense reworking. The radiocarbon dating of the shell fragment from *Laternula elliptica* yielded a radiocarbon age of 35,680±650 ^{14}C yr BP, what indicates growth of the shell in a near shore marine environment around 40.4±1 cal ka BP.

Table 4.6.1 Macro fossils identified in sediment samples from an un-named lake at 68°48.758'S; 77°56.055'E on Filla Island, 26 m a. s. l. and from recent marine mud.

Site	Benthic calc. foraminifera indet.	Agglutinating foraminifera indet.	Hydroidea indet.	*Spirorbis* sp.	Serpulidae indet.	Turbellaria *indet.*	Gastropoda indet.	*Laternula elliptica*	Ostracoda indet.	Bryozoa indet.	Echinoidea indet.	Pisces indet.	Marine algae indet.	Calcareous algae indet.	Diatoms
Un-named lake	r	-	-	r	-	-	-	a	-	-	c	-	r	r	-
Recent marine mud	a	r	r	r	-	r	c	-	r	r	a	r	-	-	a

r = rare, a = abundant, c = common.

The sediments from Skua Lake have been described as black coloured and with a bituminous smell in the field (Wagner et al., 2008). However, the sediments were rather dry and brownish oxidised, when cores were opened later in the lab.

Core Co1008-5 (153-0 cm depth) can be divided into two lithological units. The sediments of Unit I (153-110 cm depth) show layering on mm to cm scale, with changing proportions of sand, silt, and carbonate. A rock fragment of 4 cm in diameter, embedded in a sandy matrix, at 130 cm depth could be IRD. The minerogenic fraction shows a relatively constant composition, reflected by co-varying Ti and K intensities. Between 125 and 115 cm depth higher K intensity relative to Ti, indicates a change in composition, probably due to a higher proportion of silt and clay (Figure 4.6.3). The redox-sensitive elements Fe and Mn (e.g., Brumsack, 2006) closely co-vary in Unit I, probably either due to relatively constant redox conditions throughout sedimentation or due to a dominant detrital source of both elements with constant composition. Sulphur contents are relatively low (< 1%) which is also reflected in the low S intensities of XRF analysis. An increase in S intensities corresponds to fine gypsum layers with very small crystals in the uppermost centimetres of Unit I (Figure 4.6.3). An overall TOC content of < 0.4% points to very low incorporation of organic matter (OM) either due to low biogenic production or due to poor preservation.
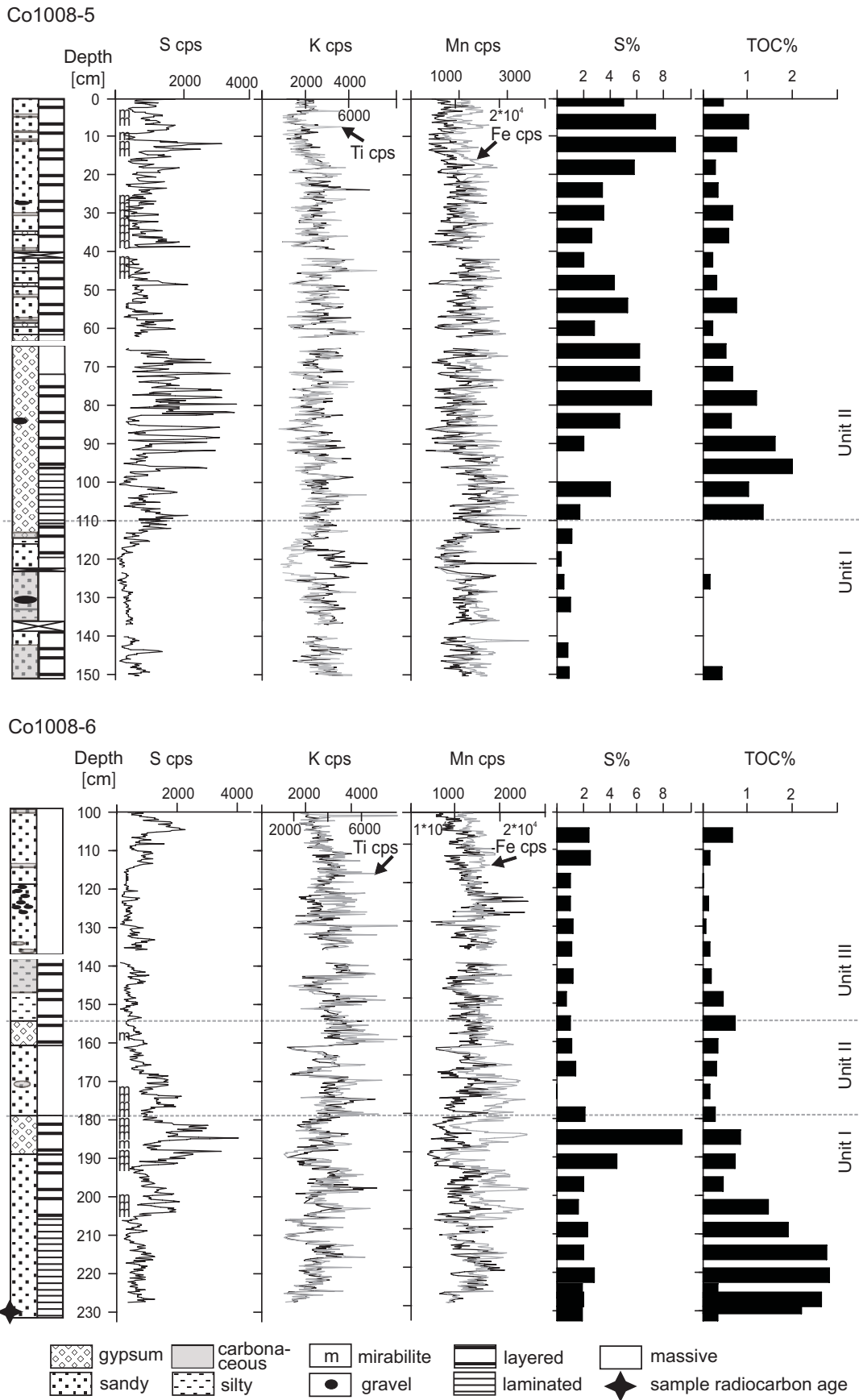
Figure 4.6.3 Lithological profiles of cores Co1008-5 and -6. Element intensities in counts per second (cps) of sulphur (S), potassium (K), titanium (Ti), iron (Fe) and manganese (Mn) from XRF core scanner and absolute concentrations of total sulphur (S), total organic carbon (TOC).

In Unit II (110-0 cm depth) TOC indicates production and biogenic sedimentation, with maximum TOC content (> 2%) between 110 and 90 cm. The minerogenic fraction is sandy and unrounded and of relatively constant composition (Figure 4.6.3). The sediment contains gypsum, which can be identified from crystals and from high S contents and S element intensities (Figure 4.6.3). From 110-90 cm layers of lensoidal gypsum crystals regularly interchange with sandy material, above, the sediment mainly consists of idiomorphic crystals. In the upper 60 cm gypsum crystals up to 0.5 cm in diameter are interspersed in the minerogenic detritus. Some horizons contain transparent crystals, which are most likely mirabilite. These crystals decayed and turned into a white powder after freeze-drying. This reaction points to a transformation of mirabilite ($Na_2SO_4*10\ H_2O$) into thenardite (Na_2SO_4) by dehydration (Gore et al., 1996). By the time of sampling the lake water was brackish, but probably not saline enough to precipitate sulphates. Precipitation of mirabilite has been ascribed to cryo-concentration of brines from freezing seawater (Marion et al., 1999). The presence of mirabilite could indicate a deep-freezing of the water column in winter, resulting in precipitation of salts. The absence of a shallow permafrost level below the lake, however, implies permanent presence of water in the lake basin.

Core Co1008-6 (231-100 cm depth) can be divided in three lithological units. Unit I (231-180 cm depth) is laminated, what implies *in situ* bedding of the sediments. A TOC content up to 2.8% is probably derived from layers of decayed microbial mats, which alternate with lighter, likely carbonaceous, layers. The minerogenic component is mainly sandy, with interspersed coarser grains, which are probably IRD. Within Unit I TOC decreases whereas gypsum crystals and mirabilite become abundant (Figure 4.6.3), which points to successive desiccation of the water column. A lacustrine origin of the sediments is likely since the formation and deposition of gypsum crystals indicates sedimentation in a basin with restricted water input.

Radiocarbon dating of one sample from 227-228 cm depth provided ages of 37,110±510 ^{14}C yr BP for the TIC and of 30,015±150 ^{14}C yr BP for the TOC fraction of the sediment (Table 4.6.2). The age offset of c. 7000 years points to either different carbon sources for carbonate precipitation and biogenic production, or to the input of reworked older material. Since both mechanisms produce "too old" ages, the age derived from TIC is most likely overestimating the actual age of deposition.

Unit II (180-150 cm depth) mainly consists of poorly sorted, sandy material. Low TOC and S contents points to low incorporation of organic matter and gypsum. The massive structure of the sediments, with several cracks and incorporated lenses of carbonaceous material, probably indicates cryoturbation due to subaerial or subglacial freezing. Unit III (150-100 cm) shows crude layering reflected by changes in grain size and sorting. While the bottom of Unit III consists of silt to fine sand, coarse sand and gravel-sized clasts are

abundant between 130 and 120 cm. TOC is almost absent (Figure 4.6.3), either due to the absence of biogenic production or due to deficient preservation of OM in the sandy sediments.

A direct correlation of the two cores Co1008-5 and -6 is not possible since common features like characteristic layers could not be observed. The comparison of the lithologies of both cores suggests that Unit I of core Co1008-5 corresponds to Unit III in core Co1008-6. Both units are low in organic carbon and gypsum crystals are almost absent. The absence of correlation tie-points indicates an inhomogeneous sedimentation, to an uneven relief of the lake bottom during deposition or to deformation after deposition.

4.6.2.3 Interpretation of the Skua Lake record

The origin of relatively large amount of salts, especially sulphates, in the sediment cores from Skua Lake point to a marine origin of the ions. Hodgson et al. (2001b) proposed that salt in the low-lying basins of Rauer Group originates from trapped seawater following isostatic uplift. Raised beach sediments on Filla Island can be found up to 8.5 m a.s.l (White et al., 2009) which is in accordance with a regional Holocene relative sea level (RSL) high stand of 8-9 m (Verleyen et al., 2005). An adjacent sill of 11.5 m a.s.l. between Skua Lake and the sea therefore precludes an ingression into Skua Lake during the Holocene (Figure 4.6.2). Gibson et al. (2009) interpreted the occurrence of marine salts in Abraxas Lake, which is located above the Holocene marine limit in Vestfold Hills, as an indication for its existence since MIS 5e, when eustatic sea level was higher. In Skua Lake, however, salt probably reaches the basin as aerosols (e.g., from sea spray) or it is derived from washed out surficial salt from the catchment (Gore et al., 1996). The radiocarbon ages from Skua Lake indicate deposition of the laminated sediments around 37-30 ^{14}C ka PB (41-34 cal ka BP) in a lacustrine environment and suggest that Filla Island was ice-free for some time during the late MIS 3. The shell from the un-named lake furthermore points to, probably coevally existing, marine environments around 35 ^{14}C ka BP (40.4 cal ka BP). The following period of minerogenic sedimentation (Unit III, Co1008-6 and Unit I, Co1008-5) was characterised by negligible biogenic sedimentation. Due to a lack of further radiocarbon ages neither this period nor the onset of the following productive conditions can be dated so far.

Further evidence for ice-free conditions in Rauer Group within the last glacial comes from a sediment core (Co1010), recovered in a marine inlet at Filla Island (Berg et al., 2009; Figure 4.6.2). The sapropelic sediments at the base of core Co1010 indicate open marine conditions and input of meltwater from the ice sheet during late MIS 3 (Berg et al., 2009; Berg et al. *submitted*). Except for one sample (KIA35024) the radiocarbon ages, obtained from the humic acid free fraction (HAF) of bulk organic carbon of the sediments, are in stratigraphic order and range from 40-37 ^{14}C ka BP (44.7-41.7 cal ka BP; Table 4.6.2). Since all three sites are located at or near Filla Island, the ice sheet margin in Rauer Group

was probably not expanded beyond its present position for more than 6 km around 40-30 ^{14}C ka BP (44.7-34 cal ka BP). Although the chronology of core Co1008 is poorly constrained, the presence of a lacustrine environment on Filla Island around that time implies a maximum RSL of 11.5 m a.s.l above present sea level. Marine conditions and a sill depth of 18 m in the inlet at Filla Island on the other hand suggest a minimum RSL of 18 m below present. RSL in Rauer Group around 40-30 ^{14}C ka BP (44.7-34 cal ka BP) can therefore tentatively be estimated to have been within ±15 m of present RSL.

4.6.3 Late Pleistocene in coastal East Antarctica

Radiocarbon dating is widely used to date late Quaternary sediments. The range of this method is limited by instrumental-based constraints to approximately 64-47 ka (Taylor and Southon, 2007). However, in older studies radiocarbon ages beyond 35 ka have been considered as questionable, due to contamination effects (Berkman et al., 1998). Since the limit of radiocarbon dating falls within the time period considered in this study, comparison to alternative dating methods can be used to confirm interpretations. Apart from technical considerations, radiocarbon age determination of natural samples from Antarctica combines several difficulties. In Antarctic marine samples, an Antarctic marine reservoir effect (AMRE), which results from the special oceanographic conditions around the continent, has to be considered (e.g., Stuiver and Braziunas, 1993). From radiocarbon ages of samples with known age a modern AMRE of c. 1130±200 yr has been estimated for Antarctica (Reimer et al., 2004). Reservoir ages for the last glacial, however, are unknown. In lacustrine environments, persisting ice cover and a restricted gas exchange with the atmosphere can lead to depletion in radiocarbon and results in very high reservoir ages. In perennial ice-covered lakes in the McMurdo Dry Valleys region reservoir effects of several thousand years have been reported (Doran et al., 1999). An overestimation of the actual age of a sample can also arise from the input of old carbon, especially in ice-proximal settings where meltwater from ice sheets and glaciers can deliver depleted radiocarbon. When bulk organic carbon samples are dated, incorporated re-deposited organic material in the sediments provides a source of misleading radiocarbon ages.

4.6.3.1 Queen Maud Land

Schirmacher Oasis (70°45'S; 11°40'E) is a small (34 km[2]) ice-free area that crops out as a narrow band between the Novolarevskaja ice shelf and the polar plateau. Numerous lakes fill the morphological depressions, with Glubokoje Lake being the deepest (34.5 m water depth; Schwab, 1998). Several sediment sequences from the deepest part of Lake Glubokoje gave radiocarbon ages older than 26 ^{14}C ka BP (30 cal ka BP, Table 4.6.2; Schwab, 1998). Although the dated macroscopic algae material is most likely not *in situ* (Schwab, 1998), the old radiocarbon ages indicate production and therefore at least partly ice free conditions around that time. The radiocarbon ages have been confirmed by an

infrared stimulated luminescence (IRSL) date from the same cores, which gave 36.2±4.3 ka (Schwab, 1998). From discontinuities in the sediment sequences Schwab (1998) concludes a subsequent glacial overriding during the LGM.

Table 4.6.2 Radiocarbon dates of late Pleistocene age, reported from coastal ice-free areas. Calibration was made with the programme CalPal-2007 online (Danzeglocke et al. 2008) with the calibration dataset CalPal2007 Hulu (Weninger and Jöris 2008); Age range of the calibrated ages is given within 1σ confidence interval.

Site	Lat.	Long.	Sample site	Sample ID	[14]C age	Error ±	cal yr BP	1σ-range	Reference	Dated material
Queen Maud Land										
Schirmacher Oasis	70°46'S	11°50E	L. Glubokoje	KIA-1396	41,500	1390	45,118	1409	Schwab, 1998	Lacustrine TOC
Schirmacher Oasis	70°46'S	11°50E	L. Glubokoje	KIA-1397	39,530	1070	43,531	836	Schwab, 1998	Lacustrine TOC
Schirmacher Oasis	70°46'S	11°50E	L. Glubokoje	KIA-1398	39,430	1390	43,508	1012	Schwab, 1998	Lacustrine TOC
Schirmacher Oasis	70°46'S	11°50E	L. Glubokoje	KIA-1399	44,350	2050	48,064	2467	Schwab, 1998	Lacustrine TOC
Schirmacher Oasis	70°46'S	11°50E	L. Glubokoje	KIA-1400	39,920	1260	43,818	1004	Schwab, 1998	Lacustrine TOC
Schirmacher Oasis	70°46'S	11°50E	L. Glubokoje	OxA7320	32,300	650	36,801	1039	Schwab, 1998	Lacustrine TOC
Schirmacher Oasis	70°46'S	11°50E	L. Glubokoje	OxA7321	34,900	700	39,926	965	Schwab, 1998	Lacustrine TOC
Schirmacher Oasis	70°46'S	11°50E	L. Glubokoje	UTC-6247	29,900	400	34,096	358	Schwab, 1998	Lacustrine TOC
Schirmacher Oasis	70°46'S	11°50E	L. Glubokoje	UTC-6248	31,800	400	35,825	632	Schwab, 1998	Lacustrine TOC
Untersee Oasis	71°S	13°E	Lake Untersee	-	28,190	1800	32,664	1576	Hiller et al., 1995	mumyio
Untersee Oasis	71°S	13°E	Lake Untersee	-	33,900	3000	38,232	2891	Hiller et al., 1995	mumyio
Insel Range	72°S	11°E	Insel Range	-	28,400	1560	32,901	1286	Hiller et al., 1995	mumyio
Insel Range	72°S	11°E	Insel Range	-	37,500	5800	41,625	5736	Hiller et al., 1995	mumyio
Lützow-Holm Bay	69°00'S	39°30'E	East Ongul	Nu-1	32,350	390	36,879	848	Igarashi et al., 1995	Marine, shell
Lützow-Holm Bay	69°00'S	39°30'E	East Ongul	Nu-2	37,220	720	41,975	492	Igarashi et al., 1995	Marine, shell
Lützow-Holm Bay	69°00'S	39°30'E	East Ongul	Ar-1	33,170	630	37,829	1128	Igarashi et al., 1995	Marine, shell
Lützow-Holm Bay	69°00'S	39°30'E	East Ongul	Km-7	32,960	300	37,433	695	Igarashi et al., 1995	Marine, shell
Lützow-Holm Bay	69°00'S	39°30'E	West Ongul	Wo-32	33,960	520	39,365	1104	Igarashi et al., 1995	Marine, shell
Lützow-Holm Bay	69°00'S	39°30'E	West Ongul	Wo-54	34,070	370	39,573	942	Igarashi et al., 1995	Marine, shell
Lützow-Holm Bay	69°00'S	39°30'E	West Ongul	Wo-28	34,190	550	39,548	973	Igarashi et al., 1995	Marine, shell
Lützow-Holm Bay	69°00'S	39°30'E	West Ongul	Wo-48	34,880	480	39,958	879	Igarashi et al., 1995	Marine, shell
Lützow-Holm Bay	69°12'S	39°40'E	Langhovde	Ko-27	34,160	550	39,526	987	Igarashi et al., 1995	Marine, shell
Lützow-Holm Bay	69°12'S	39°40'E	Langhovde	Ko-21	34,780	460	39,908	863	Igarashi et al., 1995	Marine, shell
Lützow-Holm Bay	69°12'S	39°40'E	Langhovde	Ko-20	37,030	910	41,858	596	Igarashi et al., 1995	Marine, shell
Lützow-Holm Bay	69°12'S	39°40'E	Langhovde	Ko-16	33,280	510	37,956	1065	Igarashi et al., 1995	Marine, shell
Lützow-Holm Bay	69°12'S	39°40'E	Langhovde	Ko-14	33,910	410	39,428	1056	Igarashi et al., 1995	Marine, shell
Lützow-Holm Bay	69°12'S	39°40'E	Langhovde	Ko-5	35,510	540	40,347	969	Igarashi et al., 1995	Marine, shell
Lützow-Holm Bay	69°12'S	39°40'E	Langhovde	Beta-100347	46,420	1500	50,013	2511	Maemoku et al., 1997	Marine, shell
Lützow-Holm Bay	69°12'S	39°40'E	Langhovde	Beta-94675	35,970	410	41,292	359	Maemoku et al., 1997	Marine, shell
Lützow-Holm Bay	69°12'S	39°40'E	Langhovde	Beta-94676	39,760	600	43,623	655	Maemoku et al., 1997	Marine, shell
Lützow-Holm Bay	69°12'S	39°40'E	Langhovde	Beta-94677	42,710	920	46,340	1419	Maemoku et al., 1997	Marine, shell
Lützow-Holm Bay	69°12'S	39°40'E	Langhovde	Beta-100346	32,430	270	36,975	762	Maemoku et al., 1997	Marine, shell
Lützow-Holm Bay	69°12'S	39°40'E	Langhovde	Beta-100345	39,440	580	43,463	633	Maemoku et al., 1997	Marine, shell
Prydz Bay										
Larsemann Hills	69°23 S	76°23 E	Lake Nella	ANU 8826	24,950	710	29,726	847	Burgess et al., 1994	Lacustrine moss
Larsemann Hills	69°23 S	76°23 E	Heart Lake	AA-35740	21,780	160	26,052	530	Hodgson et al., 2001a	diamicton
Larsemann Hills	69°23 S	76°23 E	Heart Lake	AA35741	25,460	230	30,370	404	Hodgson et al., 2001a	diamicton
Larsemann Hills	69°23 S	76°23 E	Lake Reid	AA-35726	26,520	260	31,259	385	Hodgson et al., 2001a	Lacustrine TOC
Larsemann Hills	69°23 S	76°23 E	Lake Reid	AA-35727	43,800	2000	47,529	2340	Hodgson et al., 2001a	Lacustrine TOC

Larsemann Hills	69°23 S	76°23 E	Lake Reid	AA-35728	41,800	1500	45,521	1580	Hodgson et al., 2001a	Lacustrine TOC
Larsemann Hills	69°23 S	76°23 E	Lake Reid	CAMS-50381	> 39700	Inf.			Hodgson et al., 2001a	Lacustrine TOC
Larsemann Hills	69°24 S	76°24 E	Lake 73	CAMS-50383	32,220	880	36,734	1239	Hodgson et al., 2001a	Lacustrine TOC
Larsemann Hills	69°24 S	76°24 E	Progress Lake	AA-41165	20,920	150	25,041	380	Hodgson et al., 2001a	Lacustrine,cyano
Larsemann Hills	69°24 S	76°24 E	Progress Lake	AA-35756	43,200	1900	47,003	2232	Hodgson et al., 2001a	Lacustrine,cyano
Larsemann Hills	69°24 S	76°24 E	Progress Lake	AA-35757	> 41,800	Inf.			Hodgson et al., 2001a	Lacustrine,cyano
Larsemann Hills	69°24 S	76°24 E	Progress Lake	AA-35758	47,800	3300	52,695	4703	Hodgson et al., 2001a	Lacustrine,cyano
Larsemann Hills	69°24 S	76°24 E	Progress Lake	AA-35759	>44,400	Inf.			Hodgson et al., 2001a	Lacustrine,cyano
Larsemann Hills	69°24 S	76°24 E	Progress Lake	CAMS-50384	>43,400	Inf.			Hodgson et al., 2001a	Lacustrine TOC
Larsemann Hills	69°22'S	76°08'E	Kirisjes Pond	Beta-196950	26,650	220	31,366	355	Hodgson et al.,2009	Lacustrine TOC
Larsemann Hills	69°22'S	76°08'E	Kirisjes Pond	Beta-196951	27,000	230	31,572	180	Hodgson et al.,2009	Lacustrine TOC
Larsemann Hills	69°22'S	76°08'E	Kirisjes Pond	Beta-196952	28,750	300	33,228	458	Hodgson et al.,2009	marune TOC
Larsemann Hills	69°22'S	76°08'E	Kirisjes Pond	CAMS-50376	>43,200	Inf.			Hodgson et al.,2009	Lacustrine TOC
Rauer Group	68°49'S	77°56'E	Filla Island inl.	KIA35023	37,130	1300	41,790	1021	Berg et al., 2009	Marine, HAF
Rauer Group	68°49'S	77°56'E	Filla Island inl.	KIA35024	29,550	80	33,926	254	Berg et al., 2009	Marine, HAF
Rauer Group	68°49'S	77°56'E	Filla Island inl.	KIA35025	38,780	900	43,129	769	Berg et al., 2009	Marine, HAF
Rauer Group	68°49'S	77°56'E	Filla Island inl.	KIA34078	40,860	2000	44,795	1754	Berg et al., 2009	Marine, HAF
Rauer Group	**68°49'S**	**77°56'E**	**Unn. lake**	**KIA33455**	**35,680**	**650**	**40,463**	**1028**	**this study**	**Marine, shell**
Rauer Group	**68°49'S**	**77°56'E**	**Skua Lake**	**ETH-38772**	**37,110**	**510**	**41,909**	**396**	**this study**	**LacustrineTIC**
Rauer Group	**68°49'S**	**77°56'E**	**Skua Lake**	**ETH-38771**	**30,015**	**150**	**34,286**	**157**	**this study**	**LacustrineTOC**
Vestfold Hills	68°29'S	78°17'E	Abraxas Lake	OZH402	18,810	440	22,509	639	Gibson et al., 2009	Lacustrine TOC
Wilkes Land										
Bunger Hills	66°15'S	100°39'E	Izvilistaja inlet	OxA-5606	28,040	500	32,610	488	Kulbe, 1997	Marine TOC
Bunger Hills	66°15'S	100°39'E	Izvilistaja inlet	OxA-5620	27,900	750	32,583	660	Kulbe, 1997	Marine TOC
Bunger Hills	66°18'S	100°43'E	Figurnoye lake	OxA-6087	35,700	1300	40,289	1388	Kulbe, 1997	Lacustrine TOC
Bunger Hills	66°18'S	100°43'E	Figurnoye lake	OxA-8085	34,140	420	39,590	928	Kulbe, 1997	Lacustrine TOC
Bunger Hills	66°18'S	100°43'E	Figurnoye lake	OxA-8086	34,050	650	39,309	1165	Kulbe, 1997	Lacustrine TOC
Bunger Hills	66°18'S	100°43'E	Figurnoye lake	OxA-5621	29,150	700	33,441	651	Kulbe, 1997	Lacustrine TOC
Windmill Islands	66°28'S	110°34'E	Browning Bay	KIA8848	33,590	1000	38,556	1717	Cremer et al., 2003a	Marine HAF
Windmill Islands	66°28'S	110°34'E	Browning Bay	KIA8849	26,130	950	30,828	857	Cremer et al., 2003a	Marine HAF
Windmill Islands	66°28'S	110°34'E	Peterson Inlet	KIA8863	41,670	1520	45,370	1569	Cremer et al., 2003a	Marine HA
Windmill Islands	66°28'S	110°34'E	Peterson Inlet	KIA8863	38,120	1470	42,682	1110	Cremer et al., 2003a	Marine HAF
Windmill Islands	66°28'S	110°34'E	Peterson Inlet	KIA8864	46,860	2450	50,978	3482	Cremer et al., 2003a	Marine HAF
Windmill Islands	66°28'S	110°34'E	Peterson Inlet	KIA8865	42,690	1350	46,442	1692	Cremer et al., 2003a	Marine HA
Windmill Islands	66°28'S	110°34'E	Peterson Inlet	KIA8865	42,160	1730	46,030	1876	Cremer et al., 2003a	Marine HAF

Dated materials: TOC total organic carbon, TIC total inorganic carbon, HAF humic acid free fraction of organic carbon, HA humic acid fraction of organic carbon.

Further inland, in the mountainous regions around Untersee Oasis (71°40'S; 12°30'E), radiocarbon dating of stomach oil deposits of snow petrels indicates that there have been ice free sites occupied by nesting snow petrels from c. 34 ^{14}C ka BP (38 cal ka BP) to the present (Hiller et al., 1995; Table 4.6.2). In Figure 4.6.4 radiocarbon ages from the so-called mumiyo deposits are indicated as marine samples, since snow petrels feed on marine organisms (Ferretti et al., 2001) and are therefore affected by AMRE. The reconstructions from the mumiyo deposits are in accordance with geomorphological studies on moraine sediments, which indicate a significant lowering of the EAIS between c. 58-13 ka in the Lake Untersee surrounding (Stackebrandt, 1995).

Lützow-Holm Bay

Along Sôya Coast in eastern Lützow-Holm Bay several ice-free peninsulas have been studied for their raised beaches. Dating of macroscopic fossils of *Laternula elliptica*, incorporated in these raised beaches showed two groups of ages: a younger one is of Holocene age and an older one dates back to c. 46-32 ^{14}C ka BP (50-34 cal ka BP, Table 4.6.2; Igarashi et al., 1995; Maemoku et al., 1997; Miura et al., 1998). The late Pleistocene ages have been interpreted as an indication of ice-free conditions (Igarashi et al., 1995; Miura et al., 1998). Nevertheless, a comparison to electron-spin resonance (ESR) dating of some shells pointed to older ages (Takada et al., 2003). The altitude of the beach deposits above present sea level clearly reflects a RSL up to 20 m higher than present during late MIS 3 (Igarashi et al., 1995). Environmental conditions around 46-32 ^{14}C ka BP (50-36 cal ka BP) were characterised by meltwater inflow from the ice sheet, as indicated by relatively low δ^{18}O values of the older shells compared to the Holocene ones (Miura et al., 1998). The stratigraphy of the raised beach deposits suggests that glacial overriding during the LGM did not occur in the northern part of Sôya Coast (Miura et al., 1998).

4.6.3.2 Prydz Bay

In Prydz Bay region, seismic surveys as well as deep sediment cores revealed the long-lived history of the Lambert Glacier/Amery Ice shelf system with ice expansions onto the shelf since the Eocene (O'Brian et al., 2007; Volpi et al., 2009). LGM expansion of the Amery Ice Shelf has been documented in several sediment cores and was obviously not a shelf wide glaciation (Domack et al., 1998). Except for the Holocene diatomaceous oozes, which represent open ocean conditions, sediment sequences from Prydz Bay contain two other beds of siliceous mud and ooze, which were deposited under interstadial conditions (Domack et al., 1998; Taylor and Leventer, 2003). Radiocarbon ages indicate deposition of these biogenic units as far back as 30 ka (Domack et al., 1998), although fossil diatom species suggests the incorporation of reworked material.

Larsemann Hills

Larsemann Hills are located in eastern Prydz Bay (69°23'S, 76°53'E). While the western peninsula Stornes is supposed to have been ice covered until the Mid- to Late-Holocene (Hodgson et al., 2005), the eastern peninsula Broknes remained widely unglaciated throughout the LGM (Hodgson et al., 2001a). In fact, exposure ages and rock weathering observations from Larsemann Hills indicate deglaciation prior to 100 ka (Kiernan et al., 2009).

A sediment sequence from Progress Lake on Broknes was recovered that apparently dates back to MIS 5a and experienced no glacial overriding since then (Hodgson et al., 2006). Nevertheless, no biogenic accumulation was perceivable in the lake basin throughout the last glacial, due to coverage with non-erosive firnified snow. Evidence for biogenic

production during the last glacial comes from a moss sample, which was found *in situ* in lake deposits 2 km from the present ice sheet margin and was dated to 24.9 ^{14}C yr BP (29.7 cal yr BP, Table 4.6.2; Burgess et al., 1994). Lake sediment sequences from several lakes provided radiocarbon ages from late MIS 3 and therefore further support ice-free periods in the area (Table 4.6.3; Hodgson et al., 2001a and 2009). Sediment from a core record recovered in Kirisjes Pond, located c. 8 m a.s.l. was radiocarbon dated to 28.7 ^{14}C ka BP (33.2 cal ka BP, Table 4.6.2; Verleyen et al., 2004b; Hodgson et al., 2009), an age, which was further confirmed by thermo luminescence dating (TL; Hodgson et al., 2009). The sediment record not only indicates ice-free conditions and biogenic production in the area, but also provides evidence for a brief marine transgression around 28.7 ^{14}C ka BP (33.2 cal ka BP) what implicates a RSL of at least 8 m higher than present (Hodgson et al., 2009).

Vestfold Hills

Vestfold Hills comprise an ice-free area of about 400 km^2 in eastern Prydz Bay (68°36' S; 78°10'E). Vestfold Hills are bounded by the EAIS to the east and by Sørsdal Glacier to the south. Radiocarbon dating of bulk organic carbon from exposed marine sediments produced minimum ages in the range of 24-28 ka (Adamson and Pickard, 1983). Further stratigraphic analyses of the sediments, however, verified a Pliocene age of the material (Quilty et al., 2000). Sediment records, e.g., from lakes or marine inlets, dating back to late MIS 3 have not been reported for the Vestfold Hills. Glacial overriding of the area during the LGM was suggested from relative sea-level reconstructions, which are consistent with 600 m of ice sheet thickening and 30-40 km of ice expansion (Zwartz et al., 1998). A recent study, however, suggests only moderate ice sheet expansion during the LGM, since a lake sediment core was dated to c. 18,800±440 ^{14}C yr BP (22,300±1200 cal yr BP; Table 4.6.2), that indicates a permanent existence of the lake throughout the LGM and probably before (Gibson et al., 2009). Stratigraphic investigations from a 4 m deep excavated trench to the southwest of Davis Station provide evidence for the last EAIS overriding of the area in the interval between 3.5-2.6 Ma (Late Pliocene; Colhoun et al., 2010). Colhoun et al. (2010) propose that any later glacial processes were linked to only limited expansions of the EAIS and marginal fluctuations of Sørsdal Glacier.

4.6.3.3 Wilkes Land

Windmill Islands

Windmill Islands are located at the coast of Wilkes Land (66°20'S; 110°30'E) and consist of several islands and peninsulas, which are bounded by the EAIS in the southeast and by Law Dome, a local ice dome, to the northeast. Two cores have been recovered in two coastal marine inlets in southern Windmill Islands, which contain consolidated sapropelic material at their base, overlain by a till layer. Dating of bulk organic matter of the sapropelic sediments produced radiocarbon ages between 33 and 26 ^{14}C ka BP (38.5-30.8

cal ka BP, Table 4.6.2) from one inlet, and between 46 and 38 ^{14}C ka BP (50.9-42.6 cal ka BP, Table 4.6.2) from the other, which are not in stratigraphic order in both records (Cremer et al., 2003a). Dating of carbonate from fossil molluscs and echinoids from the same units yielded infinite radiocarbon ages and amino acid racemisation (AAR) dating confirmed the older ages to 73 to 525 ka (Kirkup et al., 2002). Cremer et al. (2003a) suggest that the older fossils are derived from re-working and conclude that the Windmill Islands have been deglaciated some time during the second half of MIS 3. Pigment and diatom analyse s of the sediments indicate that environmental conditions in the marine inlets were characterised by relatively warm conditions and high production with blooms of green algal plankton in summer (Cremer et al., 2003a; Hodgson et al., 2003). The till layers, which cover the sapropelic units in both cores, indicate a subsequent LGM ice sheet overriding of the inlets (Cremer et al., 2003a).

Bunger Hills

Bunger Hills (66°15'S; 100°50'E) consist of a larger ice-free landmass and several islands, which are bounded on the landward side by the EAIS and several outlet glaciers. Towards the sea side Bunger Hills are inundated by the Shackleton Ice Shelf. Reconstructions of Holocene environmental history of the region were made from marine and lacustrine sediment cores (Kulbe et al., 2001; Verkulich et al., 2002). Radiocarbon ages dating back to the pre-Holocene, however, are rare (Melles et al., 1994b). Basal sediments from two cores, recovered in the southwest of Bunger Hills, gave radiocarbon ages between 35 and 28 ^{14}C ka BP (40-32 cal ka BP, Table 4.6.2; Kulbe, 1997; Melles et al., 1997). The occurrence of diatoms in these sediments points to subaquatic habitats during late Pleistocene times (Kulbe, 1997). Deglaciation in Bunger Hills between 40 and 30 ka has also been reconstructed from optically stimulated luminescence (OSL) dating of glaciolacustrine, glaciofluvial and raised beach deposits (Gore et al., 2001). A major glacial re-advance during the LGM did not occur (Gore et al., 2001).

4.6.4 Late Pleistocene in East Antarctica - Discussion

From almost all larger ice-free coastal areas, which have been studied in the last decades, radiocarbon dates of late Pleistocene age have been reported. Radiocarbon ages should be interpreted with caution, if they are derived from bulk sediment, which can contain reworked organic carbon, probably from sources of different ages. Dating of macrofossils like large shell fragments avoid the problem of mixed origin, but ESR dating of fossil shells produced discrepancies to radiocarbon ages, suggesting an underestimation of age by radiocarbon dating (Takada et al., 2003). The radiocarbon age of a fossil gives the time of living of the organism, which is not necessarily identical with the age of deposition of the sediment it is incorporated in (see Kirkup et al., 2002).

Radiocarbon ages from different sites along the East Antarctic coast indicate that the EAIS probably did not cover the presently ice free areas entirely during the second half of MIS 3. In several regions like in Bunger and Larsemann hills, the interpretation of radiocarbon ages from sediment cores is confirmed by dating of geomorphological features with alternative methods. Since most radiocarbon ages reported in this review are derived from organic carbon or biogenic carbonates, climate conditions in the late MIS 3 apparently were suitable for biogenic production in lakes and coastal marine sites. The fragmentary stratigraphy of most deposits, however, does not allow continuous reconstruction of paleoclimate. Calibrated radiocarbon ages from the studied sites span the whole period between c. 50 ka, and the onset of MIS 2 around 29 ka (Figure 4.6.4). In Antarctic ice cores isotope excursions have been identified which indicate millennial-scale temperature fluctuations, with higher temperatures over the Antarctic continent at 46 ka and 37 ka (Figure 4.6.4; Blunier and Brook, 2001; EPICA, 2004; Jouzel et al., 2007). Radiocarbon ages from marine sediment records from Windmill Islands indicate relatively warm conditions around 46 cal ka BP (Cremer et al., 2003a; Hodgson et al., 2003) what probably corresponds to a warm period around 46 ka defined in Antarctic ice cores (Figure 4.6.4). Although high productivity and open water conditions have also been prevalent in Rauer Group, the record does not show such a correlation. Increased melting of the ice sheet in the vicinity of Sôya Coast and Rauer Group (Miura et al., 1998; Berg et al. *submitted*) roughly fall in the period of increased ice discharge from Antarctica and IRD deposition in the Southern Ocean (Kanfoush et al., 2000; Figure 4.6.4). However, while the IRD event at 46.5-41.7 cal ka BP coincides with increased meltwater discharge in Rauer Group, the period of increased meltwater inflow in Sôya Coast is not limited to the duration of the IRD events (Figure 4.6.4). Contrasting the findings from sedimentary records from coastal areas with continuous records from open marine and ice-core records is limited due to dating uncertainties and the fragmentary character of many records. Although the gathered evidence from the ice-free regions strongly supports ice-free conditions sometime during the last glacial, probably in the second half of MIS 3, a correlation with millennial scale climate fluctuations recorded elsewhere should not be strained.

Although the EAIS seems to lack lateral expansion along the East Antarctic coast during the second half of MIS 3, RSL reconstructions from Sôya Coast, Larsemann Hills, and also the observations from Rauer Group presented in this study indicate that RSL was comparable to or above the present. Since global sea level was 80-60 m lower than present (Lambeck et al., 2002b), higher ice load must have induced the isostatic depression, which compensated for the lower eustatic sea level. Since the RSL reconstructions from Larsemann Hills and Sôya Coast are not synchronous this is probably true for the whole time period between c. 45 and 31 cal ka BP. An increase in ice load, which did not result in an overall expansion of the ice sheet margin, was probably induced by the lower temperatures during the last glacial (Jouzel et al., 2007), and a concurrent increase in ice

viscosity. Higher viscosity permitted the development of a steeper ice profile and consequently the storage of larger ice masses per area. Additional factors, which might have facilitated the build up of higher ice load than today in coastal areas, is the grounding of ice shelves due to lower sea level and the increase in sea ice, which both could have acted as an abutment for the EAIS.
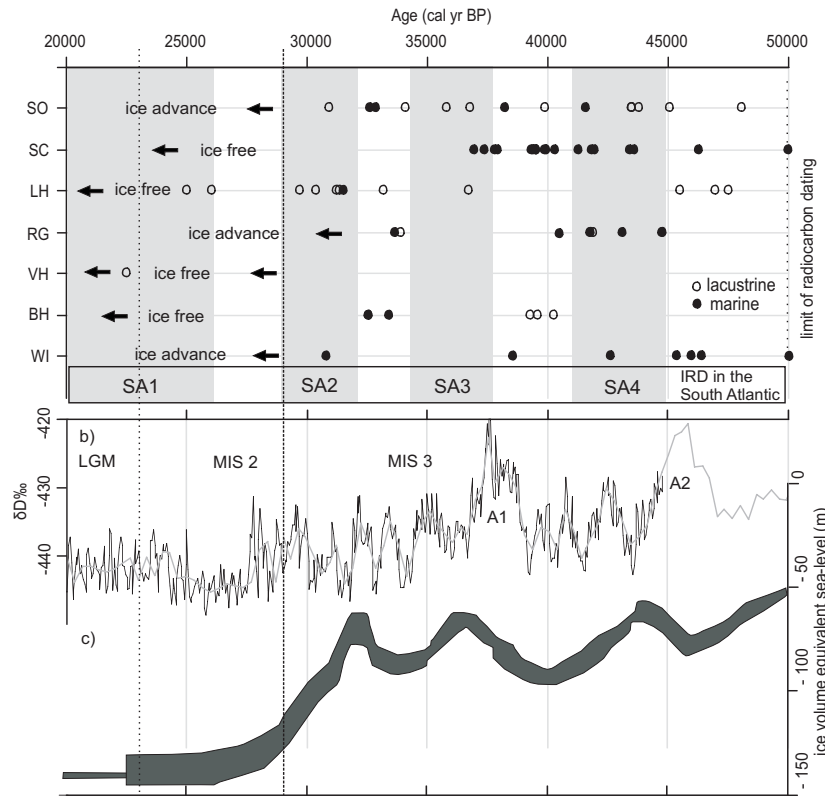
Figure 4.6.4 Calibrated radiocarbon ages from ice free coastal areas (radiocarbon ages and calibration uncertainties are given in Table 4.6.2) SO Schirmacher Oasis, SC Sôya Coast, LH Larsemann Hills, RG Rauer Group, VH Vestfold Hills, WI Windmill Island; Grey rectangles indicate periods of increased IRD deposition (SA) in the South Atlantic (Kanfoush et al., 2002) a). Deuterium record from EPICA Dome C ice core (EPICA, 2004; Röthlisberger et al., 2004), A1 and A2 indicate warm periods (Blunier and Brook, 2002) b). Ice volume equivalent sea level (time scale: cal yr BP; Yokoyama et al 2007) c).

White et al. (2009) noted that oases, which have escaped LGM glaciation, are preferentially located close to outlet glaciers enhancing draw down of ice masses. In late MIS 3 effects of fast flowing glaciers probably favoured ice-free conditions in some of the oases as well. However, the presence of clearly marine environments in Sôya Coast, Windmill Islands, Vestfold Hills, and Rauer Group strongly suggests the absence of completely grounded ice shelves on the seaward sides of these oases. Therefore the EAIS configuration, with an extent comparable to the present, probably was not limited to the relatively small ice-free areas. The inference, that the EAIS apparently developed a steeper than present profile could provide geological evidence for the physical properties of the ice sheet in glacial times.

4.6.5 Conclusion

Radiocarbon ages from three different sedimentary archives on Filla Island, Rauer Group, provided ages ranging from 40-30 ^{14}C ka BP (44.7-34 cal ka BP). The sediment record from Skua Lake and a dated shell from (reworked) marine sediment indicate ice-free conditions on the island and the presence of near shore marine environments within the second half of MIS 3. This interpretation is supported by a marine sediment core (Co1010) from an inlet at Filla Island. The chronology of the lake sediment core from Skua Lake, however, has to be further validated by additional radiocarbon dating. Climate conditions were warm enough to allow production in coastal marine and also in lacustrine environments in Rauer Group, as well as in other sites around East Antarctica. However, the large uncertainties in the radiocarbon ages, due to unknown reservoir effects, incorporation of old material and fragmentary records, hamper the correlation of the palaeoenvironmental observations from single records and sites with each other as well as with ice core records.

Radiocarbon ages as well as other dating methods strongly suggest that the EAIS did reach insignificantly further than today in the late Pleistocene, in the second half of MIS 3 at presently coastal ice-free areas. RSL observations on the other hand point to increased ice load in the vicinity to the coasts in eastern Prydz Bay and also in Sôya Coast. This apparent discrepancy between ice load and ice expansion could be resolved, considering a steeper than present ice sheet topography.

5. Synthesis

5.1 Reconstructing paleoenvironments in Rauer Group, East Antarctica - an assessment

In this thesis, sediment records from marine inlets and one lake in Rauer Group, East Antarctica, have been investigated for their sedimentological, geochemical, and paleontological properties to reconstruct the environmental and climatic history of the area.

During a field campaign in 2007 sediment cores from three marine inlets have been recovered. The morphology of the inlets that are separated from the ocean by subaquatic sills impedes the intrusion of icebergs and the related disturbance of the sediments. The restricted water exchange of the bottom water with the open ocean leads to the formation of oxygen-depleted conditions at the sediment/water interface, favouring a good preservation of organic material in the sediments. Due to the continuity of the records and high sedimentation rates, high-resolution reconstructions of Holocene environmental and climatic conditions could be obtained. Position of the marine basins in different distances from the present ice sheet margin provided the possibility to reconstruct the glacial history of Rauer Group.

The recovery of long ranging lake sediment sequences from Rauer Group turned out to be problematic. Unlike in Vestfold Hills, where streams and lakes are fed by meltwater from the ice sheet margin, the islands of Rauer Group are presently free of permanent snowfields or ice masses. Due to the dry conditions shallow lake basins are not permanently filled with water. By the time of sampling in March 2007 many lakes have been completely desiccated. Except for the comparatively deep Skua Lake on Filla Island sediment sequences from very shallow lakes probably represent only fragmentary records. Preliminary results from core Co1008 from Skua Lake indicate that the sediment sequence reaches back to pre-Holocene times. The chronology of core Co1008, however, has to be improved by additional radiocarbon dates.

The interpretation of radiocarbon ages from the Antarctic marine and lacustrine realm is usually complicated due to reservoir effects and input of old carbon, e.g., from melting ice masses or from re-worked sediments. In the three studied marine inlets surficial ages of the sediments were very similar, pointing to a consistent recent local reservoir effect of c. 900 years in Rauer Group. The chronologies presented in this thesis for the marine cores (Co1010, Co1011, Co1014) were obtained from dating of bulk organic matter. Since radiocarbon ages show no age reversals, dating of the presumably dominantly diatom derived organic material provides reliable core chronologies.

In this multi-proxy study on the environmental and climatic history of Rauer Group, several proxies turned out to be especially sensitive. While concentration of organic carbon

and nitrogen provide evidence for changes in production and preservation of organic material, diatom species composition proved to be a suitable proxy for the evaluation of salinity and sea ice conditions in the inlets. Estimations of relative temperature changes can be made from annual duration and thickness of the sea ice cover inferred from diatom ecology. However, diatom response to sea surface temperatures is relatively small (McMinn et al., 2001) and the interpretation of diatom assemblages is in some cases limited due to the poorly known ecology of species from the near coastal environment.

The preliminary study on oxygen isotope composition of diatom derived silica from the marine sediments of core Co1010 proposes this proxy as a valuable tool, in order to assess local meltwater input and, less distinct, changes in temperature. Since the sediments from the marine inlets of Rauer Group contain very high amounts of diatom frustules, complete sample purification prior to the measurement of oxygen isotopes is possible and therefore provides the basis for valid data sets.

The sensitivity of marine inlets to changes in precipitation is much lower than of lacustrine systems, whose hydrology is directly linked to precipitation and evaporation. Nevertheless, our study indicates that precipitation changes in the catchments are reflected by the amount and composition of minerogenic matter, which is transported in the marine inlets; e.g., due to changes in wind speed or due to moister conditions on land. In this respect, the ITRAX XRF core scanner provided high-resolution data, which allowed recognition of relative changes in elemental composition of the sediment sequences; however, more studies should be carried out to better determine the interaction of physical sediment properties (e.g., water content and sample inhomogeneity) and elemental data.

The well-dated sediment sequences, studied in the course of this thesis, are very valuable archives for Holocene environmental and climatic changes, since they comprise undisturbed, long-ranging records. The situation in Rauer Group during the Last Glacial Maximum, however, needs further clarification. While the records from Filla and Flag Island inlet can be used to date the timing of post-glacial onset of biogenic production, the geomorphological studies carried out on Rauer Group provide a profound picture of the relative glacial history of the area. They, however, lack a precise chronology. Geochronological approaches like exposure dating of erratics could further improve the picture of the late Quaternary glacial history of Rauer Group.

5.2 Glacial history and relative sea level - reconstructions from Rauer Group and regional implications

5.2.1 Late Pleistocene

Radiocarbon ages from different sediment records sampled on Rauer Group indicate ice-free conditions between 40-30 ^{14}C ka BP (44.7-34 cal ka BP). Marine sediments, recovered in core Co1010 from Filla Island inlet, a shell fragment from a redeposited marine

sediments and a lacustrine sediment sequence from Skua Lake, both from Filla Island, support a position of the ice sheet margin of at most 6 km the west of its present position during that time (Chapters 4.3, 4.4, and 4.6). The altitudes of the sampling sites indicate that RSL in Rauer Group was comparable to present in the second half of MIS 3. Due to the lower global sea level around that time, isostatic depression of Rauer Group can be concluded, most likely caused by increased ice load in the vicinity to the coast. The reconstructions from Rauer Group improve the picture of late Pleistocene EAIS configuration and adds evidence to previous findings from other East Antarctic oases, that the EAIS was less expanded at its margins sometime during the late Pleistocene (Chapter 4.6 and references therein). RSL reconstructions from Sôya Coast (Miura et al., 1998; Nakada et al., 2000) and Larsemann Hills (Hodgson et al., 2009) are in accordance with the observations from Rauer Group and imply that higher ice-load in coastal areas probably was an East Antarctic wide phenomenon. This circumstance could allow inferences on the physical properties of the ice sheet during glacial times.

5.2.2 Last glacial maximum (LGM)

After the ice-free period in late MIS 3, Rauer Group was most likely glaciated during the LGM. In Filla Island inlet (core Co1010) biogenic sedimentation is not recorded between c. 35 cal yr BP and the early Holocene, probably due to either subaerial exposure or glacial overriding (Berg et al., 2009; Chapter 4.3). In Flag Island inlet (core Co1011) a basal till, deposited prior to 11,200 cal yr BP, points to previous glaciation of the island. Geomorphological studies on glacial deposits and weathering style also suggest a complete glacial overriding of Rauer Group sometime during the last glacial (White et al., 2009; Chapter 4.2).

In a regional context, a complete glaciation of Rauer Group during the LGM is probably rather an exception than the norm. While the Amery Ice Shelf/Lambert Glacier system experienced a larger expansion with grounded ice shelves reaching mid-shelf areas (Domack et al., 1998), the presently ice-free coastal areas were affected by larger ice sheet expansion to a much lesser extent. Broknes Peninsula at Larsemann Hills, c. 80 km to the south of Rauer Group, remained widely unglaciated during the LGM (Hodgson et al., 2001a and 2005). A recent study from Vestfold Hills (Gibson et al., 2009) challenges previous reconstructions, which assumed heavy glaciation of the area (Zwartz et al., 1998) and suggest that the present coastline of Vestfold Hills was not covered by the EAIS during the LGM (Gibson et al., 2009). Another study even dates the last glacial overriding to the late Pliocene (Colhoun et al., 2010).

In other sectors of East Antarctica, LGM ice sheet extend is as irregular as in Prydz Bay. In the Windmill Islands, Wilkes Land, expansion of the local Law Dome completely covered the coastal area (Goodwin, 1993). Holocene raised beaches up to 30 m above present sea level indicate an LGM ice thickening of c. 770-1000 m (Goodwin and Zweck, 2000).

Other presently ice-free coastal areas have been proposed to have escaped complete glacial overriding. In Bunger Hills (Gore et al. 2001), Amery Oasis (Fink et al., 2006) and Lützow-Holm Bay (Igarashi et al., 1995) expansion of the ice sheet margin was very limited. Non-uniform expansion and retreat observed along the margin of the EAIS in individual regions is probably related to local topographic features. The regions located near larger outlet glaciers probably stayed ice-free due to the increased drawdown of ice masses by the faster flowing glaciers. Deflection of ice flow, for example, was suggested as a mechanism for keeping Larsemann Hills unglaciated during the LGM (Hodgson et al., 2001a).

5.2.3 Deglaciation and Holocene ice-sheet stability

From a circum-Antarctic perspective, deglaciation started around 19 cal ka BP when an increase in eustatic sea level marked the end of maximum global glaciation (Lambeck et al., 2002a). In the AP region deglaciation of the outer shelf areas started around 18 cal ka BP (Heroy and Anderson, 2007), while in the Ross Sea region grounding line retreat began much later, around 11-10 ^{14}C ka BP (McKay et al., 2008). The onset of deglaciation around East Antarctica commenced diachronously between c. 25 and 9 ka (Anderson et al., 2002) and retreat probably was controlled by post-LGM sea level rise (Mackintosh et al., 2007).

Deglaciation of Rauer Group began prior to the onset of biogenic sedimentation around 11,200 cal yr BP, which was dated in the inlets at Filla Island and Flag Island (Berg et al., 2009; Berg et al., *submitted*; Chapters 4.3 and 4.4). Radiocarbon ages, however, probably underestimate the first emergence of hilltops and the timing of deglaciation (Gore, 1997). Ongoing deglacial processes on the islands affected both inlets by a high terrigenous input until c. 9200 cal yr BP. The timing of deglaciation in the Prydz Bay region after the LGM is in good accordance with the results from Rauer Group. Exposure ages from nunataks in the interior of Mac.Robertson Land indicate an ice surface lowering of c. 250 m between 12-10 ka (Mackintosh et al., 2007). Inner shelf areas of Prydz Bay deglaciated between 12,600-10,500 cal yr BP, when biogenic sedimentation recommenced (Domack et al., 1991b; Sedwick et al., 2001; Taylor and McMinn, 2002; Leventer et al., 2006). An ice sheet profile comparable to the present stabilised around 7 ka, probably controlled by the slow down of post-glacial eustatic sea level rise (Mackintosh et al., 2007). In the wider East Antarctic region ice retreat in Windmill Islands started prior to 10,500 cal yr BP and commenced until c. 4000 cal yr BP (Cremer et al., 2003a). In Bunger Hills, where LGM ice expansion was less extensive (Gore et al., 2001), deglacial processes and iceberg calving from floating ice began close to the Pleistocene/Holocene transition (Melles et al., 1997).

In Rauer Group, no evidence for larger ice sheet fluctuations during the Holocene was found. Shcherbinina Island inlet contains a complete marine record of the past 4500 cal yr

BP (Core Co1014; Berg et al., *in press*; Chapter 4.5). The uniform sedimentation as well as the continuity of the record indicate that deglaciation of the islands was virtually complete prior to 4500 cal yr BP. The ice margin had reached a position comparable to the present prior to the Mid-Holocene. Geomorphological investigations of moraine sediments on the islands of Rauer Group are in accordance with the results from the marine cores, setting the Holocene ice margin within c. 500 m of its present position (White et al., 2009; Chapter 4.2). The assumption of relative stability of the EAIS margin is confirmed by observations from Bunger and Vestfold hills, where Holocene fluctuations of the ice sheet margin have been in a range of only 500 m beyond the present (Fitzsimons and Colhoun, 1995). Outlet glacier systems and marginal ice domes showed a more dynamic behaviour during the Holocene, responding to relative sea level (Melles et al., 1997), increased Holocene precipitation (Goodwin et al., 1998) and warmer climate conditions (Domack et al., 1991b). The mechanisms and climate feedbacks controlling dynamics of the EAIS and its outlet systems are manifold and their interactions need to be further investigated. Evidence for relative ice sheet stability until recent years from Rauer Group and other coastal oases is in accordance with results from radar interferometry and regional climate modelling (Rignot et al., 2008). An indication that the recent temperature increase is affecting ice sheet mass balance might be the increased ice loss, especially in coastal regions, since the year 2006 modelled by Chen et al. (2009).

5.3 Late Quaternary climate history of Rauer Group and regional implications

5.3.1 Late Pleistocene

Late Pleistocene climate in coastal East Antarctica is poorly known, due to the limited availability of records. Therefore, the records from Rauer Group are especially valuable to extend the picture of environmental and climatic conditions prior to the Holocene. Rauer Group experienced a period of relatively warm climate conditions between c. 46-40 cal ka BP, when marine conditions in Filla Island inlet were characterised by open water and relatively high meltwater input from melting ice sheets (Berg et al., 2009; Berg et al., *submitted*, Chapters 4.3 and 4.4). Open water and high productivity have also been suggested for the near coastal marine environments in Windmill Islands (Cremer et al., 2003a; Hodgson et al., 2003). Intense meltwater inflow from melting ice sheet has been reconstructed from Sôya Coast (Miura et al., 1998). Synopsis of radiocarbon dated sedimentary records from coastal East Antarctica, however, shows that a comparison to late Pleistocene continuous and high-resolution records (e.g., ice cores and marine sediments) is hampered by dating uncertainties (Chapter 4.6).

5.3.2 Holocene

The early Holocene in Rauer Group was characterised by relatively warm conditions. Deglacial processes on the islands between c. 11,200 cal yr BP and 9200 cal yr BP and

concurrent high marine productivity under relatively open water conditions point to an early Holocene optimum in Rauer Group (Berg et al. *submitted*, Chapter 4.4). The onset of post-glacial biogenic sedimentation in coastal East Antarctica has widely been reconstructed for the Pleistocene/Holocene transition, (e.g., Roberts and McMinn, 1999; Kulbe et al., 2001; Cremer et al., 2003a; Verleyen et al., 2004a; Wagner et al., 2004). Several sedimentary records e.g., from Amery Oasis (Wagner et al., 2004), Bunger Hills (Kulbe et al., 2001), and Prydz Bay (Taylor and Leventer, 2003) as well as ice core records from East Antarctica (Masson et al., 2000) agree in the recognition of an early Holocene climate optimum (Figure 5.1).

Slightly cooler climate conditions in the Early to Mid-Holocene in Rauer Group are reflected in the marine diatom assemblage in both studied inlets. After c. 8200 cal yr BP sea ice on the inlets increased during summer and higher minerogenic input points to increased aeolian activity (Berg et al. *submitted*, Chapter 4.4). In the Mid-Holocene, between c. 5700-3500 cal yr BP, climatic conditions probably have been warmer in Rauer Group, when both basins experienced more open conditions and input of freshwater from melting of the ice-sheet and increased precipitation on the islands occurred (Berg et al. *submitted*, Chapter 4.4).
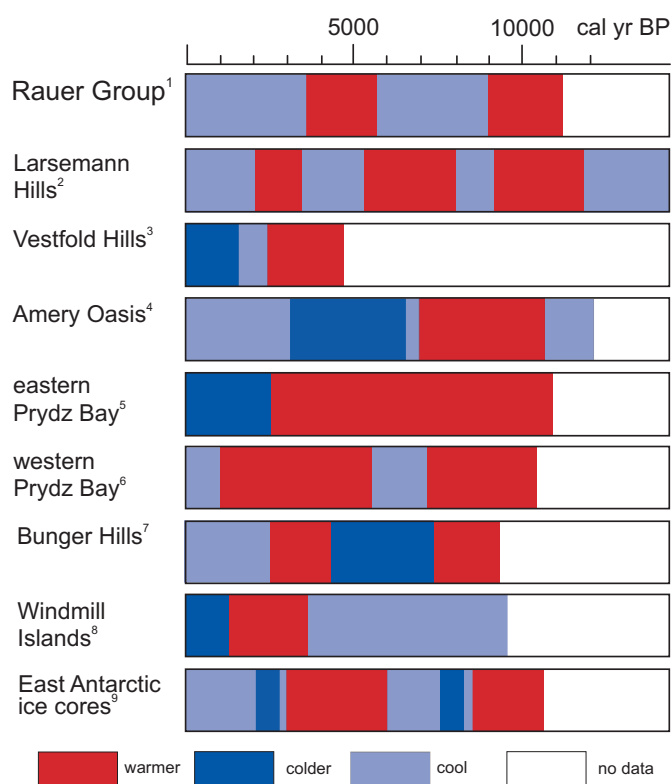
**Figure 5.1 Summary of Holocene climate reconstructions from East Antarctica. [1]Berg et al., 2009, Berg et al. submitted (Chapters 4.3 and 4.4); [2]Verleyen et al. 2004b; [3]McMinn 2000, McMinn et al., 2001, Huang et al. 2009; [4]Wagner et al., 2004; [5]Taylor and McMinn 2002; [6]Taylor and McMinn 2001; [7]Kulbe et al., 2001; Verkulich et al., 2002; [8]Cremer et al., 2003a; [9]Masson et al., 2002.**

A second climate optimum in the Mid-Holocene has been recognised in many records, albeit with slightly different timings (Figure 5.1). While East Antarctic ice cores indicate higher temperatures between 3000 and 6000 yr BP (Masson et al., 2000), a climate optimum between 4000-1000 cal yr BP was reconstructed in Windmill Islands (Cremer et al., 2003a) and between 4500-2500 cal yr BP in Bunger Hills (Kulbe et al., 2001).

Late Holocene environmental conditions in the inlets of Rauer Group are characterised by increased sea ice since c. 3000 cal yr BP and decreasing productivity since c. 1700 cal yr BP (Berg et al. *submitted*, Chapter 4.4). Neoglacial cooling, which has widely been inferred from sedimentary records in East Antarctica (McMinn 2000; Kulbe et al., 2001; McMinn et al., 2001; Taylor and McMinn, 2002; Cremer et al., 2003a; Taylor and Leventer, 2003; Figure 5.1) is, however, not very pronounced in the inlets of Rauer Group. Changes in climate conditions seem to cause only slight changes in environmental conditions in the marine inlets.

Contrasting Holocene climate reconstructions from different sites in East Antarctica reveal regional consistent climate trends as well as local characteristics. While several marine and lacustrine records provide evidence for short-term climate fluctuations in the Holocene (Roberts et al., 2001; Sedwick et al., 2001; Taylor and McMinn, 2001; Verkulich et al., 2002), response of the diatom record from the inlets of Rauer Group to Holocene changes proceeded relatively slowly. Although changes in oceanic and atmospheric circulation in Antarctica likely influence climatic conditions (Bentley et al., 2009), insolation probably is an important mechanism, which influences Holocene environmental changes in the inlets of Rauer Group by changing seasonality. The influence of insolation and seasonality on environmental conditions has also been discussed for other regions in East Antarctica (e.g., Renssen et al., 2005; Denis et al., 2009; Pike et al., 2009).

5.4 Conclusion and outlook

The outcome of this study provides valuable new information on the glacial history and climate evolution in coastal East Antarctica throughout the late Quaternary.

The present study on near coastal marine and lacustrine sediment sequences from Rauer Group shows that selection of suitable sampling sites is a precondition and that a multi-proxy approach is essential for successful reconstructions of paleoenvironments and -climate. In reconstructing paleoenvironmental and -climatic changes based on proxy data it has to be kept in mind that changes in climatic conditions can only be detected, if they have an imprint on environmental conditions as well as on the proxy under consideration. Therefore different precision and expressiveness of each record and each proxy has to be discussed. Besides classical methods like TOC and BSi analyses, the development of new tools and proxies to evaluate sediment records is one way to improve the validity of paleoenvironmental and paleoclimate reconstructions. In approaching the questions

addressed at the beginning of this thesis, the employment of an ITRAX XRF core scanner provided a valuable tool for elemental analysis, due to e.g., the high resolution of the measurement. A proxy, which is probably worth to be brought into focus, is the composition of oxygen isotopes of diatom silica. This proxy can be meaningful in order to detect changes both in water temperature and in the proportion of freshwater input into the marine realm.

Paleoenvironmental and -climatic studies are particularly depending on reliable age models, providing the basic requirement for the comparison and correlation of different sites. Nevertheless, radiocarbon ages from Antarctic sediments can rarely be interpreted straightforwardly due to inaccessible reservoir effects and tampering by input of old carbon. Dating of compound specific organic carbon could be an approach to overcome the problem of mixed organic material in Southern Ocean marine sediments (Ohkouchi and Eglinton, 2008).

Except from comprehensive fieldwork and recovery of new records, evidence from existing records should be gathered and joined with climate and ice sheet simulations so as to elucidate in what way local environmental changes are linked with regional climate (Bentley, 2010; Schmidt, 2010). Although information obtained from coastal ice-free areas is patchy and chronologies are sometimes imprecise, reconstructions of the glacial history and climate evolution of coastal areas provide a reference frame for scaling natural variability.

6. References

Adamson, D. and Pickard J. 1983 Late Quaternary ice movement across the Vestfold Hills, East Antarctica. In Oliver R.L., James, P.R. and Jago J.B. (eds.): Antarctic Earth Science: Proceedings of the Fourth International Symposium of Antarctic Earth Sciences, University of Adelaide.

Adamson, D.A. and Pickard, J. 1986a. Cainozoic history of the Vestfold Hills. In: Pickard, J. (Ed.), Antarctic Oasis, Terrestrial Environments and History of the Vestfold Hills. Academic Press, Sydney, pp. 63-97.

Adamson, D.A. and Pickard, J. 1986b. Physiography and geomorphology of the Vestfold Hills. In: Pickard, J. (Ed.), Antarctic Oasis, Terrestrial Environments and History of the Vestfold Hills. Academic Press, Sydney, pp. 99-139.

Aharon, P. 1988. Oxygen, carbon and U-series isotopes of aragonites from Vestfold Hills, Antarctica: Clues to geochemical processes in subglacial environments. Geochimica et Cosmochimica Acta 52, 2321-2331.

Anderson, J.B., Shipp, S., Lowe, A.L., Smith Wellner, J. and Mosola, A.B. 2002. The Antarctic Ice Sheet during the Last Glacial maximum and its subsequent retreat history: a review. Quaternary Science Reviews 21, 49-70.

Armand, L. K., Crosta, X., Romero, O. and Pichon, J.-J. 2005. The biogeography of major diatom taxa in Southern Ocean sediments: 1. Sea ice related species. Palaeogeography, Palaeoclimatology, Palaeoecology 223, 93-126.

Augustinus, P.C. 2002.Weathering characteristics of the glacial drifts, Bunger Hills, east Antarctica. Arctic, Antarctic and Alpine Research 34, 65-75.

Australian Antarctic Division 2002. Rauer Group, mapping project, photo control, Scale 1:40 000. http://data.aad.gov.au/aadc/mapcat/display_map.cfm?map_id=12964.

Australian Bureau of Meteorology 2009. Climate statistics from Davis Station http://www.bom.gov.au/climate/averages/tables/cw_300000.shtml (download 11 May 2007 and 18 January 2010).

Bard, E., Hamelin, B. and Fairbanks, R.G. 1990. U-Th ages obtained by mass spectrometry in corals from Barbados: sea level during the past 130.000 years. Nature 346, 456-458.

Bareille, G., Labracherie, M., Maillet, M. and Latouche, C. 1990. Quantification des teneurs en opale biogène des sédiments de l'océan austral par diffractométrie X. Clay Minerals 25, 363-373.

Bassett, S.A., Milne, G.A., Bentley, M.J. and Huybrechts, P. 2007. Modelling Antarctic sea-level data to explore the possibility of a dominant Antarctic contribution to melt water pulse 1A. Quaternary Science Reviews 26, 2113-2127.

Battarbee, R.W. 1973. A new method for estimation of absolute microfossil numbers, with reference especially to diatoms. Limnology and Oceanography 18, 647-653.

Bentley, M.J., Hodgson, D.A., Smith, J.A., Cofaigh, C.O., Domack, E.W., Larter, R.D., Roberts, S.J., Brachfeld, S., Leventer, A., Hjort, C., Hillenbrand, C.-D. and Evans, J. 2009. Mechanisms of Holocene palaeoenvironmental change in the Antarctic Peninsula region. The Holocene 19, 51-69.

Bentley, M.J. 2010. The Antarctic palaeo record and its role in improving predictions of future Antarctic Ice Sheet change. Journal of Quaternary Science 25, 5-18.

Berg, S., Wagner, B., White, D.A., Cremer, H., Bennike, O. and Melles, M. 2009. New marine core record of Late Pleistocene glaciation history, Rauer Group, East Antarctica. Antarctic Science 21, 299-300.

Berg, S., Wagner, B., White, D. and Melles, M. 2010. No significant ice sheet expansion beyond present ice margins during the past 4500 yr at Rauer Group, East Antarctica. Quaternary Research 74, 23-25.

Berg, S., Wagner, B., Cremer, H. Leng, M. and Melles, M. *submitted*. Late Quaternary environmental and climate history of Rauer Group, East Antarctica. Palaeogeography, Palaeoclimatology, Plaaeoecology, manuscript number PALAO5540

Berkman, P.A., Andrews, J.T.. Björk, S., Colhoun, E.A., Emslie, S.D., Goodwin, I.D., Hall, B.L., Hart, C.P., Hirakawa, K., Igarashi, A., Ingólfsson, O., Lopez-Martinez, J., Lyons, W.B., Mabin, M.C.G., Quilty, P.G., Taviani, M. and Yoshida, Y. 1998. Circum-Antarctic coastal environmental shifts during the Late Quaternary reflected by emerged marine deposits. Antarctic Science 10, 345-362.

Bhikhardas, A.K., Whitehead, M.D. and Peterson, J.A. 1992. Mapping Adélie penguin rookeries in the Vestfold Hills and Rauer Group, East Antarctica, using SPOT HRV data. Remote Sensing 13, 1577-1583.

Bird, M.I., Chivas, A.R., Radnell, C.J. and Burton, H.R. 1991. Sedimentological and stable-isotope evolution of lakes in the Vestfold Hills, Antarctica. Palaeogeography, Palaeoclimatology, Palaeoecology 84, 109-130.

Björk, S., Olsson, S., Ellis-Evans, C., Hakansson, H., Humlum, O. and de Lirio, J.M. 1996. Late Holocene palaeoclimatic records from lake sediments on James Ross Island, Antarctica. Palaeogeography, Palaeoclimatology, Palaeoecology 121, 195-220.

Blandford, D.C., 1975. Spatial and temporal patterns of contemporary geomorphic processes in the Vestfold Hills, Antarctica. BLitt. thesis, University of New England (Australia).

Blunier, T. and Brook, E.J. 2001. Timing of millennial-scale climate change in Antarctica and Greenland during the last glacial period. Science 291, 109-112.

Bohaty, S.M., Scherer, R.P. and Harwood, D.M. 1998. Quaternary diatom biostratigraphy and paleoenvironments of the CRP-1 drillcore, Ross Sea, Antarctica. Terra Antarctica 5, 431-453.

Böning, P., Bard, E and Rose, J. 2007. Toward direct, micron-scale XRF elemental maps and quantitative profiles of wet marine sediments. Geochemistry, Geophysics, Geosystems 8, Q05004,doi:10.1029/2006GC001480.

Bronge, C. 1996. Hydrographic and climatic changes influencing the proglacial Druhzby drainage system, Vestfold Hills, Antarctica. Antarctic Science 8, 379-388.

Brumsack, H.-J. 2006. Trace metal content of recent organic carbon-rich sediments: Implications for Cretaceous black shale formation. Palaeogeography, Palaeoclimatology, Palaeoecology 232, 344-361.

Burgess, J.S., Spate, A.P. and Shelvin, J. 1994. The onset of deglaciation in the Larsemann Hills, Eastern Antarctica. Antarctic Science 6, 491-495.

Chen, J.L., Wilson, C.R., Blankenship, D., Tapely, B.D. 2009. Accelerated Antarctic ice loss from satellite gravity measurements. Nature Geoscience 2, 859-862.

Child, D., Elliot, G., Misfud, C., Smith, A.M. and Fink, D. 2000. Sample processing for earth science studies at ANTARES. Nuclear Instruments and Method in Physics Research B 172, 856-860.

Clark, P.U. and Mix, A.C. 2002. Ice sheets and sea level of the Last Glacial Maximum. Quaternary Science Reviews 21, 1-7.

Clark, P.U., Dyke, A.S., Shakun, J.D., Carlson, A.E., Clark, J., Wohlfarth, B., Mitrivca, J.X., Hostetler, S.W. and McCabe, A.M. 2009. The Last Glacial Maximum. Science 325, 710-714.

Colhoun, E.A., Kiernan, K.W., McConnell, A., Quilty, P.G., Fink, D., Murray-Wallace, C.V. and Whitehead, J. 2010. Late Pliocene age of glacial deposits at Heidemann Valley, East Antarctica: evidence for the last major glaciation in the Vestfold Hills. Antarctic Science 22, 53-64.

Conley, D.J. 1998. An interlaboratory comparison for the measurement of biogenic silica in sediments. Marine Chemistry 63, 39-48.

Convey, P., Gibson, J.A.E., Hillenbrand, K.-D., Hodgson, D.A., Pugh, P.J.A., Smellie, J.L. and Stevens, M.I. Antarctic terrestrial life-challenging the history of the frozen continent?. Biological Reviews 83, 103-117.

Conway, H., Hall, B.L., Denton, G.H., Gades, A.M. and Waddington, E.D. 1999. Past and future grounding-line retreat of the West Antarctic Ice Sheet. Science 286, 280-283.

Cremer, H., Wagner, B., Melles, M. and Hubberten, H.-W. 2001. The postglacial environmental development of Raffles Sø, East Greenland: inferences from a 10,000-year-old diatom record. Journal of Paleolimnology 26, 67-87.

Cremer H., Gore, D., Melles, M. and Roberts, D. 2003a. Palaeoclimatic significance of late Quaternary diatom assemblages from the southern Windmill Islands, East Antarctica. Palaeogeography, Palaeoclimatology, Palaeoecology 195, 261-280.

Cremer, H., Roberts, D., McMinn, A., Gore, D. and Melles, M. 2003b. The Holocene diatom flora of marine bays in the Windmill Islands, East Antarctica. Botanica Marina 46, 82-106.

Cremer, H., Gore, D., Hultzsch, N., Melles, M. and Wagner, B. 2004. The diatom flora and limnology of lakes in the Amery Oasis, East Antarctica. Polar Biology 27, 513-531.

Cremer, H., Heiri, O., Wagner, B. and Wagner-Cremer F. 2007. Abrupt climate warming in East Antarctica during the early Holocene. Quaternary Science Reviews 26, 2012-2018.

Cromer, L., Gibson, J.A.E., Swalding, K.M. and Hodgson, D.A. 2006. Evidence for a lacustrine faunal refuge in the Larsemann Hills, East Antarctica, during the Last Glacial Maximum. Journal of Biogeography 33, 1314-1323.

Crosta, X., Pichon, J.-J. and Labracherie, M. 1997. Distribution of *Chaetoceros* resting spores in modern peri-Antarctic sediments. Marine Micropaleontology 29, 283-299.

Crosta, X., Denis, D. and Ther, O. 2008. Sea ice seasonality during the Holocene, Adélie Land, East Antarctica. Marine Micropaleontology 66, 222-232.

Croudace, I.W., Rindby, A. and Rothwell, R.G. 2006. ITRAX: description and evaluation of a new multi-function X-ray core scanner. From: Rothwell, R.G. 2006 New techniques in Sediment Core Analysis. Geological Society, London, Special Publications 267, 51-63.

Danzeglocke, U., Jöris, O. and Weninger, B. 2008. CalPal-2007online. http://www.calpal-online.de (accessed 24.2.2010)

DeMaster, D. J. 1981. The supply and accumulation of silica in the marine environment. Geochimica et Cosmochimica Acta 45, 1715-1732.

Denis, D., Crosta, X., Zaragosi, S., Romero, O., Martin, B. and Mas, V. 2006. Seasonal and subseasonal climate changes recorded in laminated diatom ooze sediments, Adélie Land, East Antarctica. The Holocene 16, 1137-1147.

Denis, D., Crosta, X., Schmidt, S., Carson, D., Ganeshram, R., Renssen, H., Bout-Roumazeilles, V., Zaragosi, S., Martin, B., Cremer, M. and Giraudeau, J. 2009. Holocene glacier and deep-water dynamics, Adélie Land region, East Antarctica. Quaternary Science Reviews 28, 1291-1303.

Denton, G.H. and Hughes, T.J. 2002. Reconstructing the Antarctic Ice Sheet at the Last Glacial Maximum. Quaternary Science Reviews 21, 193-202.

Domack E.W., Jull, A.J and Donahue, D.J. 1991a. Holocene chronology for the unconsolidated sediments at hole 740A: Prydz Bay, East Antarctica. In Barron, J., Larsen, B. (eds): Proceedings of the Ocean Drilling Program, Scientific Results 119, 747 - 750.

Domack E.W., Jull, A.J. and Nako, S. 1991b. Advance of East Antarctic outlet glaciers during the Hypsithermal: Implications for the volume state of the Antarctic ice sheet under global warming. Geology 19, 1059-1062.

Domack, E., O'Brien, P., Harris, P., Taylor, F., Quilty, P.G., De Santis, S. and Raker, B. 1998. Late Quaternary sediment facies in Prydz Bay, East Antarctica and their relationship to glacial advance onto the continental shelf. Antarctic Science 10, 236-246.

Doran, P., Berger, G.W., Lyons, W.B., Wharton, R.A., Davisson, M.L., Southon, J. and Dibb, J.E. 1999. Dating Quaternary lacustrine sediments in the McMurdo Dry Valleys, Antarctica. Palaeogeography, Palaeoclimatology, Palaeoecology 147, 223-239.

EPICA community members 2004. Eight glacial cycles from an Antarctic ice core. Nature 429, 623-628.

EPICA community members 2006. One-to-one coupling of glacial climate variability in Greenland and Antarctica. Nature 444, 195-198.

Fabel, D., Stone, J., Field, L.K., Cresswell, R.G., 1997. Deglaciation of the Vestfold Hills, East Antarctica; preliminary evidence from exposure dating of three subglacial erratics. In: Ricci, C.A. (Ed.), International Symposium on Antarctic Earth Sciences, 7. Terra Antarctica Publication, Siena, pp. 829-834.

Ferretti, V., Soave, G.E., Casaux, R. and Coria, N.R. 2001. Diet of the snow petrel *Pagodroma nivea* at Laurie Island, Antarctica, during the 1997/98 breeding season. Marine Ornithology 29, 71-73.

Fink, D., Hotchkis, M.A.C., Hua, Q., Jacobsen, G.E., Smith, A.M., Zoppi, U., Child, D., Mifsud, C., Gaast, H.A. v. d., Williams, A.A. and Williams, M., 2004. The ANTARES AMS facility at ANSTO. Nuclear Instruments and Method in Physics Research B 223-224, 109-115.

Fink, D., McKelvey, B., Hambrey, M.J., Fabel, B. and Brow, R. 2006. Pleistocene deglaciation chronology of the Radock Lake basin, Amery Oasis, northern Prince Charles Mountains, Antarctica. Earth and Planetary Science Letters 243, 285-293.

Fink, D. and Smith, A. 2007. An inter-comparison of ^{10}Be and ^{26}Al AMS reference standards and the ^{10}Be half-life. Nuclear Instruments and Methods B 259, 600-609.

Fitzsimons, S.J. and Colhoun, E.A. 1995. Form structure and stability of the Antarctic ice sheet, Vestfold Hills and Bunger Hills, East Antarctica. Antarctic Science 7, 171-179.

Fitzsimons, S.J. 1996. Paraglacial redistribution of glacial sediments in the Vestfold Hills, East Antarctica. Geomorphology 15, 93-108.

Fitzsimons, S.J. 1997. Entrainment of glaciomarine sediments and formation of thrust-block moraines at the margin of Sørsdale Glacier, East Antarctica. Earth Surface Processes and Landforms 22, 175-187.

Flower, B.P. and Kennett, J.P. 1994. The middle Miocene climatic transition: East Antarctic ice sheet development, deep ocean circulation and global carbon cycling. Palaeogeography, Palaeoclimatology, Palaeoecology 108, 537-555.

Ganzert, L., Eulenberg, A., Miller, C. and Wagner, D. 2008. Functional microbial diversity in extreme Antarctic habitats: abundance, phylogeny and ecology. (ed.) Hubberten H. Berichte zur Polarforschung (Reports on Polar Research) 583, 80-94.

Ge, L., Lai, W. and Lin, Y. 2005. Influence of and correction for moisture in rocks, soils and sediments on *in situ* XRF analysis. X-Ray Spectrometry 34, 28-34.

Gersonde, R., Crosta, X., Abelmann, A. and Armand, L. 2005. Sea-surface temperature and sea ice distribution of the Southern Ocean at the EPILOG Last Glacial Maximum - a circum-Antarctic view based on siliceous microfossil records. Quaternary Science Reviews 24, 869-896.

Gibson, J. A.E. 1999. The meromictic lakes and stratified marine basins of the Vestfold Hills, East Antarctica. Antarctic Science 11, 175-192.

Gibson, J.A.E., Paterson, K.S., White, C.A. and Swalding, K.M. 2009. Evidence for the continued existence of Abraxas Lake, Vestfold Hills, East Antarctica during the Last Glacial Maximum. Antarctic Science 21, 269-278.

Goodwin, I.D. 1993. Holocene deglaciation, sea-level change, and the emergence of the Windmill Islands, Budd Coast Antarctica. Quaternary Research 40, 70-80.

Goodwin, I.D. 1998. Did changes in Antarctic ice volume influence late Holocene sea-level lowering? Quaternary Science Reviews 17, 319-332.

Goodwin, I.D. and Zweck, C. 2000. Glacio-isostasy and glacial ice load at Law Dome, Wilkes Land, East Antarctica. Quaternary Research 53, 285-293.

Gore, D.B., Colhoun, E.A. and Bell, K. 1994. Derived constituents in the glacial sediments of the Vestfold Hills, East Antarctica. Quaternary Science Reviews 13, 301-307.

Gore, D., Creagh, D.C., Burgess, J.S., Colhoun, E.A., Spate, A.P. and Baird, A.S. 1996. Composition, distribution and origin of surficial salts in the Vestfold Hills, East Antarctica. Antarctic Science 8, 73-84.

Gore, D.B., Pickard, J., Baird, A.S. and Webb, J.A. 1996. Glacial Crooked Lake, Vestfold Hills, East Antarctica. Polar Record 32, 19-24.

Gore, D. 1997. Blanketing snow and ice, constraints on radiocarbon dating deglaciation in East Antarctic oases, Antarctic Science 9, 336-346.

Gore, D., Rhodes, E.J., Augustinus, P.C. Leishman, M.R., Colhoun, E.A. and Rees-Jones, J. 2001. Bunger Hills, East Antarctica: Ice free at the Last Glacial Maximum? Geology 29, 1103-1106.

Hall, K., Thorn, C.E., Matsuoka, N. and Prick, A. 2002. Weathering in cold regions: some thoughts and perspectives. Progress in Physical Geography 26, 577-603.

Hall, B. 2009. Holocene glacial history of Antarctica and the sub-Antarctic islands. Quaternary Science Reviews 28, 2213-2230.

Harley, S.L. 1987. Precambrian geological relationships in high-grade gneisses of the Rauer Islands, east Antarctica. Australian Journal of Earth Sciences 34, 175-207.

Harley, S.L. 1988. Proterozoic granulites from the Rauer Group, East Antarctica. I. Decompressional pressure-temperature paths deduced from mafic and felsic gneisses. Journal of Petrology 29, 1059-1095.

Harley, S.L. 1998. Ultrahigh temperature granulite metamorphism (1050°C, 12kbar) and decompression in garnet (Mg70)-orthopyroxene-sillimanite gneiss from the Rauer Group, East Antarctica. Journal of Metamorphic Geology 16, 541-562.

Harley, S.L., Snape, I. and Black, L.P. 1998. The evolution of a layered metaigneous complex in the Rauer Group, East Antarctica: evidence for a distinct Archaean terrane. Precambrian Research 89, 175-205.

Harris, P.T. and O'Brien, P. 1998. Bottom currents, sedimentation and ice-sheet retreat facies successions on the Mac.Robertson Shelf, East Antarctica. Marine Geology 151, 47-72.

Harris, P.T. 2000. Ripple cross-laminated sediments on the East Antarctic Shelf: evidence for episodic bottom water production during the Holocene? Marine Geology 170, 317-330.

Harris, P.T., Brancolini, G., Armand, L., Busetti, M., Beaman, R.J., Gioretti, G., Presti, M. and Trincardi, F. 2001. Continental shelf drift deposit indicates non-steady stat Antarctic bottom water production in the Holocene. Marine Geology 179, 1-8.

Hemer, M.A. and Harris, P.T. 2003. Sediment core from beneath the Amery Ice Shelf, East Antarctica, suggests mid-Holocene ice-shelf retreat. Geology 31, 127-130.

Heroy, D.C. and Anderson, J.B. 2007. Radiocarbon constraints on the Antarctic Peninsula Ice Sheet retreat following the Last Glacial Maximum (LGM). Quaternary Science Reviews 26, 3286-3297.

Hillenbrand, C.-D., Smith, J., Kuhn, G., Esper, O., Gersonde, R., Larter, R.D., Maher, B., Moreton, S.G., Shimmield, T.M. and Korte, M. 2009. Age assignment of a diatomaceous ooze deposited in the western Amundsen Sea Embayment after the Last Glacial maximum. Journal of Quaternary Science 25, 280-295.

Hiller, A., Hermichen, W.-D. and Wand, U. 1995. Radiocarbon-dated subfossil stomach oil deposits from petrel nesting sites; novel paleoenvironmental records from continental Antarctica. Radiocarbon 37, 171-180.

Hodell, D.A., Kanfoush, S.L., Shemesh, A., Crosta, X., Charles, C.D. and Guilderson, T.P. 2001. Abrupt cooling of the Antarctic surface waters and sea ice expansion in the south Atlantic sector of the Southern Ocean at 5000 cal yr B.P. Quaternary Research 56, 191-198.

Hodgson, D., Vyverman, W. and Sabbe, K. 2001a. Limnology and biology of saline lakes in Rauer Islands, eastern Antarctica. Antarctic Science 13, 255-270.

Hodgson, D.A., Noon, P.E., Vyverman, W., Bryant, C.L., Gore, D.B., Appleby, P., Gilmour, M., Verleyen, E., Sabbe, K., Jones, V.J., Ellis-Evans, J.C. and Wood, P.B. 2001b. Were the Larsemann Hills ice-free through the Last Glacial Maximum? Antarctic Science 13, 440-454.

Hodgson, D.A., McMinn, A., Kirkup, H., Cremer, H., Gore, D., Melles, M., Roberts, D. and Montiel, P. 2003. Colonization, succession, and extinction of marine floras during a glacial cycle: A case study from Windmill Islands (east Antarctica) using biomarkers. Paleoceanography 18, 1067, doi: 10.1029/2002PA000775.

Hodgson, D.A., Verleyen, E., Sabbe, K., Squir, A.H., Keely, B.J., Leng, M., Saunders, K.M. and Vyverman, W. 2005. Late Quaternary climate-driven environmental change in the Larsemann Hills, East Antarctica, multi-proxy evidence from a lake sediment core. Quaternary Research 64, 83-99.

Hodgson, D.A., Verleyen, E., Squir, A.H., Sabbe, K., Keely, B.J., Saunders, K.M. and Vyverman, W. 2006. Interglacial environments of coastal East Antarctica: comparison of MIS1 (Holocene) and MIS 5e (Last Interglacial) lake-sediment records. Quaternary Science Reviews 25, 179-197.

Hodgson, D., Verleyen, E., Vyverman, W., Sabbe, K., Leng, M., Pickering, M. and Keely, B. 2009. A geological constraint on relative sea level in marine Isotope Stage 3 in the Larsemann Hills, Lambert Glacier region, East Antarctica (31,366-33,228 cal yr BP). Quaternary Science Reviews 28, 2689-2696.

Huang, T., Sun, L., Wang, Y., Liu, X., Zhu, R. 2009. Penguin population dynamics for the past 8500 years at Gardner Island, Vestfold Hills. Antarctic Science 21, 131-134.

Hughen, K.A., Baillie, M.G,L., Bard, E., Bayliss, A., Beck, J.W., Bertrand, C., Blackwell, P.G., Buck, C.E., Burr, G., Cutler, K.B., Damon, P.E., Edwards, R.L., Fairbanks, R.G., Friedrich, M., Guilderson, T.P., Kromer, B., McCormack, F.G., Manning, S., Bronk Ramsey, C., Reimer, P.J., Reimer, R.W., Remmele, S., Southon, J.R., Stuiver, M., Talamo, S., Taylor, F.W., van der Plicht, J. and Weyhenmeyer, C.E. 2004. Marine04 marine radiocarbon age calibration, 0-26 cal kyr BP. Radiocarbon 46, 1059-1086

Huybrechts, P. 2002. Sea-level changes at the LGM from ice-dynamic reconstructions of the Geenland and Antarctic ice sheets during the glacial cycles. Quaternary Science Reviews 21, 203-231.

Igarashi, A., Harada, N. and Moriwaki, K. 1995. Marine fossils of 30-40 ka in raised beach deposits, and late Pleistocene glacial history around Lützow-Holm Bay, East Antarctica. Proceedings of NIPR Symposium of Antarctic Geosciences 8, 219-229.

Igarashi, A., Miura, H. and Hart, C. 1998. Amino-acid racemization dates of fossil molluscs from raised beach deposits on East Ongul Island and northern part of Langhovde, Lützow-Holm Bay region, East Antarctica. In: The 18th Symposium on Antarctic Geosciences, Program and Abstracts. NIPR: 59-61.

Ingólfsson, O. 2004. Quaternary glacial and climate history of Antarctica. In Ehlers, J. & Gibbard, P.L. (eds.): Quaternary Glaciations - Extent and Chronology, Part III, 3-43.

Ivins, E.R. and James, T.S. 2005. Antarctic glacial isostatic adjustment: a new assessment. Antarctic Science 17, 541-553.

Jansen, J.H.F., Van der Gaast, S.J., Koster, B., Vaars, A.J. 1998. CORTEX, a shipboard XRF-scanner for element analyses in split sediment cores. Marine Geology, 151, 143-153.

Jouzel, J., Masson-Delmotte, V., Cattani, O., Dreyfus, G., Falourd, S., Hoffmann, G., Minster, B., Nouet, J., Barnola, M., Chappellaz, J., Fischer, H., Gallet, J.C., Johnson, S., Leuenberger, M., Loulergue, L., Luethi, D., Oerter, H., Parrenin, F., Raisbeck, G., Raynaud, D., Schilt, A., Schwander, J., Selmo, E., Souchez, R., Spahni, R., Stauffer, B., Steffensen, J.P., Stenni, B., Stocker, T.F., Tison, J.L., Werner, M., Wolff, E.W. 2007. Orbital and millennial Antarctic climate variability over the past 800,000 years. Science 317, 793-796.

Kamatani, A. and Oku, O. 2000. Measuring biogenic silica in marine sediments. Marine Chemistry 68, 219-229.

Kanfoush, S.L., Hodell, D.A., Charles, C.D., Guilderson, T.P., Mortyn, P.G. and Ninnemann, U.S. 2000. Millennial-scale instability of the Antarctic Ice Sheet during last glaciation, Science 288, 1815-1818.

Karr, E. A., Sattley, W.M., Jung, D.O., Madigan, M.T. and Achenbach, L.A. 2003. Remarkable diversity of phototrophic purple bacteria in a permanently frozen Antarctic lake. Applied and Environmental Microbiology 69, 4910-4914.

Katz, O., Reches, Z. and Roegiers, J.-C. 2000. Evaluation of mechanical rock properties using a Schmidt Hammer. International Journal of Rock Mechanics and Mining Sciences 37, 723-728.

Kaup, E., Haendel, D. and Vaikmäe, R. 1991. Limnological features of the saline lakes of the Bunger Hills (Wilkes Land, Antarctica). Antarctic Science 5, 41-50.

Kelsey, D.E., White, R.W., Powell, R., Wilson, C.J.L. and Quinn, C.D. 2003. New constraints on metamorphism in the Rauer Group, Prydz Bay, east Antarctica, Journal of metamorphic Geology 21,739-759.

Kido, Y., Koshikawa, T. and Tada, R. 2006. Rapid and quantitative major element analysis method for wet fine-grained sediments using an XRF microscanner. Marine Geology 229, 209-225.

Kiernan, K., Gore, D.B., Fink, D., White, D. A., McConnell, A. and Sigurdsson, I.A. 2009. Deglaciation and weathering of Larsemann Hills, East Antarctica. Antarctic Science 21, 373-382.

Kinny, P.D., Black, L.P. and Shearton, J.W. 1993. Zircon ages and the distribution of Archaean and Proterozoic rocks in the Rauer Islands. Antarctic Science 5, 193-206.

Kirkup, H., Melles, M. and Gore, D.B. 2002. Late Quaternary environment of southern Windmill Islands, East Antarctica. Antarctic Science 14, 385-394.

Kudoh, S., Watanbe, K. and Imura, S. 2003. Ecological studies of aquatic moss pillars in Antarctic lakes 2. Temperature and light environment at the moss habitat. Polar Bioscience 16, 23-32.

Kulbe, T. 1997. The late Quaternary climatic and environmental history of Bunger Oasis, East Antarctica. Reports on Polar Research, 254.

Kulbe, T., Melles, M., Verkulich, S.R. and Pushina, Z.V. 2001. East Antarctic climate and environmental variability over the last 9400 years inferred from marine sediments in the Bunger Oasis. Arctic, Antarctic and Alpine Research 33, 223-230.

Lambeck, K., Yokoyama, Y. and Purcell, T. 2002a. Into and out of the Last Glacial Maximum: sea-level change during Oxygen Isotope Stages 3 and 2. Quaternary Science Reviews 21, 343-360.

Lambeck, K., Esat, T.M. and Potter, E.K. 2002b. Links between climate and sea levels for the past three million years. Nature 419, 199-206.

Leng, M. and Barker, P. 2006. A review of the oxygen isotope composition of lacustrine diatom silica for palaeoclimate reconstructions, Earth-Science Reviews 75, 5-27.

Leng, M.J. and Sloane, H.J. 2008. Combined oxygen and silicon isotope analysis of biogenic silica. Journal of Quaternary Science 223, 313-319.

Leventer, A., Domack, E., Dunbar, R., Pike, J., Stickley, C., Maddison, E., Brachfeld, S., Manley, P. and McClennen, C. 2006. Marine sediment record from the East Antarctic margin reveals dynamics of ice sheet recession. GSA Today 16, 4-10.

Lythe, M.B., Vaughan, D.G., and the BEDMAP Consortium, 2001. BEDMAP: A new ice thickness and subglacial topographic model of Antarctica. Journal of Geophysical Research 106, 11,335-11,351.

Mackintosh, A., White, D., Fink, D., Gore, D.B., Pickard, J. and Fanning, P.C. 2007. Exposure ages from mountain dipsticks in Mac. Robertson Land, East Antarctica, indicate little changes in ice-sheet thickness since the Last Glacial Maximum. Geology 35, 551-554.

Maemoku, H., Miura, H., Saigusa, S. and Moriwaki, K. 1997. Stratigraphy of the Late Quaternary raised beach deposits in the northern part of Langhovde, Lützow-Holm Bay, East Antarctica. Proceedings of NIPR Symposium of Antarctic Geosciences 10, 178-186.

Marion, G.M., Farren, R.E. and Kromrowski, A.J. 1999. Alternative pathways for seawater freezing. Cold Regions Science and Technology 29, 299-266.

Masson, V., Vimieux, F., Jouzel, J., Morgan, V., Delmotte, M., Ciais, P., Hammer, C., Johnson, S., Lipenkov, V., Mosley-Thompson, E., Petit, J-R., Steig, E., Stievenard, M. and Vaikmae, R. 2000. Holocene climate variability in Antarctica based on 11 ice-core isotopic records. Quaternary Research 54, 348-358.

Mayewski, P.A., Meredith, M.P., Summerhayes, C.P., Turner, J., Worby, A., Barrett, P.J., Casassa, G., Bertler, N.A.N., Bracegirdle, T., Naveira Garbato, A.C., Bromwich, D., Campbell, H., Hamiöton, G.S., Lyons, W.B., Maasch, K.A., Aoki, S., Xiao, C. and van Ommen, T., 2009. State of the Antarctic and Southern Ocean climate system. Reviews of Geophysics 47, DOI: 10.1029/2007RG000231.

McCormac, F.G., Hogg, A.G., Blackwell, P.G., Buck, C.E., Higham, T.F. and Reimer, P.J. 2004. SHCal04 Southern Hemisphere Calibration 0-11.0 cal kyr BP. Radiocarbon 46, 1087-1092.

McKay, R.M., Dunbar, G.B., Naish, T.R., Barrett, P.J., Carter, L. and Harper, M. 2008. Retreat history of the Ross Ice Sheet (Shelf) since the Last Glacial Maximum from deep-basin sediment cores around Ross Island. Palaeogeography, Palaeoclimatology, Palaeoecology 260, 245-261.

McMinn, A., Bloxham, J.J. and Whitehead, J. 1998. Modern surface sediments and non-deposition in Ellis Fjord, eastern Antarctica. Australian Journal of Earth Sciences 45, 645-652.

McMinn, A. 2000. Late Holocene increase in sea ice extent in fjords of the Vestfold Hills, eastern Antarctica. Antarctic Science 12, 80-88.

McMinn, A., Bleakley, N., Steinburner, K., Roberts, D. and Trenerry, L. 2000. Effect of permanent sea ice cover and different nutrient regimes on the phytoplankton succession of the fjords of the Vestfold Hills Oasis, eastern Antarctica. Journal of Plankton Research 22, 287-303.

McMinn, A., Heijnis, H., Harle, K. and McOrist, G. 2001. Late-Holocene climatic change recorded in sediment cores from Ellis Fjord, eastern Antarctica. The Holocene 11, 291-300.

Melles M., Kulbe T., Overduin P.P. and Verkulich S.R. 1994a. The expedition Bunger Oasis 1993/94 of the AWI Research Unit Potsdam. In Melles M. (ed.). The Expedition Norilsk/Tamyr 1993 and Bunger Oasis 1993/94 of AWI Research Unit Potsdam. Berichte zur Polarforschung 148, 27-80.

Melles, M., Verkulich, S.R. and Hermichen, W.-D. 1994b. Radiocarbon dating of lacustrine and marine sediments from the Bunger Hills, East Antarctica. Antarctic Science 6, 375-378.

Melles, M., Kulbe, T., Verkulich, S.R., Pushina, Z.V. and Hubberten, H.-W. 1997. Late Pleistocene and Holocene environmental history of Bunger Hills, as revealed by fresh-water and epishelf lake sediments. The Antarctic Region: Geological Evolution and Processes, 809-820.

Meredith, M.P., Brandon, M.A., Wallace, M.I., Clarke, A., Leng, M.J., Renfrew, I.A., van Lipzig, N.P.M. and King, C.J. 2008. Variability in freshwater balance of northern Marguerite Bay, Antarctic Peninsula: Results from δ^{18}O. Deep-Sea Research II 55, 309-322.

Middleburg, J.J. 1991. Organic carbon, sulphur, and iron in recent semi-euxinic sediments of Kau Bay, Indonesia. Geochimica et Cosmochimica acta 55, 815-828.

Miura, H., Maemoku, H., Seto, K. and Moriwaki, K. 1998. Late Quaternary East Antarctic melting event in the Sôya Coast region based on stratigraphy and oxygen isotopic ratio of fossil molluscs. Polar Geosciences 11, 260-274.

Mix, A.C., Bard, E. and Schneider, R. 2001. Environmental processes of the ice age: land, oceans, glaciers (EPILOG). Quaternary Science Reviews 20, 627-657.

Moriwaki, K., Iwata, S., Matsuoka, N., Hasegawa, H. and Hirakawa, K. 1994. Weathering stage as a relative age of till in the central Sør-Rondane. Proceedings of the NIPR Symposium on Antarctic Geoscience 7, 156-161.

Morley, D.W., Leng, M.J., Mackay, A.W., Sloane, H.J., Rioual, P. and Batterbee, R.W. 2004. Cleaning of lake sediment samples for diatom oxygen isotope analysis. Journal of Paleolimnology 31, 391-401.

Mortlock, R.A. and Froelich, P.N. 1989. A simple method for the rapid determination of biogenic opal in pelagic marine sediments. Deep-Sea Research 36, 1415-1426.

Nakada, M., Kimura, R., Okuno, J., Moriwaki, K., Miura, H. and Maemoku, H. 2000. Late Pleistocene and Holocene melting history of the Antarctic ice sheet derived from sea-level variations. Marine Geology 167, 85-103.

Norman, F.I. and Ward, S.J. 1990. Foods of the South Polar Skua at Hop Island, Rauer Group, East Antarctica. Polar Biology 10, 489-493.

O'Brien, P.E., Goodwin, I., Forsberg, C.-F., Cooper, A.K. and Whitehead, J. 2007. Late Neogene ice drainage changes in Prydz Bay, East Antarctica and the interaction of Antarctic ice sheet evolution and climate. Palaeogeography, Palaeoclimatology, Palaeoecology 245, 390-410.

Ohkouchi, N. and Eglinton, T.J. 2008. Compound specific radiocarbon dating of Ross Sea sediments: a prospect for constructing chronologies in high-latitude oceanic sediments. Quaternary Geochronology 3, 235-243.

Petit, J.R. and Delmonte, B. 2009. A model for large glacial/interglacial climate-induced changes in dust and sea salt concentrations in deep ice cores (central Antarctica): palaeoclimatic implications and prospects for refining ice core chronologies. Tellus B 61, 768-790.

Pickard, J. 1986. The Vestfold Hills: a window on Antarctica. In: Pickard, J. (Ed.), Antarctic Oasis, Terrestrial Environments and History of the Vestfold Hills. Academic Press, Sydney, pp. 63-98.

Pickard, J., Adamson, D.A. and Health, A. 1986. The evolution of Watts Lake, Vestfold Hills, east Antarctica, from marine inlet to freshwater lake. Palaeogeography, Palaeoclimatology, Palaeoecology 53, 271-288.

Pike, J., Crosta, X., Maddison, E.J., Stickley, C., Denis, D., Barbara, L. and Renssen, H. 2009. Observations on the relationship between the Antarctic coastal diatoms *Thalassiosira antarctica* (Comber) and *Porosira glacialis* (Grunow) Jørgensen and sea ice concentrations during the late Quaternary. Marine Micropaleontology 73, 14-25.

Quilty, P.G., Lirio, J.M. and Jillet, D. 2000. Stratigraphy of the Pliocene Sørsdal Formation, Marine Plain, Vestfold Hills, East Antarctica. Antarctic Science 12, 205-216.

Reimer, P.J., Baillie, M.G., Bard, E., Bayliss, A., Beck, J.W., Bertrand, C.J.H., Blackwell, P.G., Buck, C.E., Burr, G.S., Cutler, K.B., Damon, P.E., Edwards, R.L., Fairbankes, R.G., Friedrich, M., Guilderson, T.P., Hogg, A.G., Hughen, K.A., Kromer, B., McCormac, G., Manning, S., Ramsesy, C.B., Reimer, R.W., Remmele, S., Southon, J.R., Stuiver, M., Talamo, S., Tayloer, F.W., van der Plicht, J. and Weyhenmeyer, C.E. 2004. IntCal04 terrestrial radiocarbon age calibration, 0-26 cal kyr B.P. Radiocarbon 46, 1029-1058.

Renssen, H., Goosse, H., Fichefet, T., Masson-Delmotte, V. and Koç, N. 2005. Holocene climate evolution in the high-latitude Southern Hemisphere simulated by a coupled atmosphere-sea ice-ocean-vegetation model. The Holocene 15, 951-964.

Rignot, E., Bamber, J.L., van der Broeke, M.R., Davis, C., Li, Y., van de Berg, W.J. and van Meijgaard, E. 2008. Recent Antarctic ice mass loss from radar interferometry and regional climate modelling. Nature Geoscience 1, 106-110.

Roberts, D. and McMinn, A. 1999. A diatom-based paleosalinity history of Ace Lake, Vestfold Hills, Antarctica. The Holocene 9, 401-408.

Roberts, D., van Ommen, T.D., McMinn, A., Morgan, V. and Roberts, J.L. 2001. Late-Holocene East Antarctic climate trends from ice-cores and lake-sediment proxies. The Holocene 11, 117-120.

Röthlisberger, R., Bigler, M., Wolff, E.W., Joos, F., Monnin, E. and Hutterli, M.A. 2004. Ice core evidence for the extent of past atmospheric CO_2 change due to iron fertilisation. Geophysical Research Letters 31, L16207, doi:10.1029/2004GL020338.

SCAR (Scientific Committee on Antarctic Research) 2007. Some Antarctic Statistics. URL: http://www.scar.org/information/statistics/index.html (date of access 15. January 2010)

Schwab, J. 1998. Reconstruction of the Late Quaternary climatic and environmental history of the Schirmacher Oasis and the Wohlthat Massif (East Antarctica). Reports on Polar Research 293.

Schmidt, G.A. 2010. Enhancing the relevance of paleoclimate model/data comparisons for assessments of future climate change. Journal of Quaternary Science 25, 79-87.

Sedwick, P.N., Harris, P.T., Robertson, L.G., McMurtry, G.M., Cremer, M.D. and Robinson P. 2001. Holocene sediment records from the continental shelf of Mac. Robertson Land, East Antarctica. Paleoceanography 16, 212-225.

Shakesby, R.A., Matthews, J.A. and Owen, G. 2006. The Schmidt hammer as a relative-age dating tool and its potential for calibrated-age dating in Holocene glaciated environments. Quaternary Science Reviews 25, 2846-2867.

Spate, A., Burgess, J. and Shevlin, J. 1995. Rates of rock surface lowering, Princess Elizabeth Land, eastern Antarctica. Earth Surface Processes and Landforms 20, 567-573.

Stackebrandt, W. 1995. Moraines around Lake Untersee- indicators for the late-Quaternary regional glacial history.- in Borman, P. and Fritzsche, D.(eds): The Schirmacher Oasis, Queen Maud Land, East Anrtarctica, and its surroundings. Gotha, pp. 237-242.

Sternbeck, J., Sohlenius, G. and Hallberg, R.O. 2000. Sedimentary trace elements as proxies to depositional changes induced by a Holocene fresh-brackish water transition. Aquatic Geochemistry 6, 325-345.

Stickley, C.E., Pike, J., Leventer, A., Dunbar, R., Domack, E.W., Brachfeld, S., Manley, P. and McClennen, C. 2005. Deglacial ocean and climate seasonality in laminated diatom sediments, Mac.Robertson Shelf, Antarctica. Palaeogeography, Palaeoclimatology, Palaeoecology 227, 290-310.

Stone, J.O., 2000. Air pressure and cosmogenic isotope production. Journal of Geophysical Research, B, Solid Earth and Planets 105, 23,753-23,759.

Strand, K., Passchier, S. and Näsi, J. 2003. Implications of quartz grain microstructures for onset Eocene/Oligocene glaciation in Prydz Bay, ODP Site 1166, Antarctica. Palaeogeography, Palaeoclimatology, Palaeoecology 198, 101-111.

Streten, N.A. 1986. Climate of the Vestfold Hills. In: Pickard, J. (Ed.), Antarctic Oasis, Terrestrial Environments and History of the Vestfold Hills. Academic Press, Sydney, pp. 141-164.

Stuiver, M. and Braziunas. T.F. 1993. Modelling atmospheric ^{14}C influences and ^{14}C ages of marine samples to 10 00 BC. Radiocarbon 35, 137-189.

Stuiver, M., Reimer, P.J. and Reimer, R.W. 2005. CALIB 5.0 (www program and documentation)

Sugden, D.E., Balco, G., Cowdery, S.G., Stone, J.O. and Sass, L.C. 2005. Selective glacial erosion and weathering zones in the coastal mountains of Marie Byrd Land, Antarctica. Geomorphology 67, 317-334.

Takada, M., Tani, A., Miura, H., Moriwaki, K. and Nagatomo, T. 2003. ESR dating of fossil shells in the Lützow-Holm Bay region, East Antarctica. Quaternary Science Reviews 22, 1323-1328.

Taylor, F., McMinn, A. and Franklin, D. 1997. Distribution of diatoms in surface sediments of Prydz Bay, Antarctica. Marine Micropaleontology 32, 209-229.

Taylor, F. and McMinn, A. 2001. Evidence from diatoms for Holocene climate fluctuation along the East Antarctic margin. The Holocene 11, 455-466.

Taylor, F. and McMinn, A. 2002. Late Quaternary diatom assemblage in Prydz Bay. Quaternary Research 57, 151-161.

Taylor, F. and Leventer, A. 2003. Late Quaternary paleoenvironments in Prydz Bay, East Antarctica: interpretation from marine diatoms. Antarctic Science 15, 512-521.

Taylor, R.E. and Southon, J. 2007. Use of natural diamonds to monitor ^{14}C AMS instrument backgrounds. Nuclear Instruments and Methods in Physics Research B 259, 282-287.

Tjallingii, R., Röhl, U., Kölling, M. and Bickert, T. 2007. Influence of the water content on X-ray fluorescence core-scanning measurement in soft marine sediments. Geochemistry, Geophysics, Geosystems 8, Q02002,doi:10.1029/20006GC001393

Vaughan, D.G., Marshall, G., Connolley, W.M., Parkinson, C., Mulvaney, R., Hodgson, D.A., Pudsey, C.J., Turner, J., Wolff, E., 2003. Recent rapid regional climate warming on the Antarctic Peninsula. Climate Change 60, 243-274.

Verkulich, S.R., Melles, M., Hubberten, H.-W. and Pushina, Z.V. 2002. Holocene environmental changes and development of Figurnoye Lake in the southern Bunger Hills, East Antarctica. Journal of Paleolimnology 28, 253-267.

Verleyen, E., Hodgson, D.A., Sabbe, K., Vanhoutte, K. and Vyverman, W. 2004a. Coastal oceanographic conditions in the Prydz Bay region (East Antarctica) during the Holocene recorded in an isolation basin. The Holocene 14, 246-257.

Verleyen, E., Hodgson, D.A., Sabbe, K. and Vyverman, W. 2004b. Late Quaternary deglaciation and climate history of the Larsemann Hills (East Antarctica). Journal of Quaternary Science 19, 361-375.

Verleyen, E., Hodgson, D.A., Milne, G.A., Sabbe, K. and Vyverman, W. 2005. Relative sea-level history from the Lambert Glacier region, East Antarctica, and its relation to deglaciation and Holocene glacier readvance. Quaternary Research 63, 45-52.

Voelker, A. and workshop participants 2002. Global distribution of centennial-scale records for Marine Isotope Stage (MIS) 3: a database. Quaternary Science Reviews 21, 1185-1212.

Vogel, H., Rosen, P., Wagner, B., Melles, M. and Persson, P. 2008. Fourier transform infrared spectroscopy, a new cost-effective tool for quantitative analysis of biogeochemical properties in long sediment records. Journal of Paleolimnology 40, 689-702.

Volpi, V., Rebesco, M. and Diviacco, P. 2009. New insights in the evolution of Antarctic glaciation from depth conversion of well-log calibrated seismic section of Prydz Bay. International Journal of Earth Sciences 98, 1991-2007.

Wagner, B., Cremer, H., Hultzsch, N., Gore, D. and Melles, M. 2004. Late Pleistocene and Holocene history of Lake Terrasovoje, Amery Oasis, East Antarctica, and its climatic and environmental implications. Journal of Paleolimnology 32, 321-339.

Wagner B., Bennike, O., Berg, S., Fritz, M., Klatt, o., Klug, M., Muhle, K., Ortlepp, S., Vogel, H., White, D. and Melles, M. 2008. Late Quaternary environmental history of the Rauer Group, as deduced from lake and marine basin sediments. (ed.) Hubberten H. Berichte zur Polarforschung 583, 80-94.

Weltje, G.J. and Tjallingii, R. 2008. Calibration of XRF core scanners for quantitative geochemical logging of sediment cores: Theory and application. Earth and planetary Science 274, 423-438

Weninger, B. and Jöris, O. 2008. A ^{14}C age calibration curve for the last 60 ka: the Greenland-Hulu U/Th timescale and its impact on understanding the Middle to Upper Paleolithic transistion in Western Eurasia. Journal of Human Evolution 55, 772-781.

White, D.A. 2007. Cenozoic Glacial History and Landscape Evolution of Mac.Robertson Land and the Lambert Glacier-Amery Ice Shelf System, East Antarctica. PhD Thesis, Department of Physical Geography, Macquarie University, Sydney.

White, D.A., Bennike, O., Berg, S., Harley, S.L., Fink, D., Kiernan, K., McConnell, A. and Wagner, B. 2009. Geomorphology and glacial history of Rauer Group, East Antarctica. Quaternary Research 72, 80-90.

Wilson, C.J.L., Quinn, C., Tong, L. and Phillips, D. 2007. Early Proterozoic intratectonic shears and post-tectonic cooling in the Rauer Group, Prydz Bay, East Antarctica constrained by [40]Ar/[39]Ar thermochronology. Antarctic Science 19, 339-353.

Wingham, D.J., Sheperd, A., Muir, A., Marshall, G.J., 2006. Mass balance of the Antarctic Ice Sheet. Philosophical Transactions of the Royal Society A 364, 1627-1635.

Yabuki, T., Suga, T., Hanawa, K., Matsuoka, K., Kiwada, H. and Watanbe, T. 2006. Possible source of the Antarctic bottom water in the Prydz Bay region. Journal of Oceanography 62, 649-655.

Yevteyev, S.A. 1962. Marine terraces along the Antarctic coast. Soviet Antarctic Information Bulletin 4, 73-76.

Yokoyama,Y., Kido, Y., Tada, R., Minami, I., Finkel, R.C. and Matsuzaki, H. 2007. Japan Sea oxygen isotope stratigraphy and global sea-level changes fort he last 50,000 years recorded in sediment cores from the Oki Ridge. Palaeogeography, Palaeoclimatology, Palaeoecology 247, 5-17.

Zielinski, U. and Gersonde, R. 2002. Plio-Pleistocene diatom biostratigraphy from ODP Leg 177, Atlantic sector of the Southern Ocean. Marine Micropaleontology 45, 225-268.

Zwartz, D. 1995. The recent history of the Antarctic Ice Sheet: constraints from sea-level change. PhD Thesis, Research School of Earth Sciences, The Australian National University.

Zwartz, D., Bird, M., Stone, J. and Lambeck, K. 1998. Holocene sea-level change and ice sheet history in the Vestfold Hills, East Antarctica. Earth and Planetary Science Letters 155, 131-145.

Appendix

Table A1 List of investigated cores from marine inlets and lakes in the Rauer Group, coring locations are indicated in Figure 2.1.

Core no.	Coring location	latitude	longitude	Water depth [m]	Sediment depth [cm]	Coring device
Co1010-1	Filla Island inlet	S 68°48.142′	E 077°53.355′	38.0	0-116	GC
Co1010-2	Filla Island inlet	S 68°48.142′	E 077°53.355′	38.0	0-111	GC
Co1010-3	Filla Island inlet	S 68°48.142′	E 077°53.355′	38.0	0-113	GC
Co1010-4	Filla Island inlet	S 68°48.142′	E 077°53.355′	38.0	0-116	GC
Co1010-5	Filla Island inlet	S 68°48.142′	E 077°53.355′	38.0	50-345	U-PC
Co1010-6	Filla Island inlet	S 68°48.142′	E 077°53.355′	38.0	250-550	U-PC
Co1010-7	Filla Island inlet	S 68°48.142′	E 077°53.355′	38.0	450-746	U-PC
Co1010-8	Filla Island inlet	S 68°48.142′	E 077°53.355′	38.0	650-948	U-PC
Co1010-9	Filla Island inlet	S 68°48.142′	E 077°53.355′	38.0	850-1148	U-PC
Co1010-10	Filla Island inlet	S 68°48.142′	E 077°53.355′	38.0	1050-1346	U-PC
Co1010-11	Filla Island inlet	S 68°48.142′	E 077°53.355′	38.0	1250-1546	U-PC
Co1010-12	Filla Island inlet	S 68°48.142′	E 077°53.355′	38.0	1450-1732	U-PC
Co1010-13	Filla Island inlet	S 68°48.142′	E 077°53.355′	38.0	1650-1947	U-PC
Co1010-14	Filla Island inlet	S 68°48.142′	E 077°53.355′	38.0	1850-2137	U-PC
Co1010-15	Filla Island inlet	S 68°48.142′	E 077°53.355′	38.0	0-112	GC
Co1010-16	Filla Island inlet	S 68°48.142′	E 077°53.355′	38.0	2050-2332	U-PC
Co1011-1	Flag Island inlet	S 68°49.563′	E 077°46.293′	7.8	0-78	GC
Co1011-2	Flag Island inlet	S 68°49.563′	E 077°46.293′	7.8	0-80	GC
Co1011-3	Flag Island inlet	S 68°49.563′	E 077°46.293′	7.8	0-296	U-PC
Co1011-4	Flag Island inlet	S 68°49.563′	E 077°46.293′	7.8	240-533	U-PC
Co1011-5	Flag Island inlet	S 68°49.563′	E 077°46.293′	7.8	480-777	U-PC
Co1011-6	Flag Island inlet	S 68°49.563′	E 077°46.293′	7.8	675-969	U-PC
Co1011-7	Flag Island inlet	S 68°49.563′	E 077°46.293′	7.8	860-1099	U-PC
Co1014-1	Shcherbinina Island inl.	S 68°49.984′	E 077°55.574′	6.3	0-45	GC
Co1014-2	Shcherbinina Island inl.	S 68°49.984′	E 077°55.574′	6.3	0-56	GC
Co1014-3	Shcherbinina Island inl.	S 68°49.984′	E 077°55.574′	6.3	0-47	GC
Co1014-4	Shcherbinina Island inl.	S 68°49.984′	E 077°55.574′	6.3	0-262	U-PC
Co1014-5	Shcherbinina Island inl.	S 68°49.984′	E 077°55.574′	6.3	0-149	U-PC
Co1008-5	Filla Island (Skua Lake)	S 68°48.714'	E 077°52.173'	1.2	0-149	E-PC
Co1008-6	Filla Island (Skua Lake)	S 68°48.714'	E 077°52.173'	1.2	100-231	E-PC

GC = gravity corer, U-PC = UWITEC piston corer, E-PC Eijkelkamp piston corer

Table A2. List of radiocarbon ages and calibrated ages obtained from sediments of Rauer Group.

Core	Lab. No.	Dated material	Core depth [cm]	^{14}C age [^{14}C yr BP]	Calendar age [cal yr BP]	Mean± dev. [cal yr BP]	Remarks*
-	KIA33455	shell	-	35680±650	39435-41491	40463±1028	Chapter 4.6
Co1008	ETH-38771	TOC	227-228	30015±150	34129-34443	34286±157	Chapter 4.6
Co1008	ETH-38772	TIC	227-228	37110±510	40694-41486	41090±396	Chapter 4.6
Co1010	KIA34076	HAF	4-6	920±80	-3-149	73±76	Chapter 4.4
Co1010	KIA35015	HAF	273-275	2335±35	1257-1396	1326±70	Chapter 4.4
Co1010	KIA35016	HAF	678-680	4230±70	3401-3779	3590±189	Chapter 4.4
Co1010	KIA35017	HAF	957-959	5690±55	5329-5590	5459±130	Chapter 4.4
Co1010	KIA35019	HAF	1237.7-1239.7	7140±80	6896-7268	7082±186	Chapter 4.4
Co1010	KIA35020	HAF	1441-1443	7810±70	7575-7864	7719±145	Chapter 4.4
Co1010	KIA35020	HA	1441-1443	8130±40	-	-	
Co1010	KIA35021	HAF	1593-1595	7750±260	7176-8185	7680±505	Chapter 4.4
Co1010	KIA37749	HAF	1700-1702	9125±50	9058-9381	9219±162	Chapter 4.4
Co1010	KIA37749	HA	1700-1702	9445±55	-	-	
Co1010	KIA34077	HAF	1873-1875	10,880±40	11,193-11,417	11,305±112	Chapter 4.4
Co1010	KIA34077	HA	1873-1875	10,505±40	-	-	
Co1010	KIA35022	HAF	1894-1896	12,490±80	13,246-13,491	13,368±123	Chapter 4.4
Co1010	KIA35023	HAF	1946-1948	37,130±1300	40,769-42,811	41,790±1021	Chapter 4.6
Co1010	KIA35024	HAF	2001-2003	29,550±180	33,672-34,180	33,3926±254	Chapter 4.6
Co1010	KIA35024	HA	2001-2003	45,360±2000	46,422-51,750	49,086±2664	Chapter 4.6
Co1010	KIA35025	HAF	2103.5-2105.5	38,780±900	42,360-43,898	43,129±769	Chapter 4.6
Co1010	KIA35025	HA	2103.5-2105.5	42,200±2000	44,036-48,226	46,131±2095	Chapter 4.6
Co1010	KIA34078	HAF	2143-2145	40,860±2000	43,041-46,549	44,795±1754	Chapter 4.6
Co1010	KIA34078	HA	2143-2145	34,840±360	39,107-40,797	39,952±845	Chapter 4.6
Co1011	KIA37742	HAF	2-4	985±30	-	-	
Co1011	KIA37742	HA	2-4	890±25	-3-66	32±35	Chapter 4.4
Co1011	KIA37743	HA	147-149	3370±30	2483-2707	2595±112	Chapter 4.4
Co1011	KIA37745	HAF	619-621	7265±45	-	-	
Co1011	KIA37745	HA	619-621	7210±40	7134-7309	7222±88	Chapter 4.4
Co1011	KIA37746	HA	900-902	8530±45	8369-8561	8465±96	Chapter 4.4
Co1011	KIA37748	HAF	1087-1089	9890±60	11125-11404	11264±140	Chapter 4.4
Co1014	KIA38366	HAF	3-4	1000±25	-3-66	31±34	Chapter 4.5
Co1014	KIA38366	HA	3-4	880±20	-	-	
Co1014	KIA38367	HAF	27-28	1815±30	656-785	720±64	Chapter 4.5
Co1014	KIA38367	HA	27-28	1495±30	-	-	
Co1014	KIA38368	HAF	134-135	2785±30	1630-1828	1729±99	Chapter 4.5
Co1014	KIA38368	HA	134-135	2590±25	-	-	
Co1014	KIA38369	HAF	254-255	5000±35	4400-4615	4507±107	Chapter 4.5
Co1014	KIA38369	HA	254-255	4925±30	-	-	

HA humic acid fraction of organic material, HAF humic acid free fraction of organic material*calibration of radiocarbon ages is discussed in the respective chapters.

A3 Further data, obtained from sediment cores discussed in this study, will be available at the geoscientific database PANGAEA: http://www.pangaea.de.

Erklärung

Ich versichere, dass ich die von mir vorgelegte Dissertation selbstständig angefertigt, die benutzten Quellen und Hilfsmittel vollständig angegeben und die Stellen der Arbeit-einschließlich Tabellen, Karten und Abbildungen-, die anderen Werken in Wortlaut oder dem Sinn nach entnommen sind, in jedem Einzelfall als Entlehnung kenntlich gemacht habe; dass diese Dissertation noch keiner anderen Fakultät oder Universität zur Prüfung vorgelegen hat; dass sie- abgesehen von unten angegebenen Teilpublikationen- noch nicht veröffentlicht worden ist sowie, dass ich eine solche Veröffentlichung vor Abschluss des Promotionsverfahrens nicht vornehmen werde. Die Bestimmungen der Promotionsordnung sind mir bekannt. Die von mir vorgelegte Dissertation ist von Prof. Dr. Martin Melles betreut worden.

Nachfolgend genannte Teilpublikationen liegen vor:

1) Berg, S., Wagner, B., White, D.A., Cremer, H., Bennike, O. and Melles, M. 2009. New marine core record of Late Pleistocene glaciation history, Rauer Group, East Antarctica. Antarctic Science 21, 299-300.

2) White, D.A., Bennike, O., Berg, S., Harley, S.L., Fink, D., Kiernan, K., McConnell, A. and Wagner, B. 2009. Geomorphology and glacial history of Rauer Group, East Antarctica. Quaternary Research 72, 80-90.

3) Berg, S., Wagner, B., White, D. and Melles, M. 2010. No significant ice sheet expansion beyond present ice margins during the past 4500 yr at Rauer Group, East Antarctica. Quaternary Research 74, 23-25.

4) Berg, S., Wagner, B., Cremer, H. Leng, M.J. and Melles, M. *eingereicht*. Late Quaternary environmental and climate history of Rauer Group, East Antarctica. Palaeogeography, Palaeoclimatology, Palaeoecology, Manuskript Nummer PALAO5540.

Köln, den 5.05.2010